



Universidade Federal de Ouro Preto  
Escola de Minas  
Departamento de Engenharia Civil  
Programa de Pós-Graduação em Engenharia Civil



# Thermal Properties of Cement-based Composites

**Autora:** Júlia Castro Mendes

**Orientador:** Prof. Dr. Ricardo André Fiorotti Peixoto

Ouro Preto, Novembro de 2019



Universidade Federal de Ouro Preto  
Escola de Minas  
Departamento de Engenharia Civil  
Programa de Pós-Graduação em Engenharia Civil



## **Thermal Properties of Cement-based Composites**

**Autora:** Júlia Castro Mendes

**Orientador:** Prof. Dr. Ricardo André Fiorotti Peixoto

Tese apresentada ao programa de Pós-Graduação em Engenharia Civil da Escola de Minas da Universidade Federal de Ouro Preto, como parte dos requisitos para obtenção do título de Doutor em Engenharia Civil.

Ouro Preto, Novembro de 2019

SISBIN - SISTEMA DE BIBLIOTECAS E INFORMAÇÃO

M538t Mendes, Julia Castro .  
Thermal Properties of Cement-based Composites. [manuscrito] / Julia Castro  
Mendes. - 2019.  
110 f.: il.: color..

Orientador: Prof. Dr. Ricardo André Fiorotti Peixoto.  
Tese (Doutorado). Universidade Federal de Ouro Preto. Departamento de  
Engenharia Civil. Programa de Engenharia Civil.  
Área de Concentração: Estruturas e Construção.

1. Thermal conductivity. 2. Specific heat. 3. Pore System. 4. solid residues -  
Reuse. 5. Building performance. I. Mendes, Julia Castro . II. Peixoto, Ricardo André  
Fiorotti. III. Universidade Federal de Ouro Preto. IV. Título.

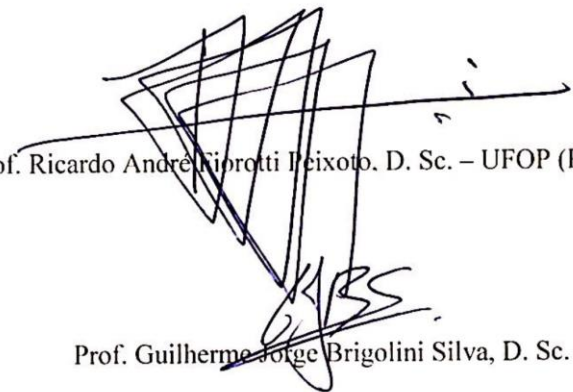
CDU 624.01

Bibliotecário(a) Responsável: Maristela Sanches Lima Mesquita - CRB: 1716

# THERMAL PROPERTIES OF CEMENT-BASED COMPOSITES

**AUTORA: JÚLIA CASTRO MENDES**

Esta tese foi apresentada em sessão pública e aprovada em 22 de novembro de 2019, pela Banca Examinadora composta pelos seguintes membros:



Prof. Ricardo André Fiorotti Peixoto, D. Sc. – UFOP (Presidente)



Prof. Guilherme Jorge Brigolini Silva, D. Sc. – UFOP



Profa. Maria Teresa Paulino Aguilar, D. Sc. – UFMG



Prof. José Maria Franco de Carvalho, D. Sc. – UFV



Prof. Fernando da Costa Baêta, D. Sc. – UFV

## AGRADECIMENTOS

É importante deixar claro que nem o primeiro passo teria sido dado sem o amor, o carinho, a inspiração e o apoio incondicional dos meus pais e heróis: Rosemary e Tarcísio; e do irmão parceiro Thales. Em todos os momentos, sobretudo quando a pressão era forte, o suporte da minha família (longe ou perto) garantiu a minha permanência no rumo, sem desanimar. E também a minha gratidão ao amor Alexandre, cuja presença e o incentivo foram fundamentais durante todo esse período.

Em especial, agradeço ao professor, orientador e amigo Ricardo André Fiorotti Peixoto, que sempre compartilhou generosamente seu conhecimento e suas experiências, dentro e fora da UFOP. Expresso minha sincera e profunda gratidão por seus ensinamentos e, principalmente, pelo seu apoio e paciência ao longo dessa jornada.

Agradeço também imensamente aos membros do grupo RECICLOS, pelo apoio e contribuição tanto na forma de conhecimento quanto na forma de suor e trabalho. São eles também os responsáveis pela conclusão desta etapa. Em especial, gostaria de agradecer os ensinamentos e sugestões do prof. Guilherme Jorge Brigolini Silva; o auxílio dos parceiros de bancada Rodrigo Barreto, Laís Costa, Arthur Castro, Fernanda Elói e Júnio Batista; e todas as boas discussões com os colegas José Maria Carvalho, Wanna Fontes, Keoma Defáveri, Juliana Natalli, Aline Figueiredo, Marina Caetano e Humberto Andrade.

Finalmente, agradeço ao PROPEC, à CAPES, à Fapemig e ao CNPq pelo apoio organizacional e financeiro. Agradeço, também, ao Laboratório de Microscopia Eletrônica Nanolab, da REDEMAT, Escola de Minas, UFOP, pelos ensaios relacionados à microscopia eletrônica de varredura. E à todas as pessoas que contribuíram para a realização deste trabalho, direta ou indiretamente, meu sincero muito obrigada.

# ABSTRACT

---

Heat transfer through a solid building element is primarily controlled by its thermal conductivity in the steady-state, and by an association of thermal conductivity and specific heat in transient situations. The thermal properties of the construction materials are some of the main responsible factors for the habitability and energy demand of a building. Therefore, the present work assesses how the chemical composition, physical properties and microstructure influence the thermal properties (specific heat and thermal conductivity) of cement-based composites. For this purpose, we investigated three mortar mixes with cement and hydrated lime (1:3, 1:1:6 and 1:2:9); three types of aggregates (river sand, iron ore tailings, friable quartzite); and three dosages of air-entraining admixture (0%, 0.05% and 0.5%). Physical and chemical characterisation of the aggregates were performed; along with physical, thermal and microstructural evaluation of the resulting mortars. Lastly, the correlation between thermal conductivity and ultrasonic pulse velocity (UPV) was also investigated. As result, mortars with iron ore tailings (IOTm) presented the lowest thermal conductivity and highest specific heat among all materials tested. The air-entraining admixture reduced the thermal conductivity of the mortars up to 40% but did not significantly influenced the specific heat. It was observed that the microstructure of the resulting matrix is more relevant to the thermal properties of mortars than the chemical composition of their components. Also, the pore system generated by the aggregates in the mortars is more influential to their thermal conductivity and UPV than their specific gravity. A satisfactory determination coefficient ( $R^2 > 0.9$ ) was obtained between thermal conductivity and UPV of the mortars when they were grouped under similar components and pore structure. These results demonstrate the importance of using methodologies that keep the microstructure of the matrices mostly intact. Based on the thermal properties obtained, residue-based mortars are promising alternatives to improve the energy efficiency of buildings. In conclusion, this work hopes to contribute to the technological and sustainable development of cement-based composites.

**Keywords:** Thermal conductivity; Specific heat; Pore System; Reuse of solid residues; Building performance;

## RESUMO

---

A transferência de calor através de um elemento construtivo sólido é controlada principalmente pela sua condutividade térmica no estado estacionário e por uma associação de condutividade térmica e calor específico em situações transientes. A condutividade térmica dos materiais de construção é um dos principais fatores responsáveis pela habitabilidade e demanda energética de uma edificação. Dessa forma, o presente trabalho investiga como a composição química, as propriedades físicas e a microestrutura influenciam as propriedades térmicas (calor específico e condutividade térmica) de matrizes cimentícias. Para este fim, foram investigados três traços de argamassa com cimento e cal hidratada (1:3, 1:1:6 e 1:2:9); três tipos de agregados (areia de rio, rejeito de barragem de minério de ferro e quartzito friável); e três dosagens de aditivo incorporador de ar (0%, 0.05% e 0.5%). Inicialmente foi realizada a caracterização química e física dos agregados, além da avaliação física, térmica e morfológica das matrizes resultantes. Por fim, a correlação entre a condutividade térmica e a velocidade de pulso ultrassônico (UPV) também foi investigada. Como resultado, argamassas com rejeito de barragem de minério de ferro (IOTm) apresentaram a menor condutividade térmica e o maior calor específico entre todos os materiais testados. O aditivo incorporador de ar reduziu a condutividade térmica das argamassas em até 40%, mas não influenciou significativamente o calor específico delas. Foi observado que a microestrutura da matriz é mais relevante para as propriedades térmicas das argamassas do que a composição química de seus componentes. Ainda, o sistema de poros gerado pelos agregados é mais correlacionado com as condutividades térmicas e UPVs das argamassas do que sua massa específica aparente. Um coeficiente de determinação satisfatório ( $R^2 > 0.9$ ) foi obtido entre a condutividade térmica e a UPV das argamassas quando estas foram agrupadas em matérias-primas e estruturas de poros similares. Esses resultados demonstram a importância de se usar metodologias que mantem praticamente intacta a microestrutura das matrizes. Com base nas propriedades térmicas obtidas, as argamassas à base de resíduos são alternativas promissoras para melhorar a eficiência energética dos edifícios. Em conclusão, este trabalho espera contribuir para o desenvolvimento tecnológico e sustentável de matrizes cimentícias.

**Palavras-chaves:** Condutividade Térmica; Calor Específico; Matrizes Cimentícias Não-Convencionais; Tecnologia dos materiais; Desempenho de edificações;

# ABBREVIATION LIST

---

AEA – Air-Entraining Admixture  
GHP – Guarded Hot Plate  
HFM – Heat Flow Meter  
HVAC - Heating, ventilation, and air conditioning  
IOT – Iron Ore Tailings from Tailings Dams  
IOTm – Mortars produced with iron ore tailings  
IR - Infrared  
LAS - Linear Alkyl Benzene Sodium Sulfonate  
LDA – Lee Disc Apparatus  
PCM – Phase Change Material  
QTZ – Friable Quartzite  
QTZm – Mortars produced with friable quartzite  
REFm – Mortars Produced with natural aggregates  
SEM – Scanning Electron Microscope  
UPV – Ultrasonic Pulse Velocity  
UV – Ultraviolet  
w/c – water/cement ratio  
w/b – water/binders ratio  
XRD – X-Ray Diffraction  
XRF – X-Ray Fluorescence

# SUMMARY

---

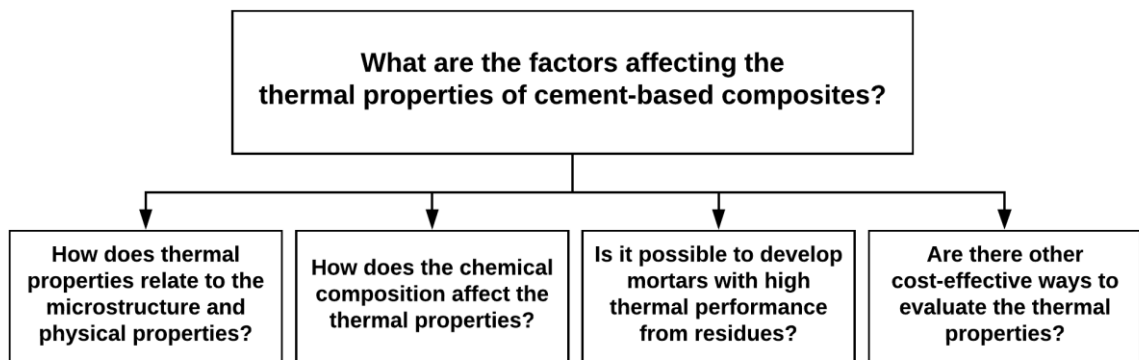
Abstract .....	V
Resumo .....	VI
Abbreviation List .....	VII
Summary .....	VIII
1 Introduction .....	2
1.1 Current Context.....	2
1.2 Motivation.....	2
1.3 Objectives .....	4
1.4 Originality and Contribution to Society.....	4
1.5 Thesis Structure .....	5
2 Literature Review .....	7
2.1 Non-Conventional Cement-Based Composites .....	7
2.1.1 Iron Ore Tailings (IOT).....	7
2.1.2 Quartzite Mining Waste (QTZ).....	10
2.1.3 Linear Alkyl Benzene Sodium Sulfonate (AEA).....	12
2.2 Heat Transfer .....	17
2.2.1 One-dimensional, steady-state thermal conduction .....	17
2.2.2 Thermal conductivity measurement.....	20
2.2.3 Specific Heat .....	23
2.2.4 Specific heat measurement.....	24
2.2.5 Other thermal properties .....	27
2.3 Thermal Performance of Buildings.....	30
2.3.1 Heat transfer in cement-based composites.....	30
2.3.2 Thermal Properties of cement-based composites.....	31
2.3.3 Buildings and Energy.....	40
2.3.4 Strategies to improve thermal performance in buildings .....	43

2.3.5	Building Energy Simulation.....	44
2.3.6	Thermal Performance at Brazilian Buildings.....	45
2.4	Ultrasonic Pulse Velocity .....	49
3	Materials and Methodology .....	53
3.1	Materials .....	53
3.2	Material Characterisation.....	54
3.3	Mixture Design and Preparation .....	55
3.4	Physical Characterisation of the mortars .....	56
3.5	Thermal Characterisation of the mortars .....	56
3.6	Microstructural Characterisation .....	58
3.7	Ultrasonic Pulse Velocity .....	60
4	Results and Discussion.....	62
4.1	Material Characterisation.....	62
4.2	Physical Characterisation of the mortars .....	65
4.2.1	Characterisation of the mortars in the fresh state.....	65
4.2.2	Characterisation of the mortars in the hardened state .....	67
4.3	Thermal Conductivity .....	69
4.4	Microstructural Characterisation .....	71
4.5	Specific Heat.....	74
4.6	Discussions on the energy perspective .....	77
4.7	Ultrasonic Pulse Velocity .....	79
4.7.1	Average UPV .....	79
4.7.2	Thermal Conductivity versus Specific gravity.....	82
4.7.3	Thermal Conductivity versus UPV .....	83
5	Conclusion.....	88
	References.....	93
	Publications by the author .....	107

# 1

---

## Chapter 1: Introduction



# 1 INTRODUCTION

---

## 1.1 CURRENT CONTEXT

The suitable choice of materials is an essential criterion to ensure the performance of a building. This factor is responsible for aspects such as habitability, durability and aesthetics, enhancing the construction's value. In addition, materials play a key role regarding the energy efficiency, as they will influence the greater or lesser need for artificial conditioning throughout the whole operation of the building.

The consolidation of sustainability as one of the fundamental criteria in building design leads to a greater focus in the project stages. This new mindset also promotes the use of novel materials and project processes, such as software for building energy simulation. With the intensification in project detailing, the widespread use of software, the tightening of fire regulations, and the consolidation of performance standards, the thermal properties of materials are increasingly demanded.

In general, the physical and mechanical properties of cement-based composites (i.e., pastes, mortars and concretes) are found in the literature with relative ease, unlike their thermal characterisation. Due to the high cost and technical limitations, few laboratories have the necessary equipment and trained personnel to evaluate them. Thus, the development of fast, inexpensive and reproducible methods for assessing the thermal properties of construction materials would contribute to the development of new materials and to the examination of existing ones.

In summary, the technological development of the construction industry requires new, efficient, sustainable, and cost-effective materials. In this scenario, the present work studies the factors influencing the thermal properties of cement-based composites, assesses the thermal performance of residue-based mortars, and evaluates a novel methodology for their characterisation.

## 1.2 MOTIVATION

Nowadays, it is evident that sustainability and social responsibility are among the main responsibilities of governments, companies and institutions. In recent years, the rising population, the urbanisation and the economic growth in developing countries have led to an extensive demand for natural resources. Consequently, billions of tons of mining tailings and industrial wastes are generated and disposed of every year, at high environmental and social costs (Edraki, et al., 2014) (Franks, et al., 2011).

The volume of tailings generated each year makes unavoidable their disposal in large containment basins, yards and/or landfills. This situation brings serious consequences for the ecosystems that they are part of, as well as massive expenses with transportation, operation, maintenance and monitoring of these sites (Franks, et al., 2011).

Mining and industrial operations must be conducted in environmental, economic and socially acceptable manners (Franks, et al., 2011). Waste management technologies that offer opportunities for reuse of tailings should be preferentially adopted (Edraki, et al., 2014) (Allesch & Brunner, 2014) (McPhail, 2006).

At the same time, civil construction stands out as one of the sectors that demand greater consumption of natural resources for its production processes. According to the National Association of Entities of Producers of Construction Aggregates, 45 billion tons of aggregates were produced worldwide in 2014 (ANEPAC, 2015). From these, 741 million tons were generated in Brazil alone (ANEPAC, 2015).

On the other hand, civil construction is also a segment with significant potential to absorb waste from other sectors and itself. For example, Weishi, et al. (2018) and Fontes et al. (2016) verified the application of iron ore tailings from tailings dams (IOT) as aggregate for concretes and mortars; and Galvão et al. (2018) and Fontes et al. (2018), as pigment for paints and cement tiles. The technical feasibility of processed steelmaking slag as aggregate and secondary binder is also well-established (Carvalho, et al., 2019) (Marinho, et al., 2017) (Silva, et al., 2016). Some other residues such as recycled aggregates, agricultural waste, sewage sludge and industrial ashes have been extensively studied as aggregates, fibres, binders, mineral admixtures, among others.

The use of residues as construction materials implies a significant reduction in the embodied energy of a building (Tuladhar & Yin, 2019) (Passuello, et al., 2014), since it mitigates the consumption of natural resources. This practice has the potential to reduce the construction costs (Gonçalves, et al., 2016), and often improve the technical properties of cement-based composites (Sant'Ana Filho, et al., 2017) (Silva, et al., 2016). Additionally, the environmental and social impacts of the deposit of these residues are also reduced. In summary, the use of tailings in construction materials implies a significant reduction in the overall carbon footprint of a building, and in the impacts of the mining, industrial and construction sectors.

In the present work, non-conventional cement-based composites are those that incorporate solutions aiming at a lower environmental impact. These solutions may be replacing one traditional component (e.g. Portland cement by residue-based binders, or

natural aggregates by recycled ones), or including new environmentally friendly components (e.g. residue-based fibres and mineral admixtures, and low-impact chemical admixtures).

The inclusion of these alternative materials will affect the thermal properties of the resulting composite (Demirboga & Gül, 2003) (Khan, 2002). A lower thermal conductivity is desired to improve insulation in buildings and reduce their energy demand. Conversely, a higher value can potentially reduce pathologies caused by thermal gradients. At the same time, a higher specific heat increases the energy storage of the envelope, being useful in climates with high daily thermal amplitudes; while a lower specific heat reduces overheat in places with low daily amplitudes (Felix & Elsamahy, 2017) (Lamberts, et al., 1997). In this sense, it is imperative to understand how the new materials will influence the thermal properties of the non-conventional cement-based composites.

### **1.3 OBJECTIVES**

The main goal of the present work is to investigate how the chemical composition, physical properties and microstructure influence the thermal properties (specific heat and thermal conductivity) of cement-based composites.

The specific objectives are:

- Evaluate how the adopted residues and admixtures affect the properties of the mortars produced;
- Investigate which parameters are more influential to the thermal properties of conventional and non-conventional cement-based composites;
- Explore more efficient and cost-effective alternatives for the determination of thermal conductivity and specific heat of construction materials;

### **1.4 ORIGINALITY AND CONTRIBUTION TO SOCIETY**

The conducted literature review demonstrated that the thermal properties of non-conventional cement-based composites are poorly disseminated. In fact, considering the wide variety of materials available and the high cost of the analyses involved, information about thermal properties is scarce even for some conventional composites. A comprehensive investigation of how the microstructure (porosity and pore structure) of cement-based composites and their thermal properties are related was not found in the literature.

Given the importance of these properties in the design and construction scenarios today, efficient methods to obtain them are also demanded. There are already a few low-cost alternatives for this determination, such as the Lee's disc apparatus (Philip & Fagbenle, 2014). However, most of these devices either have extremely long measurement times or low precision. Thus, inexpensive and effective methods to evaluate the thermal properties of building materials is a highly required tool.

In the light of the current context and the state-of-the-art of the present theme, this work seeks to contribute in the following areas:

- Materials Science, by providing clarification of the factors that involve the thermal properties in the scope of building materials;
- Architecture and Civil Construction, by encouraging the production of building elements with greater energy-efficiency and lower environmental impacts;
- Community, by assisting in the improvement the thermal performance of buildings and endorsing the reduction of risks and impacts of waste disposal;
- Environment, by contributing to reducing the consumption of natural resources, the energy use of buildings, the greenhouse gas emissions and the impact of the residues on ecosystems.

## **1.5 THESIS STRUCTURE**

The two initial chapters introduce an overview of the problem and the main concepts addressed in order to level the readers. Chapter 3 presents the materials and methodologies adopted. The results of the evaluations performed are disclosed and discussed in Chapter 4. The final chapter, 5, presents the conclusions of the thesis. It is followed by the bibliography and an appendix containing the published papers up to the date of presentation of this thesis.

# 2

---

## Chapter 2: LITERATURE REVIEW

**Non-conventional  
Cement-based composites**

**Fundamentals of Heat  
Transfer and Thermal  
Properties**

**Thermal Comfort and  
Energy-Efficient Buildings**

**Ultrasonic Pulse Velocity in  
Cement-Based Composites**

## 2 LITERATURE REVIEW

---

### 2.1 NON-CONVENTIONAL CEMENT-BASED COMPOSITES

#### 2.1.1 Iron Ore Tailings (IOT)

Only in 2017, Brazil mined 585 million tons of iron ore, being the world's 3<sup>rd</sup> largest exporter (Ministry of Mines and Energy, 2018). According to the Brazilian Ministry of Mines and Energy (2018), this ore had an average iron content of 54.4%.

After mining, a beneficiation process is necessary to concentrate the iron ore for commercial purposes. This long process includes crushing, grinding, separating and concentrating. Although modern methods do not include water in the process, Brazilian industries heavily rely on water-based ones (Ávila, 2012). As output, the concentrated ore is sold to steel industries worldwide, while the mining companies are left with a slime composed of poor (low-grade) iron ores, sand, clay and water, the iron ore tailings (IOT). Figure 2-1 shows the IOT after drying.



**Figure 2-1 – Dry Iron Ore Tailings**

Conventional IOT typically ranges 30–50% solids (Franks, et al., 2011). Because of the fluid rheology, tailings dams are the typical destination of this residue in Brazil (Ávila, 2012). Tailings dams are often built using the coarse fraction of the tailings themselves with steep slopes and successive heightening (Gomes, et al., 2016). However, with the progress of mining activities and the increase in the operation scale, these dams started to present structural risks (Ávila, 2012). Tailings dams failures occur due to inadequate application of methods, poorly prepared projects, bad supervision during construction or disregard of vital aspects in operational phases (Kossoff, et al., 2014).

As a result of the high volumes of production and poor management of residues, two major dam failures occurred in the state Minas Gerais in 2015 and 2019. These disasters led to the release of millions of cubic meters of IOT, several casualties, and an expressive impact in properties and on the ecosystems.

Despite the socio-environmental issues arising from the implementation of a mining facility, the mining industry responds to a significant portion of Brazilian economy. Therefore, it is imperative that companies develop cleaner and less risky production technologies and provide social services to the communities affected (Jenkins & Yakovleva, 2006). Some examples of improved waste management technologies are the thickening of the tailings, leaving the material in a more stable and inert form (Gomes, et al., 2016); deep-sea tailings placement and storage in empty mining pits.

Currently, there is no agreed policy by international institutions and industry associations to guide the sustainable management of tailings (Franks, et al., 2011). This lack of directives leaves the communities and the wildlife subjected only to corporate social responsibility and (often faulty, profit-driven) local regulations (Jenkins & Yakovleva, 2006).

Currently, policies are being established in Brazil to improve the monitoring of dams, reduce the production of tailings and encourage their reuse. In 2016, the Brazilian Federal Prosecution Service issued a recommendation that mining companies should incorporate at least 70% of their residues in other economic sectors until 2025 (Brazil, 2016).

In the civil construction sector, as examples, Carrasco, et al. (2017), Fontes, et al. (2016), Shettimma, et al. (2016), Zhao, et al. (2016), Ma, et al. (2016), and Yellishetty, et al. (2008) have successfully used IOT as aggregate for cement-based composites. Galvão, et al. (2018), Fontes, et al. (2018) and Pereira & Bernardin (2012) have proven the feasibility of the residue as colorant; and Defáveri, et al. (2019), Duan, et al. (2016), and Cheng, et al. (2016) as geopolymer and binder.

The fineness of IOT is one of its most important features. The study of Fontes et al. (2016), among others, showed that more than 50% of the material has particle size smaller than 75 $\mu$ m. Consequently, the particle size distribution of IOT is out of the Brazilian standard useable zone for concrete aggregates. This result affects several properties of cement-based composites both in fresh and hardened states.

Together with the fineness, the morphology of IOT is one of the main reasons why incorporating it into concretes and mortars increases the water demand and decreases workability (Carvalho, et al., 2019) (Zhao, et al., 2016). This might be attributed to the IOT's

high water absorption, angular surface area and fine texture. These same characteristics enhance the property of water retention in mortars with IOT (Fontes, et al., 2016).

On the other hand, the finer particles of IOT work as filler, refining and optimising the pore structure. As result, compressive strength, flexural strength, carbonation resistance and abrasion resistance are increased, as observed by de Carvalho et al. (2019), Sant'Ana Filho et al. (2017), Shettimma et al. (2016), among others; given that the w/c ratio required for a specific workability is not excessive.

In this sense, when applied to cement-based composites, most authors indicate an optimum content of IOT. This happens since the beneficial attributes of the IOT are sometimes surpassed by the harmful effects of the increased water requirement. The high water/binder ratio from mortars with high IOT content promotes cracking due to drying shrinkage (Fontes, et al., 2016). In the case of concretes, this characteristic reduces durability and compressive strength (Sant'Ana Filho, et al., 2017) (Shettima, et al., 2016) (Yellishetty, et al., 2008). On the other hand, when IOT is incorporated at optimum concentrations, it acts as filler, closing off the existing voids in the mortar, not compromising its plasticity and improving mechanical performance (Sant'Ana Filho, et al., 2017) (Fontes, et al., 2016). It is also worth mentioning that the deleterious effect caused by the IOT's fineness could potentially be diminished through the use of chemical admixtures. Not many studies were found in this subject.

Regarding chemical composition, it varies according to the origin of the iron ore and the processing method. Most researchers find iron (8-68%), aluminium (0.2-17%) and silicon (20-68%) oxides in varied proportions (Carvalho, et al., 2019) (Defáveri, et al., 2019) (Fontes, et al., 2018) (Duan, et al., 2016) (Fontes, et al., 2016) (Cheng, et al., 2016) (Yellishetty, et al., 2008). In minor contents (<3%), potassium, manganese, zinc and phosphorus oxides may also appear. The main crystalline phases usually found are quartz, gibbsite, hematite, goethite, dolomite and kaolinite (Carvalho, et al., 2019) (Defáveri, et al., 2019) (Fontes, et al., 2018) (Duan, et al., 2016) (Fontes, et al., 2016) (Cheng, et al., 2016) (Yellishetty, et al., 2008). This composition is responsible for the high unit weight of IOT, as all authors notice.

Finally, the leaching and dissolution analyses performed by Fontes, et al. (2016) and Bastos, et al. (2016) for the IOT confirm their environmental feasibility. For the leaching test, the IOT presented all results within the prescriptions of environmental standard NBR 10004 (ABNT, 2004a). Dissolution tests presented only aluminium, iron and phenols contents slightly above the standard limit. The samples were thus classified as Class II A,

non-dangerous and non-inert. Shettima, et al. (2016) found similar results. Therefore, the IOT does not present hazardous characteristics such as corrosivity, reactivity, toxicity, pathogenicity or flammability (ABNT, 2004a).

### 2.1.2 *Quartzite Mining Waste (QTZ)*

Quartzite is a metamorphic rock typically used for coating and decorating. Some examples of its use are floors, walls, tiles, tiles, parallelepipeds, benches, etc. The extraction of this material comprises three stages: soil mantle disintegration; removal of weathered / friable quartzite and dismantling of commercial quartzite (Santos, 2015). Depending on the amount of mica and degree of weathering of the deposit, the layer of friable and foliated quartzite may be larger or thinner. The disposal of this sterile layer is one of the main challenges of the industry (Ramirio, et al., 2008).

According to Ramirio, et al. (2008), who analysed quartzite mining companies in the state of Minas Gerais, Brazil, the amount of tailings generated can reach 92% of the extracted material in some situations. Only São Thomé das Letras, one of the cities with the largest mining activity, produced 400 thousand tons of commercial material in 2008, creating 900 thousand tons of waste (FEAM, 2009). Since the 1950s, it has been estimated that at least 26.7 million tons of shards, small blocks and quartzite sand have accumulated in the municipality (FEAM, 2009).

This mining waste builds up in the environment, leading to air and land pollution, increased cost of the final product, and even the closure of companies for environmental reasons (Faleiro & Lopes, 2010). Among the impacts caused by these high volumes of tailings, which are usually linked to inappropriate management, it is possible to mention siltation of rivers, dust generation and visual degradation (Faleiro & Lopes, 2010) (FEAM, 2009).

Figure 2-2 shows some examples of the poor management of residues in São Thomé das Letras.



**Figure 2-2 - Environmental impact related to quartzite extraction (FEAM, 2009)**

The quartzite is mainly composed by silicon (74-98%), aluminium (1.1-15.9%), potassium (0.2-26%), and sulphur (1.3-7.6%) oxides (Carvalho, et al., 2019) (Dias, et al., 2017) (Santos, 2015) (FEAM, 2009). Its main mineral constituent is the quartz ( $\text{SiO}_2$ ), but it may also present muscovite, kaolinite, biotite, and sericite (Carvalho, et al., 2019) (Dias, et al., 2017) (Santos, 2015).

Environmental analyses performed by Santos (2015) indicated classification II B - not dangerous and inert (ABNT, 2004a), the most benign configuration. Although results of leaching and solubilisation tests showed potassium and aluminium levels above the regulatory limits for some samples, the friable quartzite does not present contamination potential or hazardous characteristics. In other words, there is no difference, from an environmental point of view, between cement-based composites produced with the residue or conventional river sand.

Although its chemical composition is stable and close to the natural aggregates commonly used, the application of friable quartzite in civil construction is still little studied. As a few examples, we can cite the works of Ramirio, et al. (2008), who characterised the materials for civil construction purposes; Dias (2017) and Santos (2015) who used the fine fraction for high-technology mortars; Carvalho et al. (2019), who studied its packing efficiency for use as supplementary cementing material; and Adom-Asamoah et al. (2014) who studied the coarse fraction for concretes.

In all these cases, the technical feasibility of the tailings is observed after grinding or granulometric processing. This is necessary since, because of its friable nature, the quartzite has a high pulverulent content that may interfere with the properties of the resulting composites (Figure 2-3). Adom-Asamoah et al. (2014) also highlighted the weathering condition of the material, stating that little or partially weathered quartzites can reach

strengths similar to granite conventional aggregate. However, highly weathered aggregates failed to meet standard requirements regarding abrasion resistance, water absorption and crushing strength, and thus must not be employed without further study (Adom-Asamoah, et al., 2014).

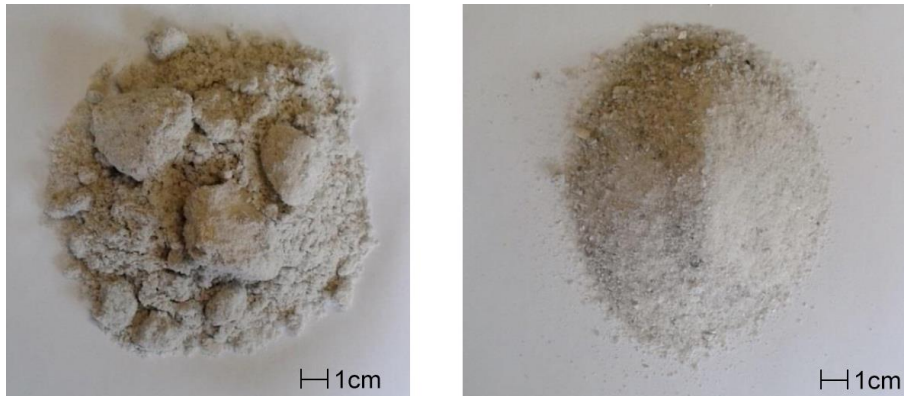


**Figure 2-3 – Friable quartzite *in natura* (left) and sieved for use as fine aggregate (right) (Santos, 2015)**

Therefore, the use of friable quartzite as aggregate in cement-based composites is feasible, provided that it is not highly weathered. Considering the physical, chemical, mineralogical and microstructural characteristics, as well as aspects related to durability and environmental contaminants, this is a waste with high employability potential.

### 2.1.3 Linear Alkyl Benzene Sodium Sulfonate (AEA)

Sodium dodecylbenzenesulfonate or linear alkyl benzene sodium sulfonate (LAS), shown in Figure 2-4, is a biodegradable surfactant present in typical washing-up (dishwashing) liquids. In a previous work, Mendes, et al. (2017) verified the technical feasibility of this substance as an air-entraining admixture (AEA) for cement-based composites.



**Figure 2-4 - Molecule of LAS**

According to Powers (1968), there are two main sources of entrained air in cement-based composites. The first is the infolding of the air into the matrix by vortex action, as in

stirring a liquid. In the second phenomenon, also called three-dimensional screen, air bubbles are formed by aggregates cascading upon themselves during mixing.

Due to the free surface energy, air voids in the fresh concrete are inherently unstable (Du & Folliard, 2005). Left unchecked, the air voids tend to coalesce (combine together), collapse, emerge to the surface, or diffuse into larger surrounding bubbles (Ramachandran, 1995). The function of the AEA is to stabilise the air bubbles or voids within the matrix. Thus, the addition of air-entrainment agents aims to promote a pore system of suitably sized and homogeneously distributed voids in the hardened concrete or mortar.

The mechanism of action of the surfactants in the AEA comprises two processes (Figure 2-5): the interaction in the air-water phase and in the solid-water phase. In the air-water phase, the polar groups are oriented towards the aqueous phase, reducing the surface tension, promoting the formation of bubbles and reducing the tendency of the already formed bubbles to dissolve (Lea, 1971). Simultaneously, in the solid-water interface, the polar groups adsorb to the cement, maintaining the nonpolar parts oriented towards the aqueous phase, converting the cement surface hydrophobic. This configuration reduces friction between the solid particles, improving the workability of the matrix, and allows the air to remain stably linked to the solid particles in the form of bubbles (Lea, 1971).

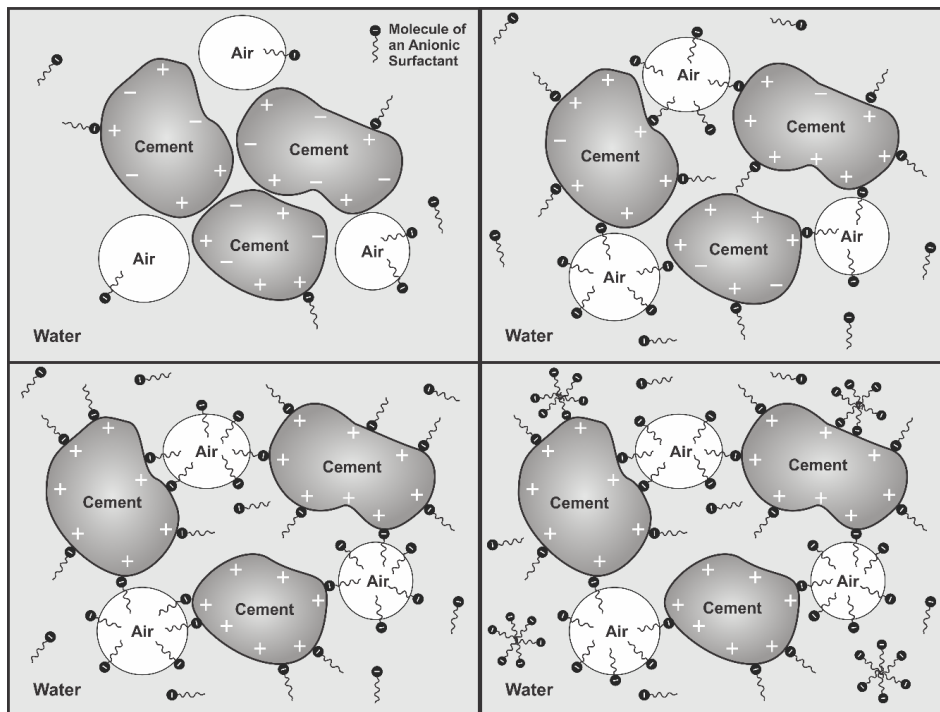


**Figure 2-5 - Mechanisms of Air-Entrainment from Anionic Surfactants (Mendes, et al., 2017).**

Pure water has a surface tension of approximately 76 mN /m, and at small surfactant contents, this value does not vary (Ouyang, et al., 2008). In this sense, a minimum dose of surfactants in the cement matrix is necessary to promote relevant effects, as Figure 2-6 shows. As the AEA is added, the surface tension is reduced, with the formation and maintenance of a stable foam system (Figure 2-7).

Above a certain critical concentration, however, the surfactant monomers are chemically prone to group as micelles, which do not contribute to reducing the surface tension (Lea, 1971). Even if more AEA is added to the matrix, the concentration of surfactant monomers will remain roughly constant and the concentration of micelles will increase (Ouyang, et al., 2008) (Du & Folliard, 2005). This is the reason why the workability and the entrained air content do not increase significantly after a certain dosage of surfactant.

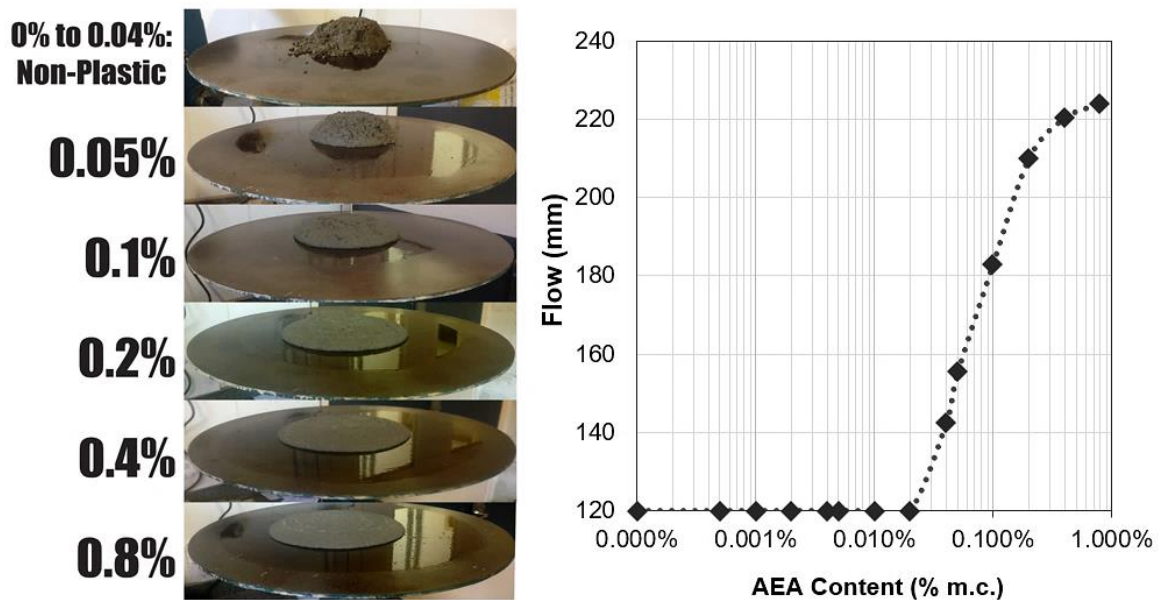


**Figure 2-6 - Flow test for reference mortar (0%), and mortars with LAS-based AEA (0.0005% to 0.8%) with the same water/cement ratio (Mendes, et al., 2017).**

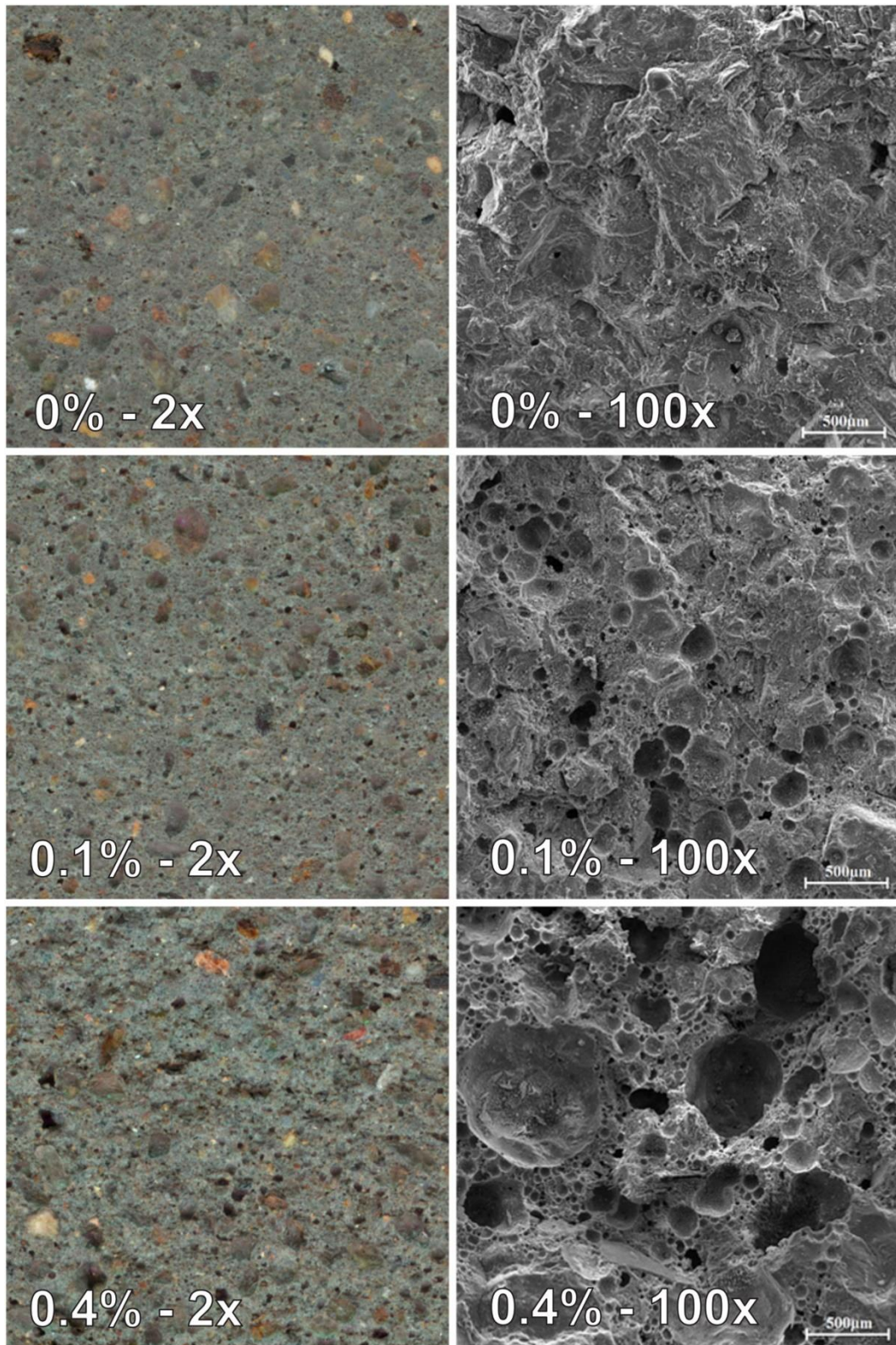


**Figure 2-7 – Microstructure of mortars (1:3) with LAS-based AEA (0%, 0.1% and 0.4%). Left column: Scanned sections, magnification 2x. Right column: Scanning Electron Microscopy, magnification 100x (Mendes, et al., 2017).**

As result, the homogeneously distributed microbubbles promoted by the AEA improve the cohesion and workability in the fresh state, as well as reduce the tendency of segregation and bleeding (Mendes, et al., 2019) (Mehta & Monteiro, 2014) (Ramachandran, 1995). In the hardened state, the AEA decreases the specific gravity of the composite, reduces water penetration by capillary action, and promotes no change on water absorption, up to a certain dosage (Mendes, et al., 2019) (Mendes, et al., 2017) (Ouyang, et al., 2008). However, the mechanical properties are strongly affected by the pore system generated (Mendes, et al., 2019) (Mendes, et al., 2017) (Ouyang, et al., 2008).

In summary, biodegradable washing up liquids based on LAS are effective air-entraining agents. They produce a stable foam system, which can improve the properties of cement-based composites if used within suitable contents.

## 2.2 HEAT TRANSFER

Heat transfer is the transport of energy that results from temperature difference. For a space occupied by living beings, this transport might be desirable or undesirable. In order to control the temperature inside a building, it is important to understand the mechanisms behind its gains and losses. If the temperatures on each end of a material become different, the specific heat and the thermal conductivity properties will largely determine how the temperature gradient will form within that material and how long it will take to level this difference (Hall, 2010).

### 2.2.1 *One-dimensional, steady-state thermal conduction*

Thermal conduction is the transfer of internal energy as heat, which occurs between neighbouring molecules of a solid, liquid or gas (and between different materials in close contact with each other), without the need for any bulk movement of the materials. From a fundamental perspective, “thermal conduction corresponds to the transfer of a particle’s vibrational energy to adjacent particles without any motion of the matter, mainly by collision” (Burger, et al., 2016).

The model currently accepted for heat transport comprises individual atoms vibrating about their lattice sites and occasionally pushing their neighbours into activity by their excess of energy (Ziman, 1960). This collective excitation in a periodic, elastic arrangement of atoms or molecules in condensed matter is called a phonon. Phonons bear the same relation to the vibrations of solid matter as photons do to the vibrations of the electromagnetic field (Ziman, 1960). Heat conductivity in non-metals is mainly due to them. In a simplified form, thermal conductivity through a crystalline material is explained by Burger, et al. (2016) and shown in Figure 2-8 as follows:

- a) Thermal energy is first transmitted to surface atoms of the sample. The surface atoms gain vibrational energy.
- b) Since the atoms are bound together by chemical bonds, the thermal energy of the surface atoms is then transferred to the adjacent atom(s), as in a wave.
- c) The thermal energy then diffuses in the sample, with a common vibrational mode (or a phonon) to the whole crystal.
- d) When heat reaches the opposite surface of the sample, it is then partially transferred by conduction, convection or radiation to the surroundings.

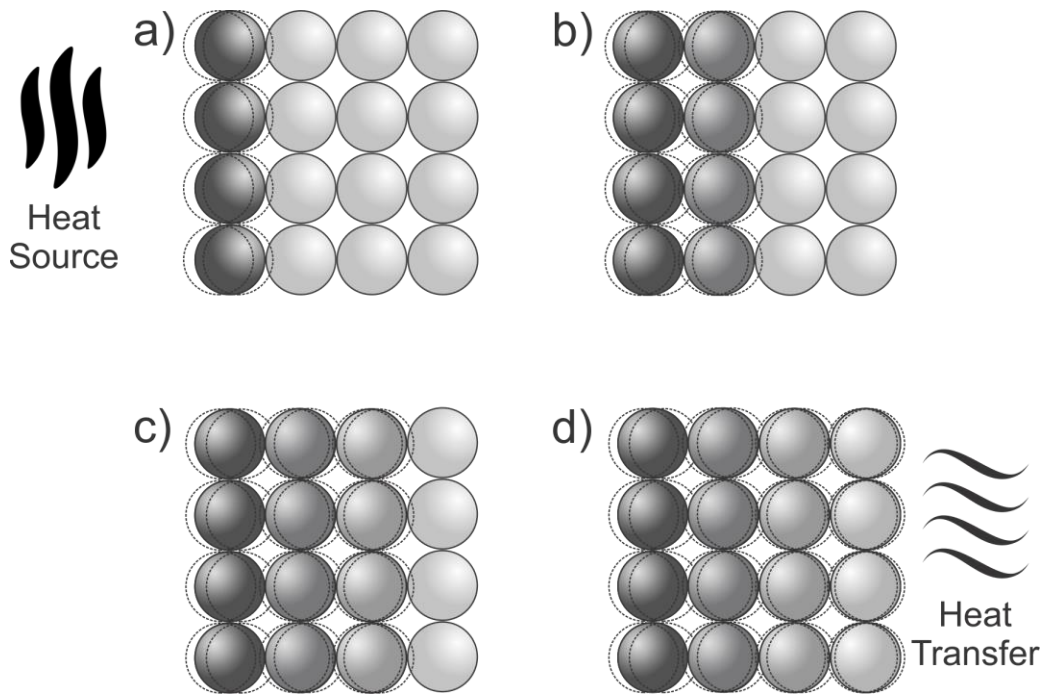


**Figure 2-8 - Thermal conductivity mechanism in a crystalline material  
(adapted from Burger, et al., 2016).**

The complexity of the mechanism of thermal conduction through solids arises from the many parameters to be considered. The material's nature is critical for thermal conductivity: plastics do not conduct heat as well as metals or crystalline non-metals. For example, polypropylene has an average thermal conductivity of  $0.11 \text{ W}/(\text{m}\cdot\text{K})$  (Han & Fina, 2011), while copper reaches  $400 \text{ W}/(\text{m}\cdot\text{K})$  (Burger, et al., 2016) and natural diamond can surpass  $2000 \text{ W}/(\text{m}\cdot\text{K})$  (Slack, 1964). The more rigid and sane the crystalline structure, the more quickly the initial vibration will be diffused to the opposite face. In solids with disordered structures, such as amorphous materials and conventional polymers, the chaotic vibrations and rotations of all the atoms around their equilibrium position reduce the efficiency of heat transfer (Burger, et al., 2016).

Also, defects in the crystal, such as dislocations or grain boundaries, negatively influence the thermal conductivity. These imperfections lead to phonon scattering – that is, phonons are reflected, diffracted or refracted, shortening the mean free path and hence reducing thermal conductivity (Burger, et al., 2016) (Ziman, 1960). Finally, size and shape also matter significantly, i.e. the thicker and sound the material, the more time for the heat to reach the opposite face. In this sense, thermal conductivity ( $\lambda$ ) can be defined as a measure of the ability of the material to conduct heat from a temperature difference.

It is possible to quantify the conduction heat transfer for a one-dimensional plane wall as Equation 2-1 (Incropera, 2007), also known as Fourier's Law. As heat flows from a location of higher temperature,  $T$  (in K), to one of lower temperature, the perpendicular heat flux  $q$  (W/m<sup>2</sup>) will be proportional to the thermal conductivity of the material. The minus sign reflects the condition of the heat being transferred in the direction of decreasing temperature.

$$q_x'' = -\lambda \frac{dT}{dx} \quad \text{Equation 2-1}$$

Under the steady-state conditions, where the temperature gradient is linear, this property relates the amount of heat ( $\Delta Q$ ) transmitted in time interval ( $\Delta t$ ) through a material of thickness  $L$ , in the normal direction to the section of area  $A$ , with the fixed temperature difference  $\Delta T$  imposed at the ends. Assuming that there are no sources of heat other than those maintained at the ends, the thermal conductivity can be determined by Equation 2-2 (Incropera, 2007):

$$\lambda = \frac{\Delta Q}{\Delta t} \cdot \frac{L}{A \cdot \Delta T} \quad \text{Equation 2-2}$$

In the International System of Units (SI) the thermal conductivity is measured in units of watt per meter kelvin [W/(m·K)]. The thermal conductivity of some materials may vary with temperature, more significantly at very low ones (i.e., below 200 K) (Cahill & Pohl, 1987) (Ziman, 1960). However, it is possible to obtain relatively accurate values for a given mean temperature (Çengel & Ghajar, 2012).

It is important to notice that this hypothesis of one-dimensional steady-state heat transfer for building materials is only an approximation. Modern building envelope systems have sometimes very complex internal structure. For example, occasionally a layer of insulating material is broken by highly conductive metal or concrete components – known as thermal bridge. In such situations, heat transfer can develop two or three-dimensional character (Kośny & Kossecka, 2002). Also, for structural components containing high thermal mass, one-dimensional analysis may generate errors in building loads estimation (Kośny & Kossecka, 2002). In this sense, it is important to evaluate the suitability of the prediction model for the studied material or structural system.

### 2.2.2 Thermal conductivity measurement

The use of materials with low thermal conductivity for the insulation of the building envelope is the most effective method of reducing the artificial cooling or heating load, thus reducing energy consumption (Pacheco, et al., 2012) (Sadineni, et al., 2011) (Lamberts, et al., 1997). There are several techniques for measuring thermal conductivity. The choice of method depends on the material or set of materials, the average system temperature, sample size, and destructive/non-destructive requirements. The methods also vary according to the desired accuracy.

The techniques are divided into steady-state and transient-state methodologies. In the first method, the heat transfer through a solid material is essentially controlled by the thermal conductivity, while the latter involves a combination of thermal conductivity and specific heat (Smith, et al., 2013). In general, steady-state techniques are used when the temperature of the material does not vary significantly with time. This hypothesis is adopted for most conventional building materials (Kośny & Kossecka, 2002), although the test usually takes a relatively long period of time (3-24h) to achieve steady-state heat transfer within the sample (Guimarães & Philippi, 1993). Transient state techniques perform measurements during the heating process. This method is more realistic when dealing with elements of massive dimensions and its main advantage is the measuring velocity (Guimarães & Philippi, 1993).

The basic procedure used in determining properties such as thermal conductivity is usually the design of a theoretical model from the heat diffusion equation, describing a thermal field in the investigated sample (Stancato, 2000). For the establishment of the thermal field, the first step is to apply a heat source to the sample. Subsequently, the location of the heat source is chosen, as well as the sensors and variables for measurement (Guimarães & Philippi, 1993). The desired properties are then obtained from the comparison between the experimental and theoretical data foreseen in the model.

For obtaining the thermal conductivity of refractory materials and/or by the transient method, the hot wire and the laser flash methods are the most used (Cha, et al., 2011) (NETZSCH, 2015). In these procedures, *in situ* measurements can be achieved with heat probe methods or adapted heat flow meters (Hall, 2010).

On the other hand, the thermal conductivity of insulation materials ( $\lambda < 2 \text{ W}/(\text{m}\cdot\text{K})$ ), like most cement-based composites, is usually determined with methods based on instrumentation of plates. Some examples are the Heat Flow Meter (HFM) and the Guarded Hot Plate (GHP) (Figure 2-9). In these methods, the specimen has usually the form of a

plaque with parallel surfaces, aiming to ensure that the heat transfer occurs primarily in one direction.

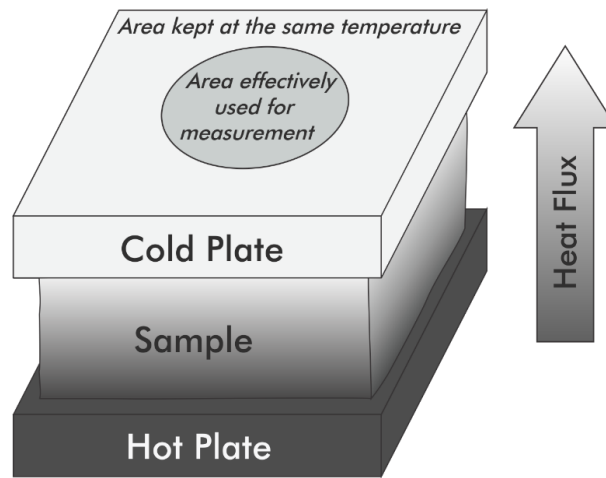


**Figure 2-9 - Principle of determination of the thermal conductivity by HFM**

The operating principle of HFM is based on the measurement of heat flowing in one direction through the sample. Thermocouples attached to the two equipment plates measure the temperature on each side of the sample. Also attached to the centre of the plates are heat flow sensors, which measure the flow through the plaque-shaped specimen. To ensure that the sensors will only measure the perpendicular heat flow, a strip of the plates around the measuring apparatus is also held in contact with the sample at the same temperature to avoid lateral heat transfer (Thermtest, 2015). Thus, the Equation 2-3 allows the calculation of the conductivity, where  $q$  is the heat flux ( $\text{W}/\text{m}^2$ ), measured by the sensors (NETZSCH, 2014). The greatest source of error in this method is the heat flow sensor itself - the calibration of the transducers is necessary and delicate (Guimarães & Philippi, 1993).

$$\lambda = \frac{q \cdot L}{\Delta T} \quad \text{Equation 2-3}$$

In the case of GHP, one-dimensional conduction is achieved using a guard ring that surrounds the hot plate at its same temperature. It seeks to restrict lateral heat losses and to mimic the thermal behaviour of an infinite plate. A temperature balance between the measuring section and the guard ring is achieved by controlling the ring power. According to NBR 15220 (ABNT, 2003), the power dissipated in the measurement section is used to determine the thermal properties of the sample.

It is noteworthy that these steady-state techniques consider the sample's thermal properties as isotropic. At the macroscopic scale, this hypothesis is verified if the composite's grains are randomly oriented in the matrix (Smith, et al., 2013).

All these measurement techniques determine the *effective* thermal conductivity. That is, the overall thermal conductivity of the material at a given temperature, including all its pores and phases, the interfacial thermal resistance generated by them and radiation effect (Stancato, 2000). The radiation component is why the effective thermal conductivity of some materials may vary with the mean test temperature, while the thermal conductivity of the solid phase remains approximately constant (Ziman, 1960). Most insulating materials, though, exhibit negligible radiation influence up to 100°C (Smith, et al., 2013), which keeps their effective thermal conductivity roughly invariable in this range.

Although highly accurate and relatively practical, HFM and GHP equipment are extremely expensive, reaching dozens of thousands of dollars. Thus, it is necessary to investigate alternatives for the determination of thermal properties, so that the development of new techniques and construction materials can proceed without limitations.

One of the currently available alternatives is the Lee Disc Apparatus (LDA) (Philip & Fagbenle, 2014), shown in Figure 2-10. The LDA consists of a cylindrical sample of material, of area  $A$  and height  $L$ , placed between two metal discs (usually bronze) of the same area, with thermocouples coupled to their centres (T1 and T2). Over the system is placed a cylindrical chamber of the same area, to where water vapour is constantly pumped. Moments after the steam is passed through the cylinder, the system 'vapour container – superior disc – sample – inferior disc – environment air' reaches the steady state. In this state, the heat conducted through the sample is equal to the heat loss of the inferior brass disc to the environment air.

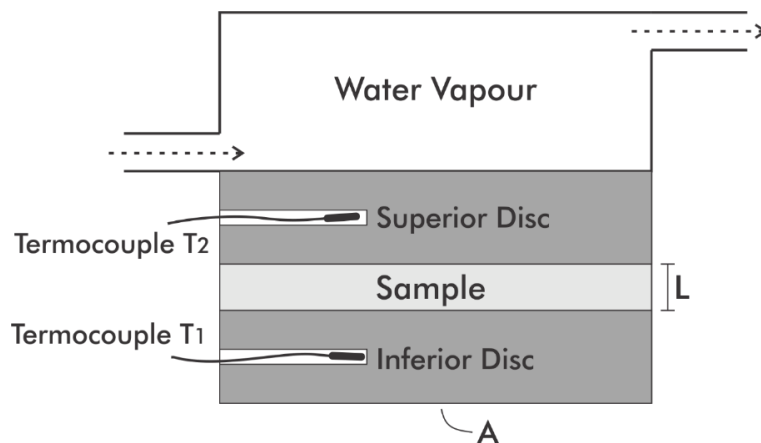


**Figure 2-10 - Schematic Figure of the Lee Disc Apparatus**

The heat conducted by the sample is given by Equation 2-4:

$$Q = \lambda \cdot A \cdot \frac{(T_2 - T_1)}{L} \quad \text{Equation 2-4}$$

At steady state, the heat conducted by the sample shall be equal to the rate of heat loss from the inferior disk to the environment air, by convection and radiation, at a measured time  $\Delta t$ . In this scenario, the rate of heat loss should be (Equation 2-5):

$$Q = m \cdot c \cdot \frac{\Delta T}{\Delta t} \quad \text{Equation 2-5}$$

Where  $\Delta T$  is the temperature difference between the inferior disc and the environment;  $m$  and  $c$  are the mass and the specific heat of the inferior disc, respectively.

Thus, the thermal conductivity is given by Equation 2-6:

$$\lambda = \frac{m \cdot c \cdot \Delta T / \Delta t}{A \cdot \frac{(T_2 - T_1)}{L}} \quad \text{Equation 2-6}$$

The LDA's limitations lie in avoiding lateral heat flow from the edges of the sample to the environment air and, in accurately measuring the rate of heat loss.

### 2.2.3 Specific Heat

The specific heat,  $c$  is the heat needed to raise the temperature of 1 kg of material by 1 K. It thus indicates a material's ability to absorb heat from the external surroundings. In the international system its unit is J/(kg·K), but it is commonly found as cal/(g·°C). The specific heat indicates how much the temperature ( $\Delta T$ ) of a certain mass of material ( $m$ ) will increase/decrease by the gain/loss of a certain amount of heat energy ( $Q$ ), not considering phase changes, as seen in Equation 2-7.

$$c = \frac{Q}{m \cdot \Delta T} \quad \text{Equation 2-7}$$

The specific heat of a substance "is governed by the manner in which the internal energy is distributed among its constituents" (Gopal, 1966). A first approximation to the energy of a system is the sum of the energies due to the various modes of motion. The molecules of a gas can have translational, rotational, vibrational, and electronic energy

levels, and each type of thermal motion contributes its share to the gas' specific heat (Pahuja, 2005) (Gopal, 1966).

The atoms in a non-metallic solid, however, are usually held fixed at their lattice sites and can at most vibrate about their mean positions (Gopal, 1966). In this sense, in most non-metallic solids, the dominant contribution to the specific heat is from phonon energy, i.e., the energy given to lattice vibrations (Pahuja, 2005). The lattice vibrations are in turn influenced by the molecular mass of the material, the crystalline structure, possible defects and, to some extent, the temperature and the changes in the matter caused by it (Callister Jr., 2001) (Gopal, 1966).

Water is a substance with relatively high specific heat - approximately 4181 J/(kg·K) at 20°C (also 4.217 J/(kg·K) at 0°C, 4.217 J/(kg·K) at 100°C, and 6.410 J/(kg·K) at 317°C), while the air is close to 1006 J/(kg·K) at 20°C (Incropera, 2007). When dealing with composite materials, the effective specific heat of a composite is not a simple weighted average of the specific heats of its constituents (Rosen & Hashin, 1970). Since the specific heat depends on molecular structure and chemical bonds, it will thus depend on the bonds created among the various phases of a composite (Xu & Chung, 1999).

#### 2.2.4 *Specific heat measurement*

One of the most used techniques to obtain the specific heat of a material is the Differential Scanning Calorimetry (DSC). To this end, the heat flow signal from the sample is compared to the signal of a standard material of known specific heat (usually sapphire) (O'Neill, 1966). Both curves are adjusted by a baseline correction experiment whereby an empty reference and empty sample crucible are placed in the furnace. In all cases, the heat flow must be measured under identical experimental conditions and temperature setup (ASTM International, 2018).

The ASTM E1269 (ASTM International, 2018) standardises this procedure in three measurements (with a linear and identical heating rate for each step, 20 °C/min recommended), summarised as follows and illustrated in Figure 2-11:

1. Sample crucible is empty for zero-line (baseline) determination ( $\phi_0$ );
2. Sample crucible contains sapphire calibration standard ( $m_{\text{standard}}, \phi_{\text{standard}}$ );
3. Sample crucible contains the sample to be measured ( $m_{\text{sample}}, \phi_{\text{sample}}$ ).

The specific heat of the sample is then calculated as follows:

$$c_{sample} = \frac{m_{standard}}{m_{sample}} \times \frac{\varphi_{sample} - \varphi_0}{\varphi_{standard} - \varphi_0} \times c_{standard} \quad \text{Equation 2-8}$$

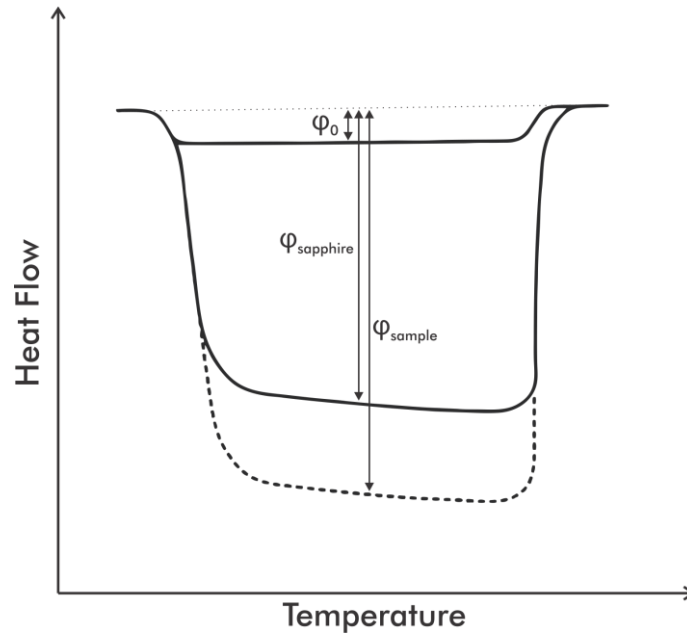


**Figure 2-11 – Scheme of calculation of specific heat via DSC: heat flow curves for empty crucible (baseline,  $\varphi_0$ ), sapphire calibration standard ( $\varphi_{sapphire}$ ) and studied sample ( $\varphi_{sample}$ )**

Despite its wide employability and accuracy, the DSC method has some limitations:

- It is a time-demanding test that requires expensive equipment.
- This method assumes that identical instrument settings and conditions are used for each experimental step (McHugh, et al., 2010).
- It also assumes that the same empty reference crucible is used for all steps and not removed from the DSC furnace (McHugh, et al., 2010).
- Only milligrams of the material are used, therefore, it must be homogeneous and representative (ASTM International, 2018).
- The occurrence of chemical changes, phase changes or mass loss during the measurement may invalidate the test (ASTM International, 2018). Therefore, the temperature range and specimen holders should be chosen to avoid these processes.

- If a specimen is heated to decomposition, toxic products may be released (ASTM International, 2018).

The specific heat can also be measured by means of an adiabatic calorimeter, as shown in Figure 2-12. In this calorimeter, the specific heat is obtained according to the equilibrium temperature between a medium (usually water) and a sample, which must necessarily present a predefined temperature difference at the beginning of the test.

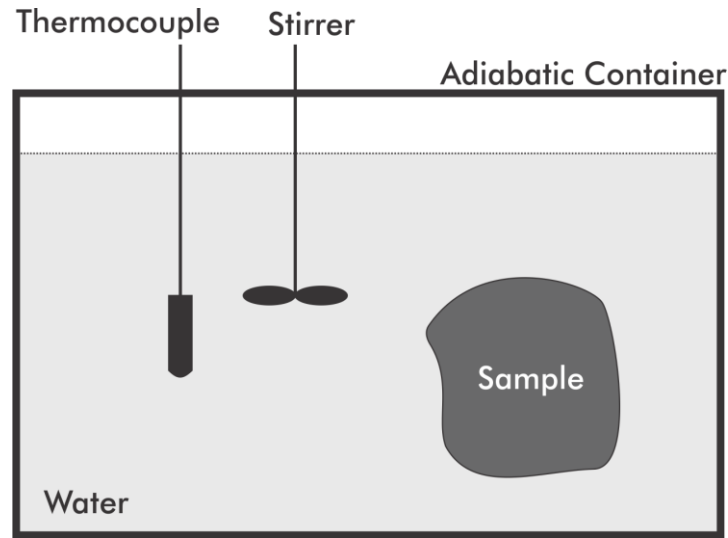


**Figure 2-12 – Scheme of an adiabatic calorimeter**

Assuming the calorimeter as an isolated system, calling  $Q$  the amount of heat transferred from the sample to the water (or vice-versa), we have that all the heat supplied inside the system is absorbed within the system:

$$Q_{\text{supplied by sample}} = Q_{\text{absorbed by water}} \quad \text{Equation 2-9}$$

$$(m c \Delta t)_{\text{sample}} = (m c \Delta t)_{\text{water}} \quad \text{Equation 2-10}$$

$$m_{\text{sample}} c_{\text{sample}} (t_f - t_{0,\text{sample}}) = m_{\text{water}} c_{\text{water}} (t_f - t_{0,\text{water}}) \quad \text{Equation 2-11}$$

The mass of the water ( $m_{\text{water}}$ ) and the sample ( $m_{\text{sample}}$ ) are known (weighed in a precision scale); as well as the initial temperature of the sample ( $t_{0,\text{sample}}$ ) and the water ( $t_{0,\text{water}}$ ), which are established by the user. The sample is then immersed in the water, which is stirred to ensure a homogeneous distribution of temperature. Within a few minutes (or hours, depending on the settings of the test), the equilibrium temperature between both

constituents will be measured with a thermocouple ( $t_f$ ). Therefore, we can isolate the specific heat of the sample ( $c_{sample}$ ) as a function of these settings and the specific heat of the water at the equilibrium temperature ( $c_{water}$ ), as shown by Equation 2-12.

$$c_{sample} = \frac{m_{water} c_{water} (t_f - t_{0,water})}{m_{sample} (t_{0,sample} - t_f)} \quad \text{Equation 2-12}$$

This method has several advantages, such as the low cost of the equipment, the speed of measurement, and, mainly, the possibility to use a macroscopic integer sample, evaluating a representative specimen with its original structure unaltered. It is thus recommended when dealing with heterogeneous or composite materials. On the other hand, some limitations of the method are:

- The assumption that the calorimeter is perfectly adiabatic;
- The assumption that the sample and the water will each be at a perfect homogeneous temperature at all times.
- The assumption that the specific heats of both sample and water are constant throughout the test, since it is known that this property varies slightly with temperature.
- The temperature range of measurement is limited to the medium's boiling point.
- The influence from the absorption of medium (water) through the sample's permeable pores during the test is not considered.

### 2.2.5 Other thermal properties

When considering the different materials that form the building envelope, the thermal conductivity alone is not enough to represent its thermal insulation. In order to evaluate the amount of energy required to increase in 1 K the temperature of a whole system, we calculate its thermal capacity (or heat capacity),  $C$ , by Equation 2-13 (ABNT, 2003); where  $m$  is the mass of the material and  $c$  its specific heat.

$$C = m \cdot c \quad \text{Equation 2-13}$$

In the case of more than one material, the equivalent thermal capacity of the system,  $C_T$ , can be determined by Equation 2-14 (ABNT, 2003), where  $d_i$ ,  $c_i$  and  $\rho_i$  are, respectively, the thickness, specific heat and specific gravity of material  $i$ .

$$C_T = \sum_{i=1}^n d_i \cdot c_i \cdot \rho_i \quad \text{Equation 2-14}$$

Therefore, while the specific heat ( $c$ ) is a constant property of a material (assumed homogeneous and isotropic), regardless of size or dimension, the heat capacity ( $C$ ) varies with the mass of this material.

An analogous correspondence is observed between the thermal conductivity ( $\lambda$ ) and the thermal resistance ( $R_T$ ) of a material. While the first is invariable for a given material, regardless of size or dimension, the second depends on the thickness of the material. For example, a 10-cm granite wall and a 1-m granite wall will have the same thermal conductivity (assuming the granite homogeneous and isotropic), but significantly different thermal resistances.

One property vastly used in building fabrics is the overall thermal transmission,  $U$  (hence the term “U-value” - W/(m<sup>2</sup>·K)).  $U$  is the inverse of  $R_T$  (also known as “R-value” – (m<sup>2</sup>·K)/W). The  $U$  and the  $R_T$  are obtained from the known thickness ( $d$ ) and thermal conductivity ( $\lambda$ ) of an element, as per Equation 2-15 and Equation 2-15 (Hall, 2010).

$$U = \frac{\lambda}{d} \quad \text{Equation 2-15}$$

$$R_T = \frac{d}{\lambda} \quad \text{Equation 2-16}$$

The thermal resistances are commutative. For example, in the case of a masonry wall, Equation 2-17 (Hall, 2010) applies to its various layers. If various materials (1, 2, ..., n) are positioned perpendicular to the heat flux, Equation 2-18 is used. Both cases are analogous to electrical resistances in series and parallel, respectively.

$$R_T = R_{\text{coating mortar}} + R_{\text{brick}} + R_{\text{coating mortar}} \quad \text{Equation 2-17}$$

$$R_T = \frac{A_1 + A_2 + \dots + A_n}{\frac{A_1}{R_1} + \frac{A_2}{R_2} + \dots + \frac{A_n}{R_n}} \quad \text{Equation 2-18}$$

U-values can be measured *in situ* through portable heat flux sensors and thermocouples, adapted probes, infrared sensors, among others. One advantage of this measurement is that the materials that compose the fabric do not necessarily need to be known. Another one is the realism of the value obtained. The actual U-values of building fabrics are often found to be higher than estimated through the equations above (Dowson, et al., 2012) (Hall, 2010). This is usually due to errors in the quality of construction, thermal bridges, deterioration, weathering and moisture accumulation (Dowson, et al., 2012) (Hall, 2010) (Olivier, 2001).

Other significant thermal properties of construction materials are:

- Reflectance, Transmittance and Absorptance, which are, respectively, the capacity of a material to reflect, transmit and absorb radiant energy from incident solar radiation. For example, an opaque material would have zero transmittance; all the incoming radiation would then be divided in reflected and absorbed energy. Those, in turn, would be determined by the material's colour and surface properties and the radiation wavelength.
- Emissivity, the effectiveness of a material in emitting energy as thermal radiation;
- Thermal diffusivity,  $\alpha$ , which correlates other thermal properties in order to evaluate the rate of heat transfer within a material from the hot side to the cold side (Equation 2-19). It is considered the "thermal inertia" of a material. Some equipment, such as the hot wire and laser flash methods, measure the thermal diffusivity of a sample and subsequently obtain its thermal conductivity or specific heat through a back calculation.

$$\alpha = \frac{\lambda}{\rho \cdot c} \quad \text{Equation 2-19}$$

## 2.3 THERMAL PERFORMANCE OF BUILDINGS

A sustainable building is much more than a construction with isolated measures for water reuse or solar energy generation. This concept encompasses not only energy and water, but also land and material conservation, environmental pollution and the quality of indoor and outdoor environments. This section focuses on the aspects of thermal performance and energy savings related to it.

### 2.3.1 Heat transfer in cement-based composites

An analysis of heat transfer through building elements is of great importance in civil engineering problems such as energy-efficient design, planning for thermal comfort, avoiding thermal bridges, thermal load of structures due to daily variations of temperature, among others. According to Smith (2013), “the heat transfer through a solid material is essentially controlled by its thermal conductivity in the steady state, and by a combination of thermal conductivity and specific heat capacity in transient situations”.

When a porous ceramic is subjected to a thermal gradient, heat transfer involves: (a) vibrational conduction in the solid phase; (b) conduction by the fluid in the pore phase; (c) natural convection through fluid in the pores; and (d) radiation either through a semi-transparent solid phase or across the fluid in the pores (Smith, et al., 2013) (Hall, 2010). For cement-based composites, the solid phase is the cement paste and the aggregates, and the fluid in the pores is usually air, a mixture of air and water, or water. When water is included, the fluid’s thermal conductivity can vary significantly, and the heat balance may also include the latent form due to condensation (Hall, 2010).

A well-compacted concrete has total porosity in the order of 10-15% at a mature age (Aligizaki, 2005). The pores in cement-based composites are usually classified in gel pores, capillary pores and macropores (Kumar & Bhattacharjee, 2003) (Mehta & Monteiro, 2014). The gel pores (1-100 nm) are those formed within the cement hydration products (Aligizaki, 2005). The capillary pores or channels (2 nm - 10  $\mu\text{m}$ ) result from the consumption or evaporation of the free water in the matrix, while macropores (> 10  $\mu\text{m}$ ) are the air voids entrapped or entrained in the matrix (Aligizaki, 2005). The voids are said *entrapped* when occur unintentionally during the mixing or pouring; and *entrained* when they are purposefully added, for example, through air-entraining agents (Aligizaki, 2005).

Since the thermal conductivity of gases is relatively small ( $\lambda < 0.1 \text{ W}/(\text{m}\cdot\text{K})$ ), it would be expected that the overall thermal conductivity of a dry porous composite should decrease continually with decreasing bulk density, finally approaching the conductivity of

the gas filling the pores. This is not the case of some lightweight insulators (e.g. fibreglass, glass wool, extruded polystyrene foam), which possess a relatively large number of interconnected voids – usually more than 95% of their volume is occupied by gas (Hall, 2010) (Larkin & Churchill, 1959). In these materials, the effective thermal conductivity is observed first to decrease and then to increase with decreasing bulk density (Larkin & Churchill, 1959). This fact suggests that convection heat transfer must be contributing to this phenomenon, reducing the efficiency of these insulators (Akutstu & Sato, 1988) (Larkin & Churchill, 1959). However, for matrices with low total porosity and pore sizes less than 5 mm, which usually correspond to cement-based composites, convection heat transfer can be neglected (Schulle & Schlegel, 1991).

Regarding radiation heat transfer, radiant transfer through a porous lightweight insulator occurs by direct transmission through the voids - by scattering, absorption and reradiation (Larkin & Churchill, 1959). Radiation contributes 5-20% of the total heat transfer through lightweight insulations (Larkin & Churchill, 1959), which are typically in the range of 0.03-0.05 W/(m·K) (ABNT, 2003). In other words, radiation through a material mainly comprised by gas contributes to only 0.01 W/(m·K) for temperatures over 200°C (Larkin & Churchill, 1959).

In a low-porosity composite, however, the radiation heat transfer from gases is generally masked by the conduction heat transfer from the solids (Kaviani, 2012). Additionally, in general, no radiation heat transfer is considered in dealing with fully or partially saturated matrices, since liquids are highly absorbing in the IR wavelength range (Kaviani, 2012).

Therefore, the radiation component at cement-based composites can be neglected, just as the convection component, since these composites are characterised by a relatively low porosity and employability at temperatures below 100°C. As result, these materials exhibit negligible variations in effective thermal conductivity from 0 to 1000°C (Smith, et al., 2013). In summary, heat transfer through conduction is the main phenomenon occurring in cement-based composites at ambient temperature, as also mentioned by Asadi et al. (2018).

### 2.3.2 *Thermal Properties of cement-based composites*

The thermal properties of cement-based composites are influenced by several factors: composition and quantity of aggregates, distribution, geometry and pore size, moisture

content, age, w/c ratio, types of admixtures, among others (Khan, 2002). Among these, Kim et al. (2003), in a comprehensive study, observed that aggregate volume fraction and moisture condition of specimen were the main factors affecting these properties, confirmed by Asadi et al. (2018).

The thermal conductivity of a cement-based composite increases with higher saturation conditions, higher aggregate volume ratio and lower w/c ratio. This is reported by Khan (2002), Siwinska & Garbalinska (2011), among others, who also indicate porosity as a significant factor. On the other hand, temperature and age were the least influencers, except for very early age (Kim, et al., 2003). Li, et al. (2016) also noticed that the composites' thermal conductivity tends to stabilise after 20 days of curing. The authors verified that, at 20 days, the phases of aluminate, ferrite and alite within cement have practically completed their hydration, taking the places originally occupied by the mix water (Li, et al., 2016).

The thermal conductivity of the cement paste varies depending on the type of cement and w/c ratio. Most authors report values around 0.5 – 0.6 W/(m·K) (Kim, et al., 2003) (Yunsheng & Chung, 2000) (Fu & Chung, 1997). The cement-based composites employed in conventional construction purposes are considered isotropic in relation to thermal properties.

Regarding air content, the thermal conductivity of construction materials is in the inverse proportion to the porosity ratio and, consequently, is inversely related to the apparent specific mass (Akutstu & Sato, 1988). This trend is due to the relatively low thermal conduction of the air – 0.025 W/(m·K) at room temperature and free of convection (ABNT, 2003) – and to the interfaces promoted by the pores. According to Smith, et al. (2013), the thermal conductivity of a porous ceramic depends on: (i) the intrinsic thermal conductivity of the solid phase and (ii) the thermal resistance due to phonon scattering at the interfaces (boundaries). In this sense, the type of material at the solid phase and the pore characteristics are thus key factors to the resulting thermal conductivity of composites. That is why the sizes and volume distribution, orientation, and interconnection of pores are relevant to the final thermal conductivity of the matrix (Smith, et al., 2013) (Francl & Kingery, 1954).

Conversely, the thermal conductivity of cement-based composites tends to increase with the increase in moisture content (Siwinska & Garbalinska, 2011) (Khan, 2002) (Kim, et al., 2003). Siwinska & Garbalinska (2011) observed a 63% increase of the thermal conductivity of mortars with cement and sand (1:3.1, in mass), when the moisture content was altered from 0% to 100%. An 85% increase was observed for mortars with cement, lime and sand (1:1:6, in mass) at the same conditions (Siwinska & Garbalinska, 2011). This result

is due to the relatively high thermal conductivity of water: 0.57-0.63 W/(m·K) at 0-40°C, respectively (Kim, et al., 2003). Furthermore, in saturated materials, the water occupies part of the air filling the pores. Thus, the more porous the matrix' and aggregates' structure, more water will be absorbed, resulting in a greater increase of thermal conductivity (Khan, 2002).

In turn, the conductivity of the aggregates is determined by their microstructure and chemical and mineralogical composition (Horai & Simmons, 1969). According to Khan (2002) and Akutsu & Sato (1988) the aggregates of crystalline structure with interconnected pores conduct more heat than aggregates of vitreous structure, with pores in discrete distribution.

The thermal conductivity of rocks commonly used as aggregates typically ranges from 1 to 9 W/(m·K) (Khan, 2002) (Horai & Simmons, 1969). According to Brigaud & Vasseur (1989) and Horai & Simmon (1969), the mineral quartz has thermal conductivity of 7.7 W/(m·K); hematite, 11.3 W/(m·K); calcite, 3.6 W/(m·K); gibbsite, 6.2 W/(m·K); and kaolinite, 2.6 W/(m·K). The specific heats of some of the minerals observed in the aggregates are: quartz, 740 J/(kg·K); kaolinite, 974 J/(kg·K); gibbsite, 1180 J/(kg·K); orthoclase, 628 J/(kg·K); phlogopite, 780 J/(kg·K); muscovite, 760 J/(kg·K); hematite, 620 J/(kg·K); calcite, 815 J/(kg·K); and wuestite, 730 J/(kg·K) (Waples & Waples, 2004).

Therefore, except for lightweight aggregates, the cement paste usually has a lower thermal conductivity than the aggregate. That is, conventional mixes with higher aggregate volume tend to present higher conductivity; in case of lightweight aggregates, the opposite holds (Asadi, et al., 2018) (Fu & Chung, 1997).

The Brazilian thermal performance standard, NBR 15520 (ABNT, 2003) presents indicative values for ordinary cement-based construction materials. Table 2-1 shows these values, which are commonly used for building simulation purposes. The standard also specifies that whenever possible, laboratory values should be used.

While low thermal conductivity is desired to improve insulation in buildings, high thermal conductivity is useful for reducing temperature gradients in structures. In massive structures subjected to large thermal gradients, such as bridges, the thermal stresses may cause mechanical degradation and even warpage in the structure (Xu & Chung, 2000a). Contrary to buildings, bridges and dams do not need thermal insulation and benefit from materials with high thermal conductivity.

**Table 2-1 - Indicative Values for Thermal Properties of some cement-based composites (ABNT, 2003).**

<b>Material</b>	<b>Density (kg/m<sup>3</sup>)</b>	<b><math>\lambda</math> (W/(m·K))</b>	<b>c (J/(kg·K))</b>
Conventional mortar	1800-2100	1.15	1000
Gypsum (or gypsum + lime) mortar	1200	0.70	840
Cellular mortar	600-1000	0.40	1000
Conventional concrete	2200-2400	1.75	1000
Lightweight concrete with expanded clay (cement content > 300 kg/m <sup>3</sup> ; density of aggregates > 350 kg/m <sup>3</sup> )	1600-1800	1.05	1000
	1400-1600	0.85	
	1200-1400	0.70	
	1000-1200	0.46	
Lightweight concrete with expanded clay (cement content > 300 kg/m <sup>3</sup> ; density of aggregates < 350 kg/m <sup>3</sup> )	800-1000	0.33	1000
	600-800	0.25	
	< 600	0.20	
Autoclaved aerated / cellular concrete	400-500	0.17	1000
Cement boards	1800-2200	0.95	840
	1400-1800	0.65	

Regarding specific heat, this property is influenced by the composition and mix proportions of raw materials, the porosity and pore system of the matrix and aggregates, the saturation condition, and the presence of mineral and chemical admixtures. The admixtures contribute to the interface bonding between the materials and thus reduce the defects that would otherwise interfere with the lattice vibrations (Xu & Chung, 1999) (Fu & Chung, 1997).

Incropera (2007) presents generic values of specific heat for concretes and mortars as 880 and 780 J/(kg·K), respectively (slightly lower than Brazilian Standards). Fu & Chung (1997) and Xu & Chung (1999), obtained 0.703-0.736 J/(kg·K) for cement pastes (0.45 and 0.35 w/c ratio, respectively); and reported 0.642 J/(kg·K) for a cement:sand mortar (1:1 in mass, 0.35 w/c ratio), all with DSC method. According to a review by Waples & Waples (2004), most minerals in construction aggregates have specific heats in the range from 600 to 900 J/(kg·K).

A high value of specific heat means a high ability for retaining heat — an ability that is desirable for energy conservation in buildings. Therefore, construction materials with high specific heat would leave the building less exposed to the variation of the external temperature (Xu & Chung, 2000a). On the other hand, in tropical regions, a reduced specific heat prevents overheating during the night (Lamberts, et al., 1997) and is thus beneficial to

the overall thermal performance of the building. Additionally, thermal energy storage through building materials is a line of research that has gain massive attention in the past few years. Researchers engineer materials with high specific heat or latent heat (e.g. phase change materials) to improve energy conservation, management and utilization.

In summary, due to their composite nature and wide variety of constituents, cement-based composites can present a wide range of thermal properties. Some of these are summarised in Table 2-2. This table highlights the several methods available to evaluate thermal conductivity, the range of values for conventional cement-based composites, and the fact that most authors focus on the effect of the addition of mineral admixtures and fibres.

It is observed that few articles address the use of residues as aggregates (Ledhem, et al., 2000) (Khan, 2002) (Marie, 2017). It is also noticed that mortars for coating (plastering), one of the most widely used types, are seldom studied (Siwinska & Garbalinska, 2011). In this sense, many different approaches can be undertaken to further enhance the desired thermal performance of cement-based composites.

**Table 2-2 – Literature review of thermal conductivity of cement-based composites**

<b>Ref.</b>	<b>Material</b>	<b>Thermal Cond. W/(m·K)</b>	<b>Method</b>
(Xu & Chung, 2000a)	Cement paste w/c ratio 0.35	0.52	Correlation among the thermal diffusivity (laser flash method), specific heat (Differential Scanning Calorimeter), and density
	Cement paste w/c ratio 0.35 + silica fume 15% in addition (by mass of cement)	0.403	
	Cement paste w/c ratio 0.35 + silica fume 15% in addition (by mass of cement) + silane 0.2% to 2% in addition (by mass of cement)	0.613-0.719	
(Fu & Chung, 1997)	Cement paste w/c ratio 0.45	0.52	Correlation among the thermal diffusivity (laser flash method), specific heat (Differential Scanning Calorimeter), and density
	Cement paste w/c ratio 0.23 + latex 20% to 30% in addition (by mass of cement)	0.38-0.28	
	Cement paste w/c ratio 0.32 + methylcellulose 0.4% to 0.8% in addition (by mass of cement)	0.42-0.32	
	Cement paste w/c ratio 0.35 + silica fume 15% in addition (by mass of cement) + methylcellulose 0.4% in addition (by mass of cement)	0.33	
	Cement paste w/c ratio 0.35 + methylcellulose 0.4% in addition (by mass of cement) + carbon fibres 0.5% to 1% in addition (by mass of cement)	0.44-0.34	
	Cement paste w/c ratio 0.35 + silica fume 15% in addition (by mass of cement) + methylcellulose 0.4% in addition (by mass of cement) + carbon fibres 0.5% in addition (by mass of cement)	0.28	
(Kim, et al., 2003)	Cement (type V) paste w/c ratio 0.25 to 0.4 (dry condition, 20°C)	0.84 – 0.66	Probe method
	Fly ash paste w/c ratio 0.57	0.86	
	Cement (type V) + Fly ash paste (50%/50%) w/c ratio 0.47	0.92	
	Blast furnace slag paste w/c ratio 0.47	0.77	
	Cement (type V) + Blast furnace slag (50%/50%) w/c ratio 0.42	0.87	
	Cement (type I) paste w/c ratio 0.4	0.99	
	Concretes with aggregate volume ratio from 0.21 to 0.70 (dry condition, 20°C)	0.86 - 1.69	
	Concretes with aggregate volume ratio from 0.21 to 0.70 (wet condition, 20°C)	1.20 – 2.12	

<b>Ref.</b>	<b>Material</b>	<b>Thermal Cond. W/(m·K)</b>	<b>Method</b>
(Xu & Chung, 2000b)	Cement paste w/c ratio 0.35	0.53	Correlation among the thermal diffusivity (laser flash method), specific heat (Differential Scanning Calorimeter), and density
	Cement paste w/c ratio 0.35 + silica fume 15% in addition (by mass of cement)	0.33	
	Mortar 1:1 (cement:sand)	0.58	
	Mortar 1:1 (cement:sand) + silica fume 15% in addition (by mass of cement)	0.54	
(Khedari, et al., 2001)	Mortar 1:2.75 (cement:sand)	1.6452	Hot Wire Method
	Mortar 1:1 (cement:sand) + Young coconut fibres 10% to 30% in addition (by mass of cement)	0.9333-0.1753	
	Mortar 1:1 (cement:sand) + Durian fibres 10% to 40% in addition (by mass of cement)	0.7961-0.1751	
(Corinaldesi, et al., 2011)	Mortar 1:3 (cement:sand)	0.739	Guarded Hot Plate
	Mortar 1:3 (cement:sand) + Polyurethane residue 10% and 30% in addition (by mass of sand)	0.648 and 0.598	
	Mortar 1:3 (cement:sand) + Polyurethane residue 10% in addition (by mass of sand)+ limestone powder 20% in addition (by mass of cement)	0.717	
(Demirboga, 2003)	Mortar 1:2 (cement:sand)	1,186	Hot Wire Method
	Mortar 1:2 (cement:sand) + silica fume 10% to 30% in replacement of cement (by mass)	0.972-0.715	
	Mortar 1:2 (cement:sand) + fly ash class C 10% to 30% in replacement of cement (by mass)	1.016-0.792	
	Mortar 1:2 (cement:sand) + blast furnace slag 10% to 30% in replacement of cement (by mass)	1.034-1.017	

<b>Ref.</b>	<b>Material</b>	<b>Thermal Cond. W/(m·K)</b>	<b>Method</b>
(Raheem & Adesanya, 2011)	Mortar 1:1 (cement:sand)	2.40	Non-standard steady state heating method involving the use of three brass blocks
	Mortar 1:1 (cement:sand) + corn cob ash 2% to 25% in replacement of cement (by mass)	2.40-0.69	
	Mortar 1:2 (cement:sand)	1.60	
	Mortar 1:2 (cement:sand) + corn cob ash 2% to 25% in replacement of cement (by mass)	1.60-0.63	
	Mortar 1:3 (cement:sand)	1.20	
	Mortar 1:3 (cement:sand) + corn cob ash 2% to 25% in replacement of cement (by mass)	1.20-0.51	
(Benmansour, et al., 2014)	Mortar approximately 1:0.37 (cement:sand) + date palm fibres (3 mm diameter) 5% to 15% in addition	0.39-0.14	Hot Wire Method
	Mortar approximately 1:0.37 (cement:sand) + date palm fibres (6 mm diameter) 5% to 15% in addition	0.63-0.22	
	Mortar approximately 1:0.37 (cement:sand) + date palm fibres (50% 3 mm / 50% 6 mm diameter) 5% to 15% in addition	0.39-0.14	
(Ledhem, et al., 2000)	cement + clay-like material from quarry waste (clay/cement ratio at 0.6)	0.67	Probe method
	cement + clay-like material from quarry waste (clay/cement ratio at 0.6) + wood shavings 9% to 29% (by mass percentage of the total dry mixture)	0.34 – 0.11	
(Khan, 2002)	Mortar 1:2.33 (cement: reddish land quarried quartz sand) – dry condition / saturated condition	1.9/2.65	Hot Wire Method
	Mortar 1:2.33 (cement: greyish river sand) – dry condition / saturated condition	1.37/1.95	
	Concrete 1:2.33:4.66 (cement : reddish land quarried quartz sand : basalt coarse aggregate) – dry condition / saturated condition	2.26/3.52	
	Concrete 1:2.33:4.66 (cement : greyish river sand : basalt coarse aggregate) – dry condition / saturated condition	1.97/3.24	

<b>Ref.</b>	<b>Material</b>	<b>Thermal Cond. W/(m·K)</b>	<b>Method</b>
	Concrete 1:2.33:4.66 (cement : reddish land quarried quartz sand : limestone coarse aggregate) – dry condition / saturated condition	2.03/2.92	
	Concrete 1:2.33:4.66 (cement : greyish river sand : limestone coarse aggregate) – dry condition / saturated condition	1.6/2.71	
	Concrete 1:2.33:4.66 (cement : reddish land quarried quartz sand : siltstone coarse aggregate) – dry condition / saturated condition	2.21/3.61	
	Concrete 1:2.33:4.66 (cement : greyish river sand : siltstone coarse aggregate) – dry condition / saturated condition	1.91/2.9	
	Concrete 1:2.33:4.66 (cement : reddish land quarried quartz sand : quartzite coarse aggregate) – dry condition / saturated condition	2.77/4.18	
	Concrete 1:2.33:4.66 (cement : greyish river sand : quartzite coarse aggregate) – dry condition / saturated condition	2.29/3.49	
(Schackow, et al., 2014)	Concrete with 55% to 65% vermiculite in volume + air-entraining admixture 1% in addition (by mass of cement)	0.5 – 0.34	Heat Flow Meter
	Concrete with 55% to 65% Expanded Polystyrene (EPS) in volume + air-entraining admixture 1% in addition (by mass of cement)	0.56 – 0.50	
(Marie, 2017)	Concrete 1:2.15:1.31 (cement : fine aggregate : coarse aggregate)	1.25	Guarded Hot Plate
	Concrete 1:2.15:1.31 (cement : fine aggregate : coarse aggregate) + recycled concrete aggregate 5% to 20% in replacement of coarse aggregate (by mass)	1.2-0.91	
	Concrete 1:2.15:1.31 (cement : fine aggregate : coarse aggregate) + crumb rubber 10% to 20% in replacement of fine aggregate (by mass)	1.0-0.9	
	Concrete 1:2.15:1.31 (cement : fine aggregate : coarse aggregate) + recycled concrete aggregate 5% to 20% in replacement of coarse aggregate (by mass) + crumb rubber 10% in replacement of fine aggregate (by mass)	1.0-0.79	

### 2.3.3 *Buildings and Energy*

A large portion of the global energy is consumed to operate buildings. The exact figure varies with each country's climate and development status. For example, the US reports an energy consumption of 39% by its buildings (D&R International, 2009); the UK, 29% (GOV.UK, 2017); while mainland China used 27% during 1999– 2001 (Yao, et al., 2005). If the current trend remains, the building's energy demand is expected to rise 50% by 2050 (IEA, 2013).

The main drivers of this significant energy consumption are economic growth, growing population, increasing demand for new electric-consuming appliances and desire for better indoor built environment, particularly winter space heating and summer comfort cooling. The International Energy Agency (2013) estimates that, currently, space heating and cooling together with water heating account for nearly 60% of the global energy consumption in buildings. Besides the extremely high carbon footprint of constructions during their entire lifetime – of decades and centuries – a country's energy supply is a strategic issue of political and economic ramifications. Therefore, the best way to alleviate the ever-growing demand for energy is to improve the competence of building designs and introduce proper building energy conservation regulations (Lam, et al., 2008).

The building envelope, or fabric, is one of the most important systems affecting energy efficiency of the building (IEA, 2013) (Sadineni, et al., 2011) (Kośny & Kossecka, 2002). This key element separates and controls the flow of energy between the indoor and outdoor environments of a building. It thus determines the quality of the indoor conditions regardless of the outside one. The fabric of the building (walls, windows, doors, floors, and roof) comprises, usually, its least altered elements. They remain standing for a long period, maybe even longer than the building's original function remains or the time that the original heating/cooling systems will work (Olivier, 2001).

The past few decades have generated several promising new envelope construction technologies. Numerous structural systems and very effective insulation materials are increasingly being used to ensure the quality of the building envelope. Still, one of the main presumed issues regarding energy-efficient design is the raise in construction costs (Bodach & Hamhaber, 2010) (Olivier, 2001). Although this concern is initially true, along the lifecycle of the building, the savings from electricity and gas bills may far surpass the initial increased price (Dowson, et al., 2012) (Olivier, 2001).

Since the 1970s, European countries promote tests to evaluate cost-effective and energy-efficient construction systems (Dowson, et al., 2012) (Olivier, 2001). This is not only a solution to energy shortages and to reduce the building's carbon footprint, but also a response to the problem of uncomfortable homes and acute social deprivation (Patino & Siegel, 2018) (Rahid, 2003).

In this scenario, Olivier (2001) mentions the case of the Salford City Council, UK. In 1978, the Council built eight experimental masonry-walled, concrete-floored houses with several energy efficiency measures. Compared to ordinary houses, these cost 4% more to build. The measured energy saving was 65% annually. On top of this large fuel saving, an increase in the internal temperature was reported: low-income tenants could now afford to heat their houses up to 21°C for a sharply lower cost (Olivier, 2001). Similar initiatives all over the world found similar performances and benefits (Pacheco-Torgal, et al., 2017).

Unfortunately, nowadays, much of the construction industry is still delivering energy-intensive and poor-quality products. The eagerness for short-term profit margins usually surpass the opportunities for the adoption of better building materials and techniques with higher added value (IEA, 2013) (Bodach & Hamhaber, 2010).

As Olivier (2001) declares, “a major change in philosophy is overdue”. Based on the current state-of-the-art of energy-efficient technologies and standards, some solutions are (IEA, 2013):

- Materials technology: develop more durable and more energy-efficient building materials; more quickly and at a lower initial cost;
- Construction: improve the training and qualification of both labour, engineers and architects; mechanise sites; and use highly labour-saving plant and equipment to the maximum.
- Management: raise the level of organisation skills through qualification and improved management processes.
- Regulation: given the urgent need to meet the challenge of climate change robustly and cost-effectively, it is essential to release more strict performance standards; set legal bodies to ensure that finished buildings meet the prescribed energy performance.
- Government: government institutions must provide a coherent strategy of monitoring, verification, education and training.

Market barriers in the buildings sector are complex and can be difficult to overcome, so the implementation and enforcement of stringent building codes will be essential to achieving widespread diffusion (Oliveira, et al., 2017) (IEA, 2013). The UK and Nordic countries are examples of how a strong leadership can produce a major step forward. Table 2-3 shows the evolution of maximum U-values allowed for building envelope materials in England. As comparison, in Brazil, the strictest U-values required are 1.5 W/m<sup>2</sup>·K for roofs and 2.5 W/m<sup>2</sup>·K for walls, in NBR 15575 (ABNT, 2013). Inconsistently, NBR 15220 (ABNT, 2003) requires the maximum of 2.0 and 2.2 W/m<sup>2</sup>·K for roofs and walls, respectively.

**Table 2-3 - Code Standard U-values for buildings in England  
(adapted from Dowson, 2012 and GOV.UK, 2016).**

<b>Building Regulations</b>	<b>Exposed Walls (W/m<sup>2</sup>·K)</b>	<b>Roofs (W/m<sup>2</sup>·K)</b>	<b>Floors (W/m<sup>2</sup>·K)</b>	<b>Windows (W/m<sup>2</sup>·K)</b>
1976	1	0.60	Not Specified	Not Specified
1982	0.60	0.35	Not Specified	Not Specified
1991	0.45	0.25	0.45	3.3
1995	0.45	0.25	0.35	3.3
2000	0.35	0.25	0.25	2.2
2006	0.35	0.16-0.25	0.25	2.0-2.2
2010*	0.30	0.20	0.25	2.0

\* Incorporating 2016 amendments

Initially, the construction industry in these developed countries opposed the proposals and warned of 'prohibitive' rises in housing costs (Olivier, 2001). Nevertheless, the measures became law for new and retrofitted buildings. In the following years, dozens of experimental dwellings were constructed to evaluate what worked, what didn't and the most effective techniques (Mendes, 2013). Gradually, materials and measures initially resisted by the construction companies became familiar and a significant improvement in building performance and user satisfaction was verified (Olivier, 2001).

Finally, attention must be given not only to the U-values of envelope materials. Commonly used highly conductive structural materials such as steel may generate thermal bridges. This is a phenomenon in which highly conducting materials create a path of least resistance, unintentionally increasing the heat transfer (Kośny & Kossecka, 2002). Thermal

bridges can significantly rise local U-values and change the dynamic response of envelope components, generating two- or three-dimensional effects around them. The effects of thermal bridges are intensified by the very high ratio between thermal conductivities of the structural and insulating materials. For example, aluminium has a thermal conductivity over 320 times that of ceramic bricks; and steel is 1800 times a better conductor than polyurethane foam (ABNT, 2003).

#### *2.3.4 Strategies to improve thermal performance in buildings*

Before the electricity and the development of mechanical means for obtaining thermal comfort, people in different climate zones cooled or heated their houses with only locally available materials and air temperature (Felix & Elsamahy, 2017). They would employ natural sources of energy and physical phenomena such as the different densities of cold and hot air (Pacheco, et al., 2012). With the advent of electricity, however, these natural mechanisms made way for more comfortable, energy-demanding appliances.

Active measures for comfort conditions are those energy-intense solutions. They include equipment for artificial ventilation and lighting, air cooling/heating and water heating. Some examples are electric resistance space heaters; electric lighting; chillers, boilers, etc. In the past few years, massive research has been put into more efficient active systems. However, they still require energy to operate.

In turn, passive measures are those directly related to architectural design and require little or no energy to be effective. The efficiency of passive measures is closely related to the nocturnal and diurnal temperature gradient, as well as wind speed and solar altitudes. Some examples of passive measures are (Guyot, et al., 2018) (Manzano-Agugliaro, et al., 2015): use of reflective surfaces; optimised orientation; shading; design for natural ventilation; improved airtightness; use of materials with high thermal mass (energy storage); and, most importantly, selection of insulating envelope materials. Considered by many authors the most important factor, the thermal properties of the construction materials are responsible for reducing the heat transfer from indoors to outdoors environments. Therefore, a poorly insulated building will demand much more energy for artificial cooling/loading to maintain thermal comfort indoors.

In the middle, there are the hybrid schemes. These use active systems to assist passive measures. For example: heat recovery ventilation, solar thermal systems, photovoltaic panels, ground source heat pumps, and so on. In general, where possible, engineers and

architects will aim to maximise the potential of passive measures, before introducing hybrid systems or active systems.

According to the International Energy Agency (2013) the technologic and policy priorities in the buildings sector in Brazil should be:

- a) Reduce cooling loads through reflective technologies (passive measure) and advanced cooling equipment (active measure);
- b) Promote solar water heating (hybrid measure);
- c) Develop suitable building codes with supporting infrastructure (education, product ratings and oversight);
- d) Improve appliance and equipment standard (promoting energy-efficient appliances, lighting, electrical loads, etc.);

In summary, the available mechanisms for thermal performance improvement in buildings are endless, from recent devices (e.g., air-conditioning chillers) to techniques dating from centuries (e.g., stack effect). Nowadays, researchers and manufacturers undergo pressure from governments and the environmentally aware population to reduce the energy consumption from the building stock. The increasing complexity of architectural projects and HVAC systems is gradually leading to the inclusion of thermal simulations as one of the main design stages of construction and retrofit.

### *2.3.5 Building Energy Simulation*

Computer building energy simulation is a technique for assessing the dynamic interactions between the external climate, building envelope and HVAC systems (Lam, et al., 2008). It is a decision-making tool that can be used to evaluate the energy performance of an envelope material, estimate the total energy used in a building, predict HVAC sizing and lighting requirements, compare retrofit strategies, among others (Sadineni, et al., 2011).

The accuracy of the building energy simulations heavily depends on the user input data such as: type of building, building geometry and orientation, construction details, material properties, geographic location, weather data, occupancy, mechanical equipment, among others (Coakley, et al., 2014). The climate is usually input as hourly weather databases (e.g., temperature, relative humidity, wind direction/velocity, solar radiation). Detailed heat-balance calculations are then carried out at discrete time-steps based on the

physical properties of the building, its mechanical systems, as well as the dynamic inputs (weather, occupancy, lighting, equipment, etc.) (Coakley, et al., 2014).

These calculations can be applied to the course of a full year or for a given number of days. Some researchers use design days, typical summer or winter days characterised by air temperature, relative air humidity, wind speed and incident solar radiation for the average hottest/coldest day of the year for the last 10 years (ABNT, 2013). This method thus condenses a large quantity of complex measured data into relatively few input points or schedules (Coakley, et al., 2014).

With all proper input on hands, the next step is to choose among the dozens of available software for thermal modelling. Some examples are: BLAST, BSim, DeST, DOE-2.1E, ECOTECH, Ener-Win, Energy Express, Energy-10, EnergyPlus, eQUEST, ESP-r, IDA ICE, IES/VES, HAP, HEED, PowerDomus, SUNREL, Tas, TRACE and TRNSYS. Apart from those, developed by several research groups worldwide, there are also specific computer programs that deal with performance simulation of specific envelope components.

As previously mentioned, proper thermal modelling requires accurate descriptions of the building envelope components. Otherwise, the model results may provide misleading information about the energy balance of the building. These can cause poor dimensioning of the envelope materials and under or overestimate the dimensioning of heating and air-conditioning systems (Kośny & Kossecka, 2002). Thus, the building may incur in higher (or lower) energy consumption in the future, besides generating discomfort for the users. Hence the importance of using precise thermal properties of building materials in energy simulations.

### *2.3.6 Thermal Performance at Brazilian Buildings*

In 2014, the Brazilian housing deficit corresponded to 6 million dwellings, of which 84% are of low-income families (Fundação João Pinheiro, 2016). Concomitantly, Paulsen & Sposto (2013) concluded that the social housing sector in Brazil presents a higher embodied energy in comparison to other countries (7.2 GJ/m<sup>2</sup> versus the world average of 5.8 GJ/m<sup>2</sup> per 50 years). These numbers express the acute social deprivation undertaken by families in developing countries. They also signal the soaring demand for quality and cost-effective social housing (Ralid, 2003).

In this scenario, erecting new houses to solve the lack of habitation is not enough. It is necessary to design the constructions considering the building's lifecycle, focusing on

energy-efficiency, maintenance and occupants' health (Triana, et al., 2015) (Viegas, et al., 2018). An enhanced thermal performance may increase not only health, but also productivity and happiness, thus reducing the social deprivation suffered by low-income families in thermally stressful environments (Patino & Siegel, 2018). The consequences are not only social but also economic and environmental, given the more rational use of resources through lower energy consumption (Triana, et al., 2015).

In Brazilian buildings, the lack of thermal performance is blatant (Oliveira, et al., 2017) (Triana, et al., 2015). Among the main reasons, it can be mentioned that most Brazilian constructions do not have a project that considers the bioclimatic conditions of the region or the thermal properties of construction materials. This is a result of expensive, inconsistent and outdated building standards – for example, Brazilian standard NBR 15220 of thermal performance has not been updated since 2005 (Oliveira, et al., 2017) (Triana, et al., 2015). This scenario is also caused by the knowledge gap of Brazilian construction professionals regarding thermal performance. Finally, the lack of construction oversight for compliance with the standards worsens the situation (Bodach & Hamhaber, 2010).

In Brazil, building performance standard NBR 15575 (ABNT, 2013) brings directives for the verification of the thermal performance of the envelope. The criteria only include maximum values for thermal transmittance and thermal capacity for the walls and roof systems. Solely in the cases in which these properties are out of the allowed range, the designer is required evaluate the thermal performance of the building by the computational simulation method.

In this situation, the Brazilian standard adopts the methodology of typical winter and summer days for eight climate zones (Figure 2-13). Brazil is a large country with an area of about 8.5 million km<sup>2</sup>. The land area stretches between a latitude of 6°N and 34°S, from the subtropical zones in the south to the tropical zones in the north. Thus, characteristics associated with continental climates can be identified, such as large annual temperature range and big variations on the maximum solar altitudes. Brazil also has vast tropical forests and a complex topography ranging from mountainous regions to flat plains. These diversities and complexities culminate in many different regions with distinct climatic features.

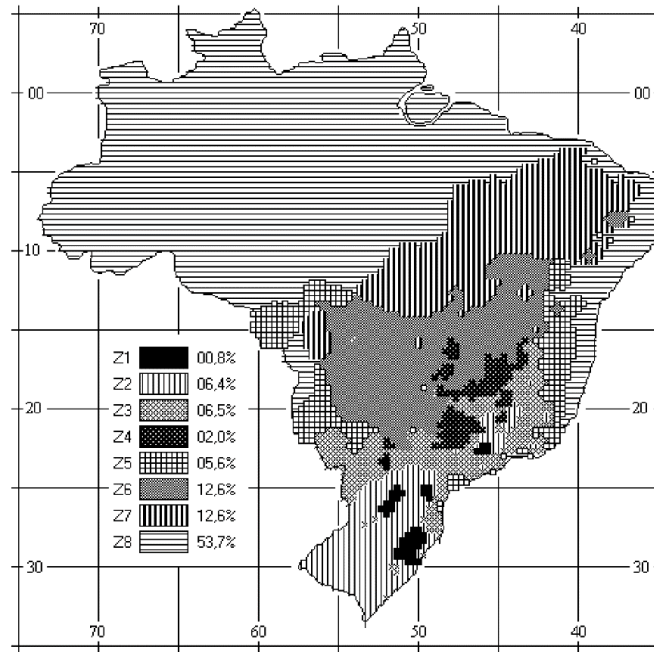


**Figure 2-13 - Brazilian bioclimatic zoning (ABNT, 2003).**

Unfortunately, the performance standard NBR 15575 (ABNT, 2013) only provides temperature data for 26 cities. If the designed building is not located in one of them, the standard suggests that the designer use a city of similar climate.

For each of these zones, a set of constructive recommendations was formulated to optimise the thermal performance of the buildings, through improved climatic adequacy. They are based on the bioclimatic study proposed by Givoni (1992). The parameters considered are: size of ventilation openings; shading of openings; external envelope (wall and roof); strategies of passive thermal conditioning. For example, Table 2-4 presents the directions for Zone 3, where the city of Belo Horizonte is situated, and Zone 8, which covers most of north and northeast regions of the country. Therefore, it is possible to infer that construction techniques and materials are highly dependent on the place where a building is located, if a suitable thermal performance is to be achieved.

**Table 2-4 - Constructive recommendations for Bioclimatic Zones 3 and 8 (ABNT, 2003).**

	<b>Parameter</b>	<b>Recommendations</b>
Zone 3	Ventilation openings	Average: 15% < % Floor area < 25%
	Shading of openings	Allow sun incidence during winter
	External envelope	Walls: Light and reflecting, with $U \leq 3.6$ W/m <sup>2</sup> ·K; Thermal lag <sup>1</sup> $\leq 4.3$ ; Solar Factor <sup>2</sup> $\leq 4.0$ ; Roof: Light and insulating, with $U \leq 2.0$ W/m <sup>2</sup> ·K; Thermal lag <sup>1</sup> $\leq 3.3$ ; Solar Factor <sup>2</sup> $\leq 6.5$ ;
	Strategies of passive thermal conditioning	Cross ventilation; solar space heating; high internal thermal mass;
Zone 8	Ventilation openings	Large: 40% < % Floor area
	Shading of openings	Shade all openings
	External envelope	Walls: Light and reflecting, with $U \leq 3.6$ W/m <sup>2</sup> ·K; Thermal lag <sup>1</sup> $\leq 4.3$ ; Solar Factor <sup>2</sup> $\leq 4.0$ ; Roof: Light and reflecting, with $U \leq 2.3 \cdot FT^3$ W/m <sup>2</sup> ·K; Thermal lag <sup>1</sup> $\leq 3.3$ ; Solar Factor <sup>2</sup> $\leq 6.5$ ;
	Strategies of passive thermal conditioning	Permanent cross ventilation;

<sup>1</sup> Time elapsed between a thermal variation in a medium and its manifestation on the opposite surface of a building component subjected to a periodic heat transfer regime

<sup>2</sup> Quotient of the rate of solar radiation transmitted through an opaque component by the rate of total solar radiation incident on the outer surface of the same component

## 2.4 ULTRASONIC PULSE VELOCITY

The Ultrasonic Pulse Velocity (UPV) is a popular method for non-destructive testing of cement-based composites because of its simplicity and cost-effectiveness. Several researches, professionals and standards worldwide suggest UPV for the assessment of compressive strength, dynamic modulus of elasticity, defects, homogeneity, and changes in properties with time (Dzaye, et al., 2018) (Al-Nu'man, et al., 2016) (Lafhaj & Goueygou, 2009) (Komlos, et al., 1996). Most nations have standardized procedures for the performance of these tests.

In the longitudinal method, which is the most adopted, pulses of elastic stress waves are generated by an electro-acoustical transducer that is held in direct contact with the surface of the tested element (Jones, 1962). After traversing through the concrete, the pulses are received and converted into electrical energy by a second transducer. The velocity is calculated as the ratio between the distance between the two transducers and the electronically measured transit time. Most standards describe three possible arrangements for the transducers (shown in Figure 2-14):

- The transducers are located directly opposite each other (direct transmission);
- The transducers are located diagonally to each other; that is, the transducers are across corners (diagonal or semi-direct transmission);
- The transducers are located at the same surface and separated by a known distance (indirect transmission).

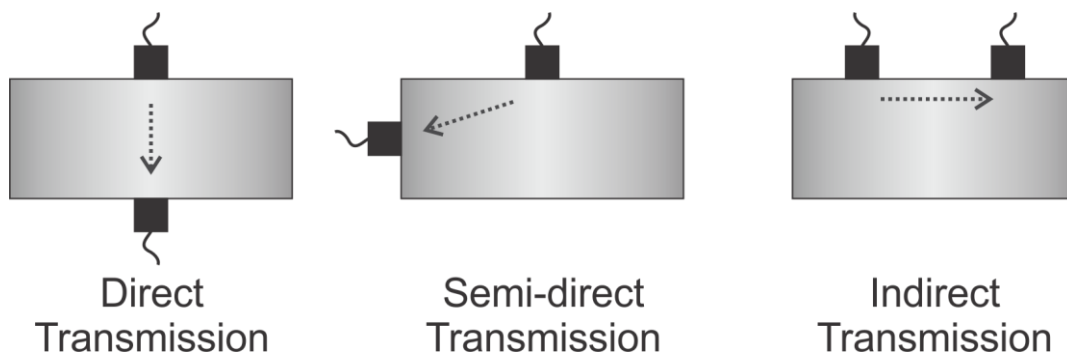


**Figure 2-14 - Different configurations of transducers**

Direct transmission is the most sensitive configuration, and indirect transmission the least sensitive (ACI Committee, 2013). Jones (1962) explained the discrepancy between the direct and indirect velocity as being due to wave dispersion. In laboratory experiments, access to opposite surfaces of a test specimen is generally available and, thus, ultrasonic tests are commonly conducted using direct transmission. In the field, however, access to opposite

surfaces of a component may not be readily available (e.g., concrete pavements, concrete slabs and bridge decks), and tests are usually conducted using indirect transmission (Yaman, et al., 2001).

Several factors affect the UPV: type of cement, type and shape of aggregate, mixture ratio, water/cement ratio, temperature and saturation (Trtnik, et al., 2009). The influence of the aggregate content cannot be neglected (Al-Nu'man, et al., 2016), neither the presence of admixtures (Demirboga, et al., 2004). Furthermore, as the ratio between the diameter of sample and the wavelength increases, the degree of distortion decreases (Popovics, et al., 1990). This suggests the importance of picking a suitable frequency when testing an element of specific geometry. A change in frequency would have less effect on pulse velocity in very large specimens (Popovics, et al., 1990).

Reflection and refraction occur when sound waves interact with interfaces of materials with differing acoustic properties (e.g., cement paste, steel reinforcement, and air). These phenomena caused by the presence of discontinuities or geometric features enable their detection and location. The pulse velocity in a cement-based material depends on its density and its elastic properties, which in turn can be related to its uniformity and compressive strength (Popovics, et al., 1990).

It is known that there is a tendency for concrete of higher density to have a higher strength, provided that it comprises conventional materials, so a general classification of quality based on the UPV is possible (Trtnik, et al., 2009) (Demirboga, et al., 2004). This is usually done with the help of a calibration curve for a given concrete. If the concrete is made of unconventional materials or in unknown proportions, this method becomes unreliable (Demirboga, et al., 2004; Al-Nu'man, et al., 2016; Komlos, et al., 1996). Popovics, et al. (1990) affirms that this method, even when used with preestablished calibration curves, is inaccurate to a degree of 20%. On the other hand, the pulse velocity vs. density curve seems applicable to all types of mixtures regardless of the composition of specimens (Popovics, et al., 1990).

The detection of defects such as voids, flaws and lack of compaction is based on the fact that they increase the transit time of the ultrasonic pulses (ACI Committee, 2013). This effect is shown in Figure 2-15. Similarly, for the determination of uniformity, standards recommend the use of a grid of points that appropriately covers the element. The non-uniformity is indicated by the variation of the pulse velocities obtained from different measurements. This is one of the most reliable techniques for UPV, if the material is

relatively homogeneous – the presence of reinforcement in concrete, for example, would impair the precision of the method (Popovics, et al., 1990).

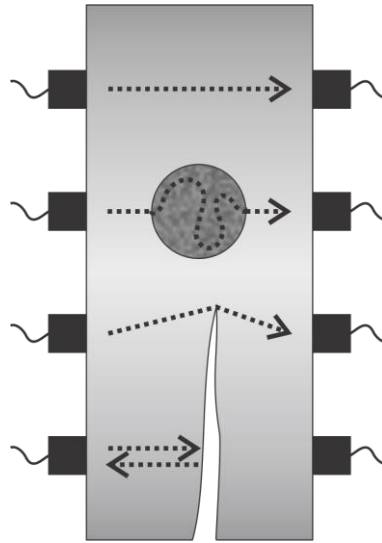


**Figure 2-15 - Effects of defects on travel time of ultrasonic pulses: in the presence of defects, the wave takes a longer time to arrive at the receiver, or does not arrive at all. (adapted from ACI Committee, 2013)**

Another way to evaluate homogeneity in cement-based composites is to use their dispersive nature. In composite materials, the velocity of the pulses increases with their frequency (Saint-Pierre, et al., 2016). This effect is stronger at high frequencies for less homogeneous materials (Popovics, et al., 1990).

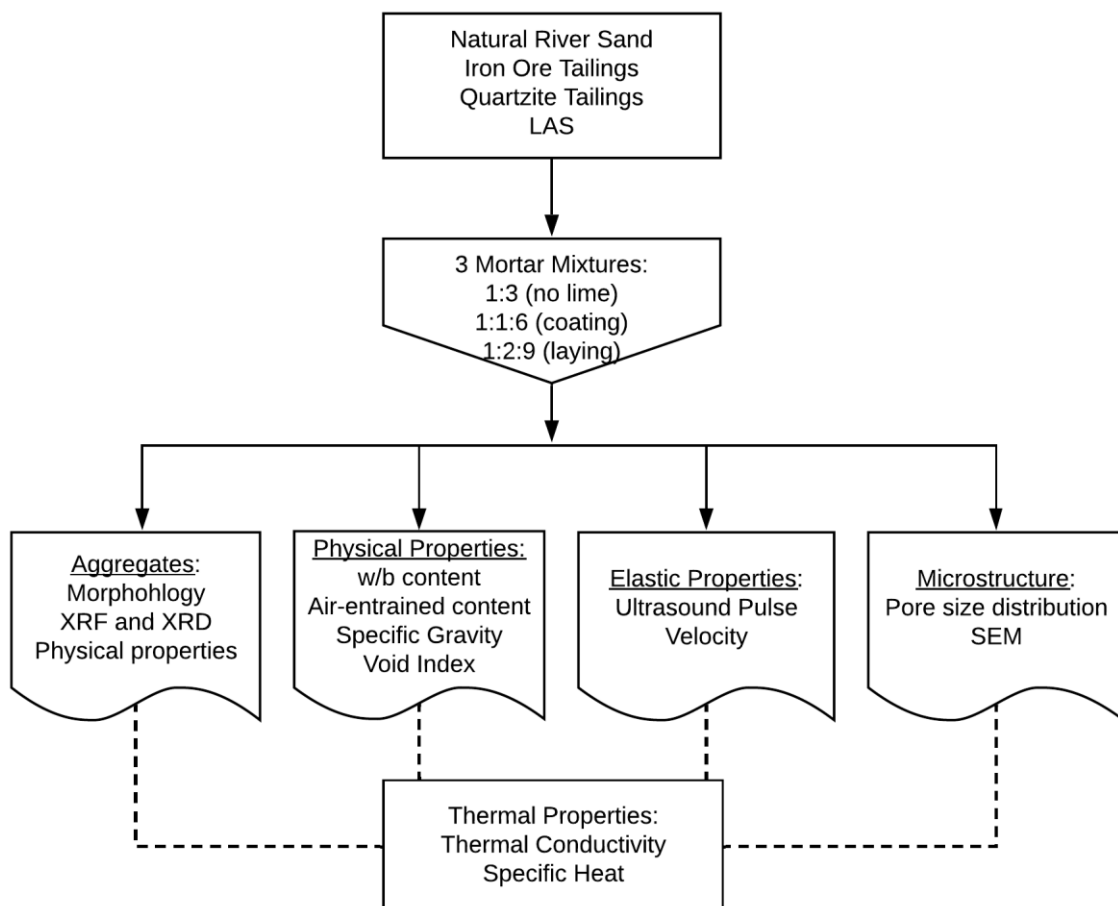
Regarding changes in the properties with time, professionals use repeated measurements of UPV at different ages with the same transducers in the same position (Dzaye, et al., 2018) (Popovics, et al., 1990). A similar methodology is adopted in assessing material deterioration *in loco*. In these cases, a reference UPV is determined in laboratory specimens. Field measurements are then compared with the reference value to assess the current condition of the material (Yaman, et al., 2001).

In summary, UPV is a fast and effective technique for evaluating properties of cement-based composites concerning the interfaces among their components and voids. It is important to notice that the precision of this method increases proportionally to the availability of previous results – used as calibration.

# 3

## Chapter 3: Materials and Methodology

What are the factors affecting the thermal properties of cement-based composites?



### 3 MATERIALS AND METHODOLOGY

---

#### 3.1 MATERIALS

For the preparation of the mortars, the following materials were used: high early strength Portland cement; hydrated lime; fine aggregates and potable water. Fine aggregates included local river sand (natural aggregate, as reference); iron ore tailings from tailing dams (IOT); and friable quartzite (QTZ). Before the mixing, the natural aggregate and all residues were sieved in the #4 (4.75 mm) mesh and oven dried at 105°C.

The residues' samples were collected according to the normative prescriptions of NBR 10007 (ABNT, 2004b) with the aid of excavation machines at different collection points. Subsequently, they were sent to the Laboratory of Civil Construction Materials, Federal University of Ouro Preto, Brazil, in plastic drums, sealed and identified.

The IOT used in the present work originates from the margins of a tailing dam located in the city of Igarapé, state of Minas Gerais, Brazil. After drying, the IOT's clay lumps and friable particles were broken down manually. No further processing was performed. The QTZ is the waste generated in the mining and cutting processes of commercial quartzite. The samples used here originated in the city of São Thomé das Letras, Brazil, and were used in their raw state.

The high early strength Portland cement (ASTM type III equivalent) was chosen since it has the lowest content of mineral admixtures among Brazilian cement types (ABNT, 2018). This product contains 90%-100% of clinker and gypsum and only 0%-10% of inert limestone filler.

**Table 3-1 - Physicochemical characteristics of the Portland cement**  
(source: manufacturer Brennand Cimentos)

<b>Parameter</b>	<b>Result</b>	<b>Standard Requirements (ABNT, 1991)</b>
Insoluble Residue	0.86%	≤1%
Loss on ignition	3.18%	≤4.5%
MgO content	1.36%	≤6.5%
SO <sub>3</sub> content	3.32%	≤4.5%
CO <sub>2</sub> content	2.56%	≤3.0%
Na <sub>2</sub> O content	0.07%	-
K <sub>2</sub> O content	0.91%	-
Specific area (Blaine method)	4.743 cm <sup>2</sup> /g	≥3.0 cm <sup>2</sup> /g

<b>Parameter</b>	<b>Result</b>	<b>Standard Requirements (ABNT, 1991)</b>
Unit Weight	3.04 g/cm <sup>3</sup>	-
Fineness Index – % retained in sieve #200	0.27%	≤6.0%
Compressive strength at 7 days	49.1 MPa	≥34.0 MPa

A hydrated lime type CH-I was adopted (ABNT, 2003a). Table 3-2 presents its chemical composition.

**Table 3-2 – Physicochemical characteristics of Hydrated Lime**  
(Source: manufacturer Ical)

<b>Components</b>	<b>Proportion (%)</b>
CaO	98.3%
SiO <sub>2</sub>	0.5%
Fe <sub>2</sub> O <sub>3</sub>	0.4%
SrO	0.3%
Al <sub>2</sub> O <sub>3</sub>	0.2%
MgO	0.1%
SO <sub>3</sub>	0.1%
Others	0.1%
Loss on ignition (1000°C)	25%
Retained in sieve #32	0.02%
Retained in sieve #200	5.07%

Finally, the LAS-based AEA, evaluated in a previous work (Mendes, et al., 2017), consists of an association of anionic surfactants between 6 and 10%: LAS; Linear Alkyl Benzene Sulfonate Triethanolamine and Sodium Lauryl Ether Sulphate (Química Amparo LTDA, 2011).

### 3.2 MATERIAL CHARACTERISATION

The particle size distribution of the aggregates was obtained by conventional sieving (ABNT, 2003b) and laser diffraction (on the fraction below 0.075mm), using a BETTERSIZE 2000 laser particle size analyser. The results show the average of two analysis for each aggregate. Apparent specific gravity was determined using a 500ml pycnometer (brand Solotest), according to NBR NM 52 (ABNT, 2009). In turn, unit weight was obtained by weighting a known standardised container filled with oven-dry aggregate, per NBR NB

45 (ABNT, 2006). In addition, the morphology of the particles was observed in an optical microscope Coleman XTB-3AT, magnification of 45x.

Chemical and mineralogical characterisations were carried out by X-Ray Fluorescence (XRF) and X-Ray Diffraction (XRD), respectively. XRF was performed in a semi-quantitative energy dispersive PANalytical Epsilon 3X equipment. The XRD analysis was carried out on a D2 PHASER from Bruker at Nanolab, Redemat, Federal University of Ouro Preto. The equipment operated with measurement setup Bragg–Brentano,  $\text{CuK}\alpha_{1,2}$  radiation ( $\lambda = 1.5408 \text{ \AA}$ ), 45 kV, 40 mA; spinning speed 8 rpm; angular range  $6^\circ\text{--}80^\circ 2\theta$ ; step size  $0.02^\circ 2\theta$ ; time per step 1s. The analysis and refinement of results were performed using the Rietveld method on a Topas 5.0 software, aided by the Crystallography Open Database (COD) 2013. Griceite (LiF), was used as an internal standard, added in the proportion of 10% to the sample’s mass. The samples were hand grounded in an agate mortar, and the fraction below  $45 \mu\text{m}$  was used.

### 3.3 MIXTURE DESIGN AND PREPARATION

Two typical coating (plastering) and laying mortars for masonry systems were produced, with cement and lime, volume mix 1:1:6 and 1:2:9 (cement : lime : fine aggregate); one extra mixture without lime was tested for comparison purposes, volume mix 1:3 (cement : fine aggregate). According to the unit weight of each material, the mass mix ratios of the mortars are found in Table 3-3. The mortars with natural river sand as aggregate were called reference mortars (REFm). In the other mixtures, the fine aggregate was completely replaced by IOT (IOTm) or friable quartzite (QTZm).

**Table 3-3 - Mortar’s mix ratios (in mass)**

Mix type	Volume Mix	Portland Cement	Hydrated Lime	Fine Aggregate
REFm	1:3	1.00	0.00	4.91
	1:1:6	1.00	0.45	9.81
	1:2:9	1.00	0.89	14.72
QTZm	1:3	1.00	0.00	4.69
	1:1:6	1.00	0.45	9.38
	1:2:9	1.00	0.89	14.07
IOTm	1:3	1.00	0.00	5.03
	1:1:6	1.00	0.45	10.06
	1:2:9	1.00	0.89	15.09

In order to study the effect of the pore system, REFm mortars (with river sand) were prepared with two dosages of AEA (0.05% and 0.5%), besides the conventional one without AEA (0%). Those dosages indicate the mass of AEA used as a percentage of the mass of cement in each batch of mortar.

The mortars were produced in a conventional mortar mixer (ABNT, 2005a). Mix procedure included 90 s in low speed, followed a 15s pause for scraping the bowl, and a final 30s in high speed. Water/cement (w/c) ratio was defined as the necessary for the mixture to reach a flow of  $260 \pm 5$  mm.

Four  $300 \times 300 \times 50$  mm plaque-shaped specimens were built for each mix and aggregate type. Demoulding was performed after 48h, followed by curing in a moist chamber for the remaining 26 days; at temperature of  $25 \pm 2^\circ\text{C}$  and relative humidity of  $90\% \pm 5\%$ .

### **3.4 PHYSICAL CHARACTERISATION OF THE MORTARS**

On the fresh state, the air entrained content was investigated by the pressure method. Similar to the flow tests, only one air entrained measurement was performed for each mortar type.

On the hardened state, the specific gravity (density) was determined by the ratio between the mass and the volume of the plaque-shaped specimens (ABNT, 2005b). The volume was measured using a calliper rule. In total, eight measurements on each dimension of the plaques were performed, and the mean value was adopted. The mass was obtained with a precision scale.

The water absorption and void index tests were performed according to NBR 9778 (ABNT, 2009) equivalent to ASTM C642. Instead of using standard cylindrical specimens, adapted specimens measuring  $2 \times 2 \times 5$  cm were cut from the interior of the plaques with a diamond saw. This adaptation sought to evaluate the pore system of the same materials used to obtain the thermal properties. Test procedure includes oven-drying the samples at  $105^\circ\text{C}$  for 72h to measure the dry weight; submerging the samples in water for 72h and boiling them for 4h to obtain the saturated weight; and subsequently hydrostatic weighing the samples. Results correspond to the average of four specimens.

### **3.5 THERMAL CHARACTERISATION OF THE MORTARS**

The thermal conductivity was obtained with a heat flow meter type Lambda HFM 436, manufactured by NETZSCH. It is seen on Figure 3-1. Before the test, the specimens were oven dried at  $80^\circ\text{C}$  and weighed each 24h until the mass loss did not exceed 0.5% in

two subsequent intervals. This procedure sought to level the free water content of all boards to the lowest possible level without damaging the mortar's microstructure. The final value of the thermal conductivity was given by the average of the measurements in the mean temperature of 20°C and delta of 10°C.



**Figure 3-1 – Steps on the fabrication and testing of the boards: a) Mould prepared b) Mould filled with mortar c) Resulting mortar board and d) Testing on HFM equipment**

The specific heat was determined by an adiabatic calorimetry (Figure 3-2). The instrument is a polystyrene calorimeter coupled to a temperature data acquisition system HOBO Onset U12-006. This method allowed the tests of roughly unaltered fragments of mortars. The specimens measured 2×2×5 cm, obtained in the same manner as those from the void index tests. Results comprehend the average of 4 samples.

Two conditions were evaluated: one with samples saturated and another with them oven-dried at 100°C. The specimens tested on dry conditions were measured after reaching a constant mass (less than 0.5% difference in 6 hours), which took approximately 48 hours. In turn, the saturated specimens were immersed in water at  $24 \pm 2^\circ\text{C}$  for 72 hours and subsequently boiled at 100°C for 4 hours, following the specifications of NBR 9778. In both cases, the specific heat was determined when immersing the specimens in 200g of water at 20°C.



**Figure 3-2 – Adiabatic Calorimeter adopted**

### **3.6 MICROSTRUCTURAL CHARACTERISATION**

For microstructural analysis of the pore system, an inner plaque of one specimen of each mixture was cut with a diamond saw (Figure 3-3). Since the HFM calculates the thermal conductivity from an interior area of the sample, this cut aimed to investigate the porosity on the cross-sections that better correlate with the conductivity results. The resulting plaques measured approximately 80×80×50 mm. The cross-sections were then polished with 100 and 400-grit sandpapers. The purpose of polishing is to remove any distortion of the surface caused during the cutting process. After each step, the sample is thoroughly rinsed to remove the material from the previous polishing period.



**Figure 3-3 – Cut performed in the inner section of the mortar specimens**

After polishing, a high contrast was established between the air voids and the matrix. To do so, based on the works of Felice, et al. (2014) and Mendes, et al. (2017), the section was initially painted with black marker. After covering section with black ink, a very fine white powder was pressed into the pores, highlighting them. Subsequently, excess powder is removed, and the section is scanned at a HP Scanjet G4050 scanner with a resolution of 1200 dpi. A strip of about 5 mm of the contour of each specimen was discarded from the analysis to prevent damage from unmoulding or sawing to be confused with pores. Figure 3-4 a) shows the final configuration of this procedure and Figure 3-4 b) shows the scanned image.

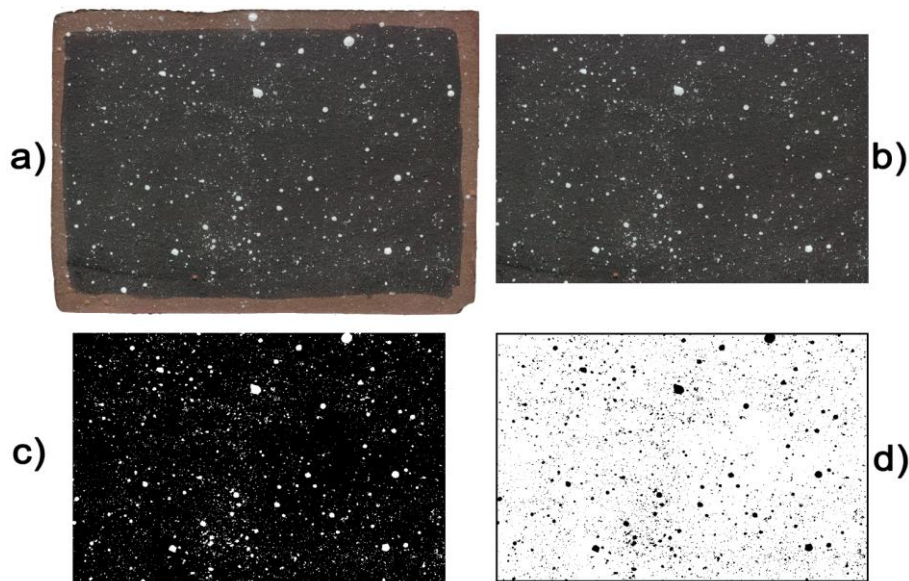


**Figure 3-4 – Steps on the preparation of section for quantitative analysis: a) scanned section of the mortars, already painted and with pores highlighted; b) inner section cropped to remove the influence of the sawed edges; c) transformation in black-and-white with image editing software; d) black-and-white image inverted for use as input in the algorithm**

The analysis of the pore size distribution was performed using a code developed by Rabbani, et al. (2014), which couples distance function and watershed segmentation, and adapted for this study. The algorithm requires a binary rectangular image as input. So, with a software for image editing, a crop was made in the centre of the scanned specimen, then the image was transformed into black and white and inverted (Figure 3-5 c) and d)).

The code's output is the radii of the round model pores equivalent to the volume of each real pore. According to the resolution of the scanner, pores with a radius above 11  $\mu\text{m}$  can be identified. Also, the total area of pores was obtained by counting the black pixels on

the image. Four images from each specimen were evaluated; the results presented herein correspond to the mean of the parameters studied. Unfortunately, the sections of reference specimens 1:1:6 and 1:2:9 were too uneven, due to their low strength, for this methodology to be applied.

The Scanning Electron Microscope (SEM) images were obtained approximately 90 days after moulding. The equipment is a Tescan Vega 3 SEM coupled with Energy Dispersive Spectroscopy (EDS), at the Nanolab Electronic Microscopy Laboratory, at the Redemat, Escola de Minas, UFOP, MG, Brazil. Samples were simply dismantled (not sawn nor sanded) and coated with gold. A magnification of 5000x was used.

### 3.7 ULTRASONIC PULSE VELOCITY

The Ultrasonic Pulse Velocity was obtained using a Proceq TICO apparatus. The transducers produce pulses of 54 kHz. Since the specimens allowed it, and given the higher precision (Yaman, et al., 2001), UPV was obtained using longitudinal direct measurements (Figure 3-5). The specimens were previously oven-dried at 80°C prior to the test, as done for the thermal conductivity tests. The centre of each plaque was evaluated since that is the location measured by the thermal conductivity equipment. A 20-mm-thick rubber mat was placed below the plaques to avoid contact with the granite counter. Petroleum jelly was adopted as couplant.



**Figure 3-5 - UPV testing**

# 4

---

## Chapter 4: Results and Discussion

## 4 RESULTS AND DISCUSSION

### 4.1 MATERIAL CHARACTERISATION

Figure 4-1 shows the particle size distribution of river sand and the residues used in the present work.

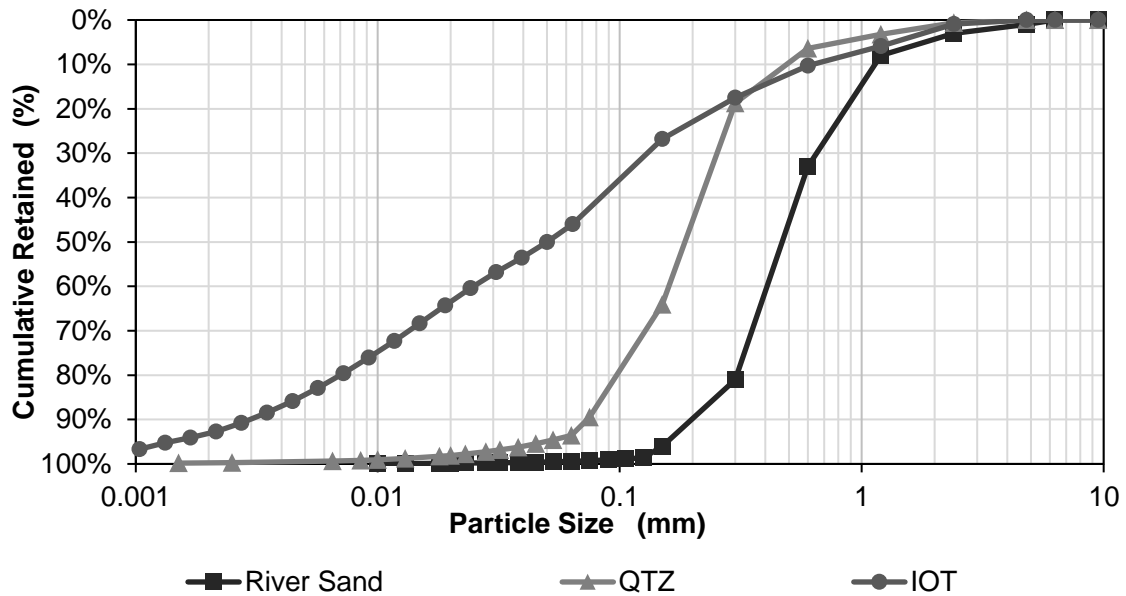


**Figure 4-1 – Particle size distribution of the river sand (natural aggregate), QTZ (friable quartzite), and IOT (iron ore tailings).**

The characteristic dimensions, D10, D50 e D90 can be seen in Table 4-1 (where DN corresponds to the diameter of a theoretical sieve, in mm, above which N% of the material passed).

**Table 4-1 - Characteristic dimensions of the aggregates: river sand (natural aggregate), QTZ (friable quartzite), and IOT (iron ore tailings).**

	River Sand	QTZ	IOT
D10 (mm)	1.100	0.490	0.600
D50 (mm)	0.480	0.190	0.050
D90 (mm)	0.200	0.073	0.002

It is noticeable that the IOT is a well-graduated and particularly fine material, with 50% of its particles smaller than 50  $\mu\text{m}$ . It is followed by the QTZ, with 50% of the material smaller than 0.2 mm; and natural fine aggregate, river sand, below 0.5 mm. The D90 in Table

4-1 shows that IOT has a significant amount of very fine particles, which will influence the specific area, and, consequently, the water demand of the composites produced with this aggregate.

Regarding chemical composition, Table 4-2 presents XRF results for the natural and residue aggregates. It is observed that river sand mainly comprises silicon and aluminium oxides, while QTZ mostly comprises by the former. Despite presenting a significant amount of silicon and aluminium oxides, iron is the main constituent of IOT.

**Table 4-2 – XRF of the aggregates: river sand (natural aggregate), QTZ (friable quartzite), and IOT (iron ore tailings).**

Oxide	River Sand	QTZ	IOT
SiO <sub>2</sub>	78.5%	87.1%	23.5%
Al <sub>2</sub> O <sub>3</sub>	10.8%	7.8%	15.7%
Fe <sub>2</sub> O <sub>3</sub>	6.0%	0.9%	59.0%
K <sub>2</sub> O	1.7%	1.6%	0.2%
TiO <sub>2</sub>	1.0%	0.2%	0.3%
SO <sub>3</sub>	0.0%	0.0%	0.1%
CaO	0.7%	1.3%	0.2%
MnO	0.1%	0.0%	0.0%
MgO	0.6%	0.4%	0.1%

**Table 4-3 – XRD of the aggregates: river sand (natural aggregate), QTZ (friable quartzite), and IOT (iron ore tailings).**

Mineral	River Sand	QTZ	IOT
Quartz	78.04%	89.60%	26.32%
Kaolinite	3.53%	4.40%	17.53%
Gibbsite	1.95%	-	5.20%
Orthoclase	5.62%	-	-
Phlogopite	2.87%	-	-
Muscovite	-	2.85%	-
Hematite	-	-	43.62%
Goethite	-	-	2.07%
Amorphous Content	7.83%	3.12%	5.25%

The XRD informed that the river sand comprises mainly quartz and kaolinite, IOT presents quartz, hematite and kaolinite, while QTZ essentially comprises quartz (Table 4-3). It is observed that all aggregates have a relatively high degree of crystallinity, all of them presenting amorphous content below 8%. It is known that amorphous materials have lower thermal conductivity (Burger, et al., 2016). The chemical elements and minerals observed in the aggregates of the present work are in agreement with findings from other authors (Fontes, et al., 2018) (Santos, 2015) (Faraone, et al., 2009) (Ramirio, et al., 2008) (Yellishetty, et al., 2008).

The fineness modulus and specific gravity of the aggregates are shown in Table 4-4. The higher apparent specific gravity of IOT is a consequence of its chemical composition. River sand and QTZ follow with very similar densities. In addition, as seen in Table 4-4, it is noticeable that IOT is a much finer material than the other aggregates. These properties, alongside the particle shape (Figure 4-2) will influence the microstructure of the mortars in the fresh and hardened state.

**Table 4-4 – Physical properties of the aggregates**

	<b>River Sand</b>	<b>QTZ</b>	<b>IOT</b>
<b>Unit Weight (g/cm<sup>3</sup>)</b>	2.65	2.63	3.53
<b>Apparent Specific Gravity (g/cm<sup>3</sup>)</b>	1.58	1.51	1.62
<b>Fineness Modulus</b>	0.61	0.93	2.22

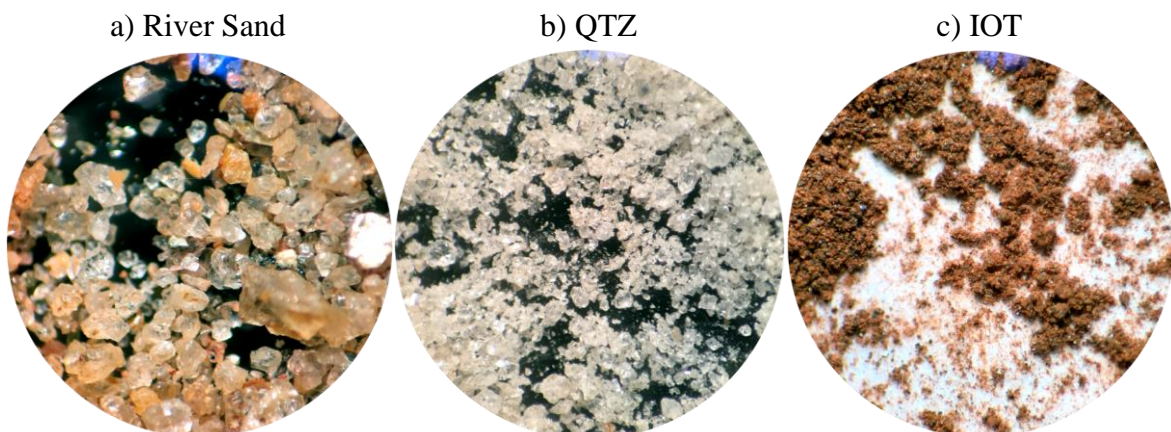


**Figure 4-2 – Stereoscopic analysis of the aggregates: river sand (natural aggregate), friable quartzite (QTZ), and iron ore tailings (IOT); magnification of 45x.**

The morphological analysis of the aggregates shows the typical characteristics of each one. River sand presents heterogeneous medium and large grains, with volumetric aspect and rounded edges. QTZ is a clear and homogeneous aggregate, with medium and small particles, notably angled and irregular. IOT, in turn, comprises small lamellar particles that gather in lumps, confirming its clay-like behaviour. The same characteristics were observed in SEM analysis performed with the same residues by Fontes et al. (2016) and Carvalho et al. (2019).

## 4.2 PHYSICAL CHARACTERISATION OF THE MORTARS

### 4.2.1 Characterisation of the mortars in the fresh state

Initially, Figure 4-3 presents the w/c and w/b ratios of the mortars, defined by fixing the flow at 260 mm. A reduction of the w/c and w/b ratios is observed as the AEA content increases. This behaviour is due to the higher workability of the mortars, a consequence of the better spread of the cement particles attributable to the action of the surfactants (Mendes, et al., 2017) (Ouyang, et al., 2008) (Ramachandran, 1995).

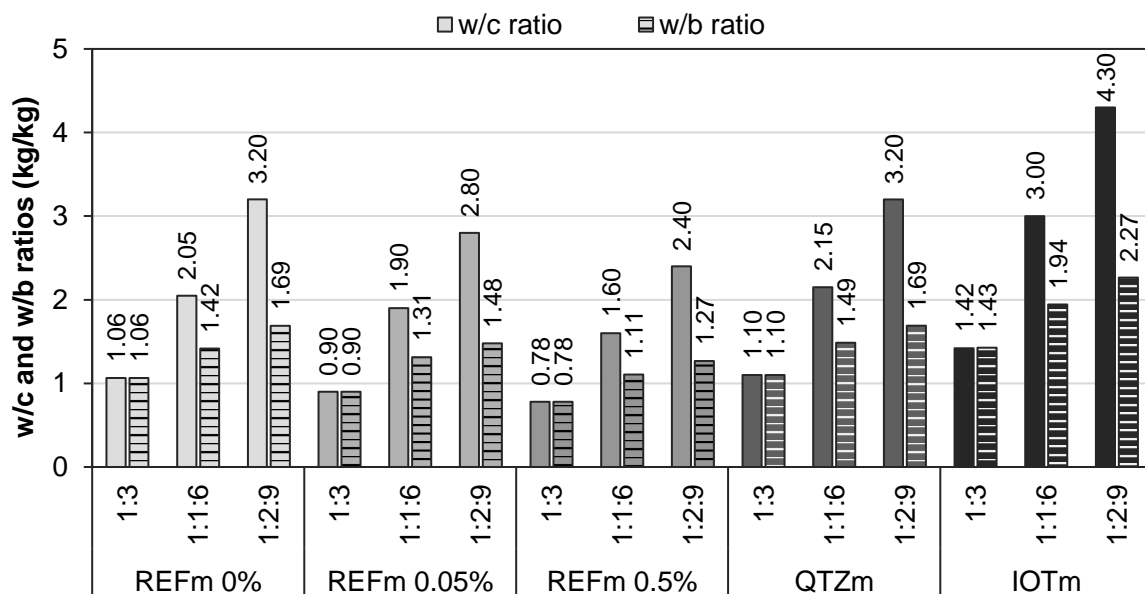


**Figure 4-3 - Water/cement (w/c) and water/binders (w/b) ratios of mortars produced with natural aggregate (REFm) with 0%, 0.05% and 0.5% AEA content; friable quartzite (QTZm) and iron ore tailings (IOTm).**

Similarly, the water demand increased along with the lime content of all mortars (from 1:3 to 1:2:9). This trend is possibly because of the chemical composition and fineness of this binder (Mehta & Monteiro, 2014) (Siwinska & Garbalinska, 2011).

Regarding the mortars with residues, IOTm were the mortars with higher water demand to achieve the set flow of 260 mm. This is directly related to the fineness and shape of IOT particles. The same factors are responsible for the slightly higher w/b ratio of QTZm in relation to REFm. Still in the fresh state, the entrained air content was evaluated. Results are shown in Figure 4-4.

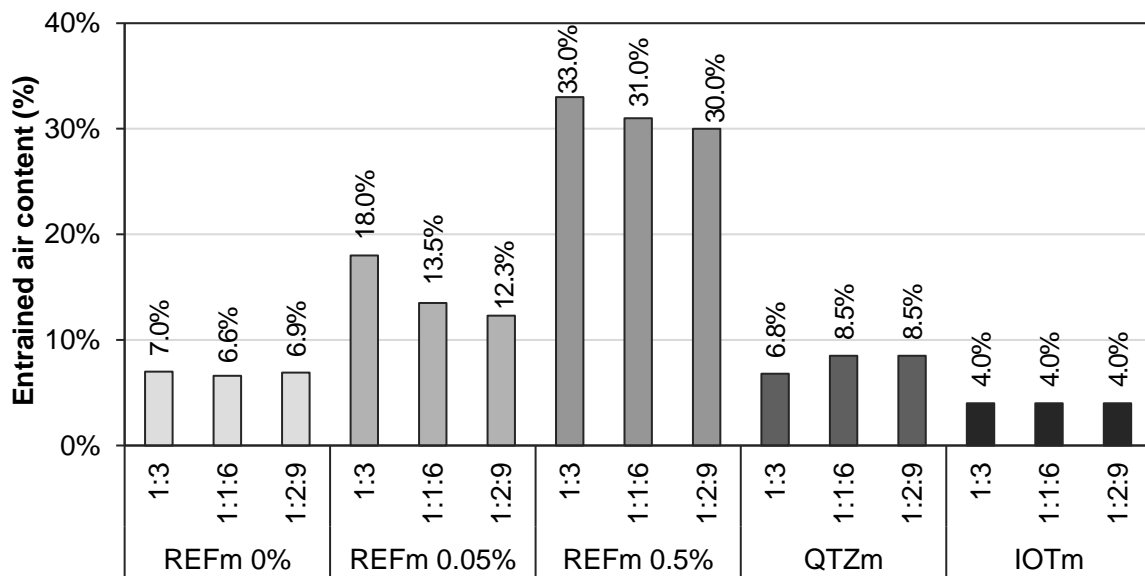


**Figure 4-4 – Entrained air content of mortars produced with natural aggregate (REFm) with 0%, 0.05% and 0.5% AEA content; friable quartzite (QTZm) and iron ore tailings (IOTm).**

Within the reference mortars, the air-entrainment increases with the increase in AEA content, as expected. However, for mortars REFm 0.05% and 0.5%, a general trend of decreasing entrapped air was observed with increase in lime content. A possible interaction between lime and AEA might be causing this behaviour. This effect has never been reported before, and is, thus, an interesting point for further investigations.

For mortars without AEA, the entrained air content varied little with the changes in lime volume and w/b content. IOTm presented a remarkably low value among them. Since IOT is a clayish material with high specific gravity, unlike conventional aggregates, it is possible that either its properties affected the precision of the equipment, or IOTm did entrapped less air during mixing. A similar trend was observed by Fontes, et al (2016).

Conversely, QTZm presented similar or higher entrained air content in relation to REFm. This is possibly due to the angled shape of QTZ particles.

#### 4.2.2 Characterisation of the mortars in the hardened state

Figure 4-5 shows the results of specific gravity (density) on the hardened state. As expected, there is a decrease in the specific gravity as the AEA content in the mixtures increases. For the REFm mortars with varying AEA content, it is observed that the specific gravity decreases slightly from mortars without AEA (0%) to those with 0.05% AEA; on the other hand, there is a sharp decline when the AEA content is increased to 0.5%.

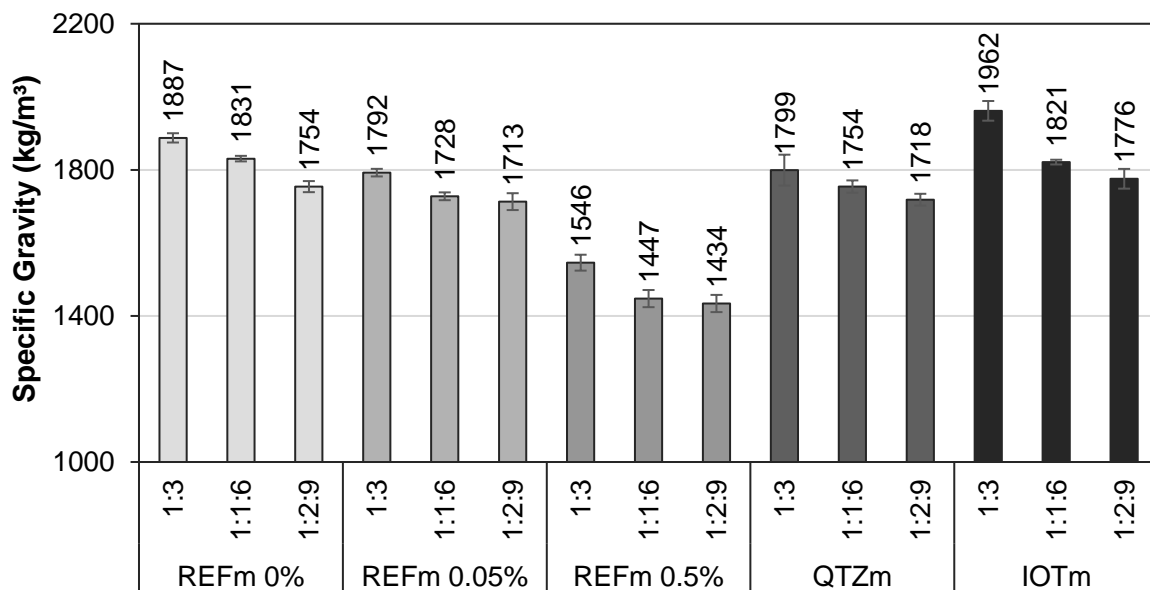


**Figure 4-5 - Specific gravity of mortars produced with natural aggregate (REFm) with 0%, 0.05% and 0.5% AEA content; friable quartzite (QTZm) and iron ore tailings (IOTm).**

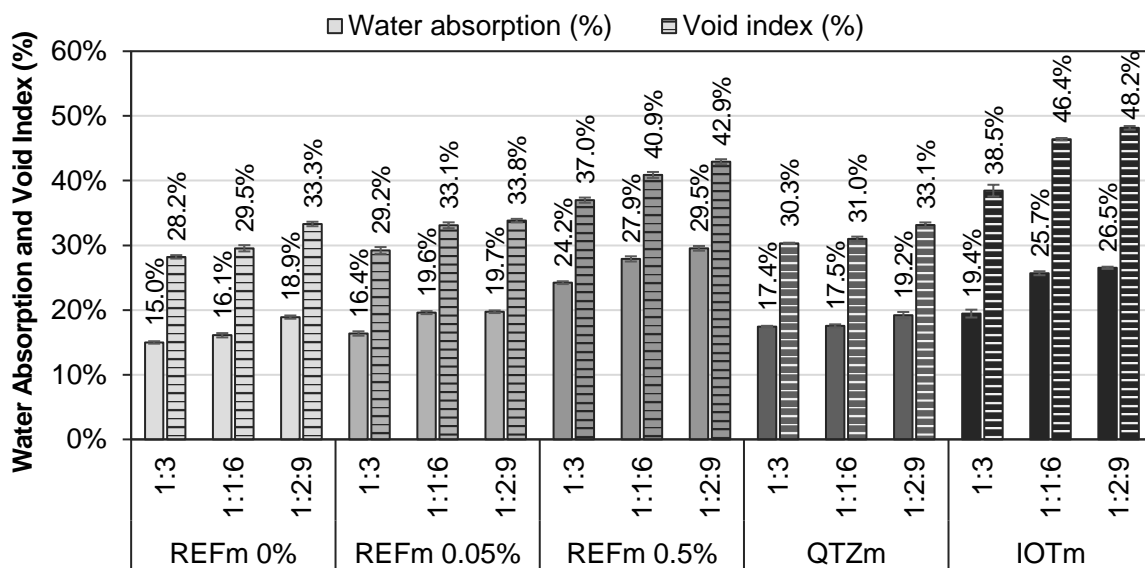
As the surfactant is added in the fresh state, the surface tension of the water is reduced, with the formation and maintenance of a stable foam system (Du & Folliard, 2005) (Ouyang, et al., 2008). Thus, the pore system increases in volume and average dimensions, making the mortars lighter (Mendes, et al., 2017) (Yang, et al., 2000). Mortars with 0.5% AEA were on average 19% lighter than the reference mortars (REFm 0%). This reduction of the specific gravity entails a reduction of the permanent loads in the structure and foundation of the buildings.

Figure 4-5 also shows that, although IOT has a much higher unit weight than the other aggregates, IOTm showed similar or slightly higher specific gravity than REFm 0%. This is probably due to the higher w/b content of IOTm. The high water retention promoted

by the IOT (Fontes, et al., 2016) possibly led to the stability of the water and air in the mortar matrix during curing, which in turn induced a higher number of voids and consequent lower specific gravity. Regarding QTZm, their specific gravity is similar to REFm, which follows the comparable specific gravities of their respective aggregates. The light reduction might have been caused by the higher air-entrainment during mixing.

For all mortars, the specific gravity decreases as the lime content increases (from 1:3 to 1:2:9). This behaviour results from both the smaller unit weight of lime and the increased porosity that this air binder promotes.

The more developed pore system of mortars with higher lime content can be observed in the water absorption and void index results, Figure 4-6. The increased porosity in the hardened state predicted for REFm 0.05%, REFm 0.5%, and, especially, IOTm was also confirmed. It should be noticed that the method adopted for this test (hydrostatic weighing) depends not only on the overall porosity of the matrices, but also on the interconnections among these pores. In other words, mortars with connected pores, such as those promoted by the evaporation of water in IOTm, can present higher water absorption and void index results without necessarily presenting a higher total porosity.



**Figure 4-6 – Water absorption and void index of mortars produced with natural aggregate (REFm) with 0%, 0.05% and 0.5% AEA content; friable quartzite (QTZm) and iron ore tailings (IOTm).**

### 4.3 THERMAL CONDUCTIVITY

Figure 4-7 presents the thermal conductivity results. The increasing content of lime promoted a general decreasing trend of the overall thermal conductivity for all mortars. This fact is probably due to the high water retention and w/b content promoted by this fine air binder. A significant amount of the water demanded in the fresh state will not react within the mortars, and, by evaporating, will thus contribute to the formation of pores and to the refinement of the pore system (Fontes, et al., 2016) (Sébaïbi, et al., 2003). The evaporation of water leads to the formation of the capillary pores or channels (2 nm - 10 µm) (Mehta & Monteiro, 2014) (Aligizaki, 2005).

An increase in total porosity leads to a reduction on thermal conductivity, a well-known relationship for ceramic materials (Francl & Kingery, 1954). This trend is due to the relatively low thermal conduction of the air filling the pores (0.025 W/(m·K) at room temperature and free of convection) (ABNT, 2003).

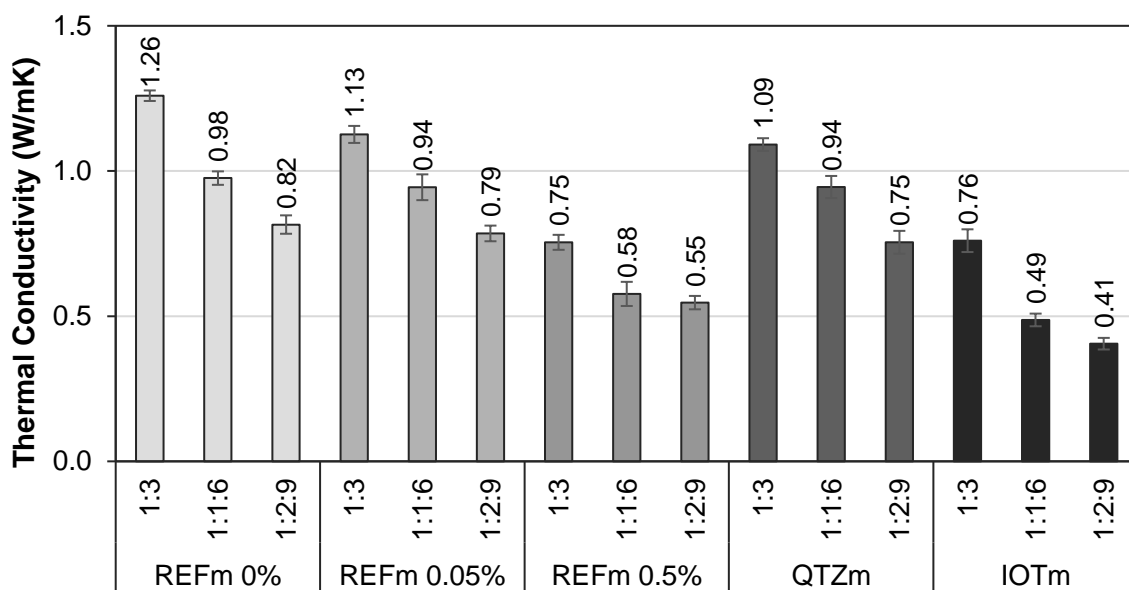


**Figure 4-7 – Thermal conductivity of mortars produced with natural aggregate (REFm) with 0%, 0.05% and 0.5% AEA content; friable quartzite (QTZm) and iron ore tailings (IOTm).**

The stabilisation of pores promoted by the AEA in mortars REFm 0.05% and 0.5% increased the total porosity of the matrices (Figure 4-4 and Figure 4-6). As result, mortars 1:2:9 and 1:1:6 with 0.5% AEA presented thermal conductivity 37% and 46% lower than their respective references, REFm 0%.

QTZm presented lower thermal conductivity than reference mortars, REFm 0%. QTZ and river sand have similar chemical composition, even though QTZ presents slightly lower amorphous content than river sand. Therefore, the average 8.5% decrease in the thermal conductivity of QTZm is probably mainly due to the slightly higher porosity of this mortars.

In general, IOTm obtained the lowest thermal conductivity of all mortars, despite presenting the highest specific gravity than them. IOT also showed the highest apparent specific gravity and hematite content (11.3 W/(m·K)), and second highest crystalline degree among the aggregates, 94.75% (Table 4-3), all characteristics of highly conductivity materials. However, the relative fineness and morphology of IOT might have influenced the results. The filler effect promoted by the smaller particles of this aggregate led to the refinement of pores (Carvalho, et al., 2019) (Sant'Ana Filho, et al., 2017) (Mehta & Monteiro, 2014). IOTm also presented high void index results, due to the high water retention of IOT, meaning that these mortars have a significant system of small, interconnected pores.

Researchers affirm that the thermal conductivity of the aggregates is one of the most important factors determining the insulating/conductive quality of concretes (Marie, 2017) (Schackow, et al., 2014) (Khan, 2002) (Akutstu & Sato, 1988). However, for mortars, it is observed that, although the aggregates correspond to 75% of the volume, the pore system generated by them affects the resulting thermal conductivity to a higher degree.

For instance, in comparison with REFm 0.5% 1:2:9, mortar IOTm 1:2:9 had significantly higher hematite content (43.6% versus 0%) and specific gravity (1962 versus 1546 kg/m<sup>3</sup>), and a slightly higher void index (38.5% versus 37%), but they presented very similar thermal conductivities. In other words, the resulting microstructure of a mortar seems to be more influential on its thermal conductivity than the chemical composition and the isolated thermal conductivity of its constituents. Similar findings were reported for cement pastes (Xu & Chung, 2000a) (Fu & Chung, 1997), sand mortars (Xu & Chung, 2000b) and fibre-reinforced mortars (Benmansour, et al., 2014) (Khedari, et al., 2001).

For example, in a study carried out by Fu & Chung (1997), the addition of carbon fibres decreased the thermal conductivity of the cement paste, even though the fibres are more conductive than the paste up to 2 times. The apparent contradiction was a result of the increase in air voids promoted by the fibres. Similarly, Khedari, et al. (2001) added a certain percentage of organic fibres to mortars and found out that the length of the fibres influenced the resulting thermal conductivity of the mortars. Albeit the mass and thermal conductivity

of the fibres were constant, short fibres were more difficult to align and pack densely and thus generated a larger number of voids.

Therefore, we cannot accurately predict the thermal conductivity of concretes by the thermal properties of their mortars, neither predict the performance of mortars or concretes based on the cement paste. According to Kumar & Bhattacharjee (2003), the pore system in the mortar of concrete is markedly different from the pores of well-compacted mortar prepared independently using identical proportions of the ingredients. The interfacial transition zone plays an important role in the resulting microstructure of cement-based composites (Mehta & Monteiro, 2014). This fact is verified by Khan (2002), who, testing on prediction models, observed that models based on the thermal conductivity of the aggregates and mortars were less effective in predicting the experimental thermal conductivity than the ones based on porosity and pore shape. Smith, et al. (2013) also proved that the pores' structure, sizes and connectiveness affect the accurate precision of several pore-related models.

#### **4.4 MICROSTRUCTURAL CHARACTERISATION**

This investigation is deepened by the quantitative and qualitative analyses performed on the mortar specimens REFm 1:3, QTZ 1:3, IOTm 1:3, 1:1:6 and 1:2:9. Figure 4-8 shows the total porosity of the cross-sections of the mortars in which this study could be performed. One should notice that this image method only evaluates the pores with radius above 11  $\mu\text{m}$ , hence, the macropores (Mehta & Monteiro, 2014) (Aligizaki, 2005). For ease of comparison, the thermal conductivity and specific gravity (density) of those specific specimens were plotted too.

Analysing the results, it is possible to infer that: 1) the thermal conductivity among different mortar types is not directly related to their specific gravity or total porosity; 2) within the same kind of aggregate, it is; 3) thermal conductivity is not only associated with the absolute porosity but also to the pore size distribution; 4) the higher the number of small pores (< 20  $\mu\text{m}$ ), the lower the thermal conductivity. This last affirmative is highlighted in Figure 4-9.

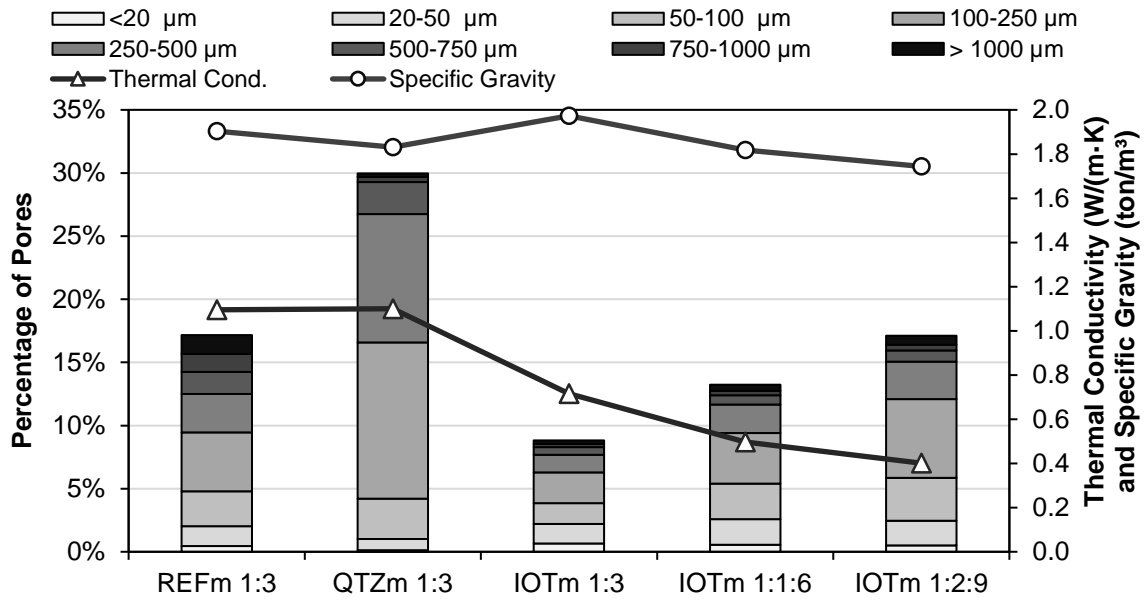


**Figure 4-8 – Total porosity and absolute pore volume distribution (by radii), along with thermal conductivity (W/(m·K)) and specific gravity (g/cm<sup>3</sup>) of mortars.**

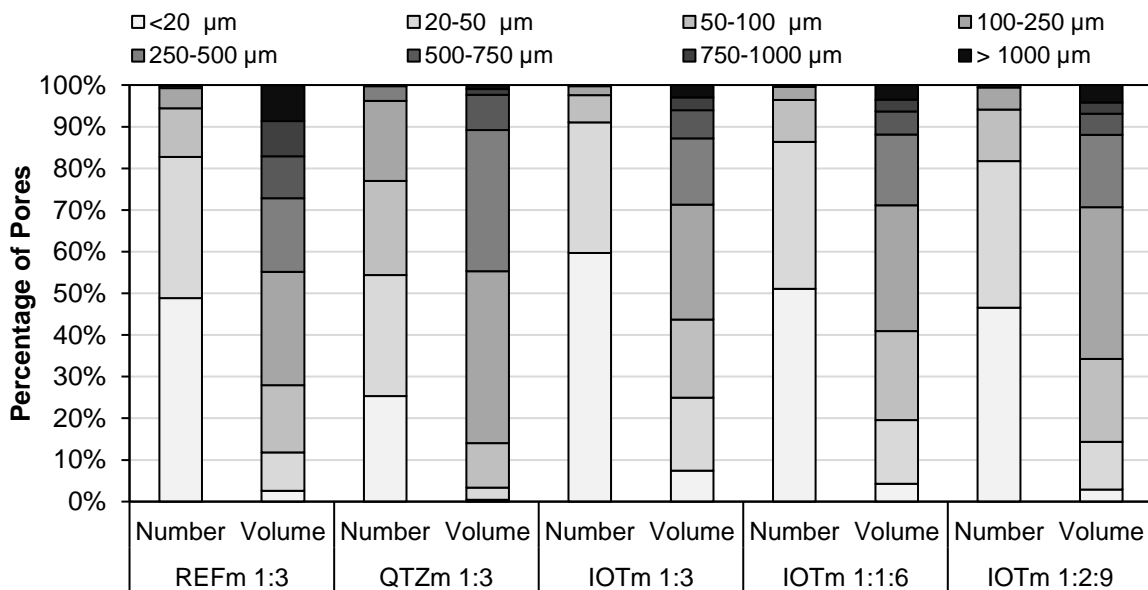


**Figure 4-9 – Relative pore distribution – by number of pores of each radius and their respective volume.**

In comparison with REFm 1:3 and QTZm 1:3, the specimen IOTm 1:3 presents a higher relative number and relative volume of pores below 20 μm. Another prove of this configuration is the fact that IOTm 1:3 presented the lowest total porosity in this image-analysis test (Figure 4-8), while it exhibited the highest void index (Figure 4-6) among 1:3 mortars. The image-analysis test only registers pores above 11 μm, while the void index is

strongly affected by the permeability promoted by the capillary channels ( $> 10 \mu\text{m}$ ). Therefore, the pores in IOTm are predominantly in the range of the capillary and gel pores.

As consequence, the thermal conductivity of IOTm is sharply lower than that of QTZm and REFm. This phenomenon is possibly related to the greater phonon scattering promoted by the increased number of interfaces, collisions with the pore walls, and disconnections in the matrix (Burger, et al., 2016) (Smith, et al., 2013). Finally, mortar QTZm 1:3 presented a system with predominantly medium-size pores, which probably justifies its thermal conductivity close to REFm 1:3 and higher than 1:3 IOTm, despite the higher total porosity.

Despite presenting the same entrained air content in the fresh state (Figure 4-4), IOTm 1:1:6 and 1:2:9 presented high porosity value in the hardened state than IOTm 1:3, considering both the image analysis (Figure 4-8) and the void index results (Figure 4-6). Since no air-entraining or foam-inducing admixtures were added to these mortars, this result indicates that the pressure method is not accurate to evaluate the entrained air content of mortars with this type of aggregate. Therefore, the pore system exhibited in IOTm is probably related to the high specific area (related to the fineness and morphological properties), the filler effect and the high water retention promoted by the IOT. These factors possibly led to the formation of a larger number of smaller pores.

Figure 4-10 presents SEM images that show the configuration observed in the quantitative analysis. Among the hydration products, the pore system of each mortar is observed (in black). In general, the reference mortars present a more compact matrix, with fewer amounts of isolated bigger voids. QTZm mortars present a wider range of pores sizes and shapes. Finally, the SEM images show that mortars with IOT presented a significant number of pores smaller than  $11 \mu\text{m}$ , as expected. With the increase in lime content, a refinement of pores is observed, confirming the results for thermal conductivity (Figure 4-7) and pore analysis (Figure 4-8 and Figure 4-9).

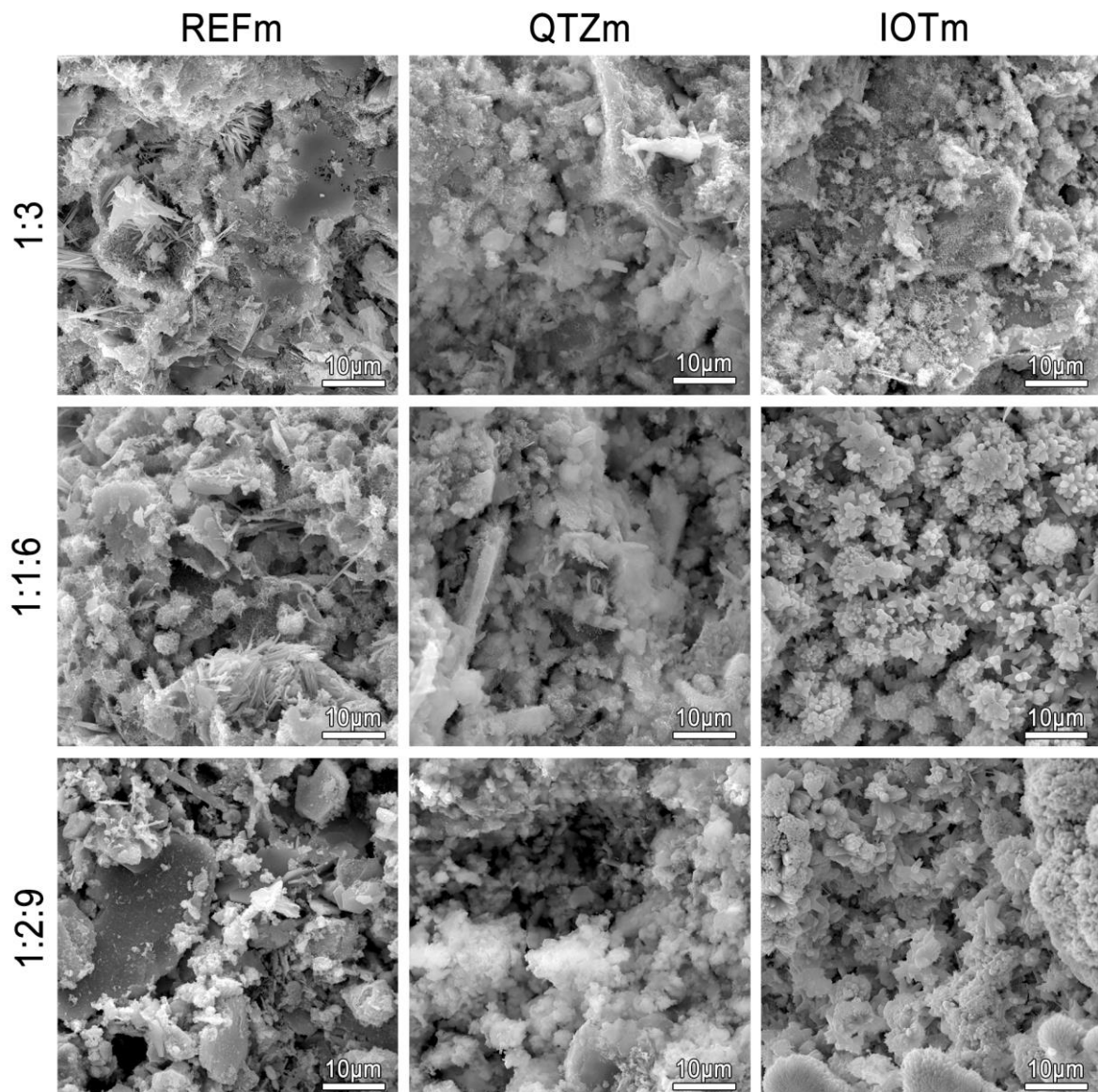


**Figure 4-10 – SEM images of the mortars – 5000x magnification**

#### 4.5 SPECIFIC HEAT

The specific heat of the conventional and non-conventional mortars is presented in Figure 4-11. No clear trend is observed between the results of specific heat and those of thermal conductivity (Figure 4-7). This fact is probably due to the physical mechanisms behind each property. Thermal conduction corresponds to the transfer of the vibrational energy of a particle to adjacent particles (Burger, et al., 2016); while the specific heat of a substance relates to the manner in which the internal energy of its constituents is distributed (Gopal, 1966).

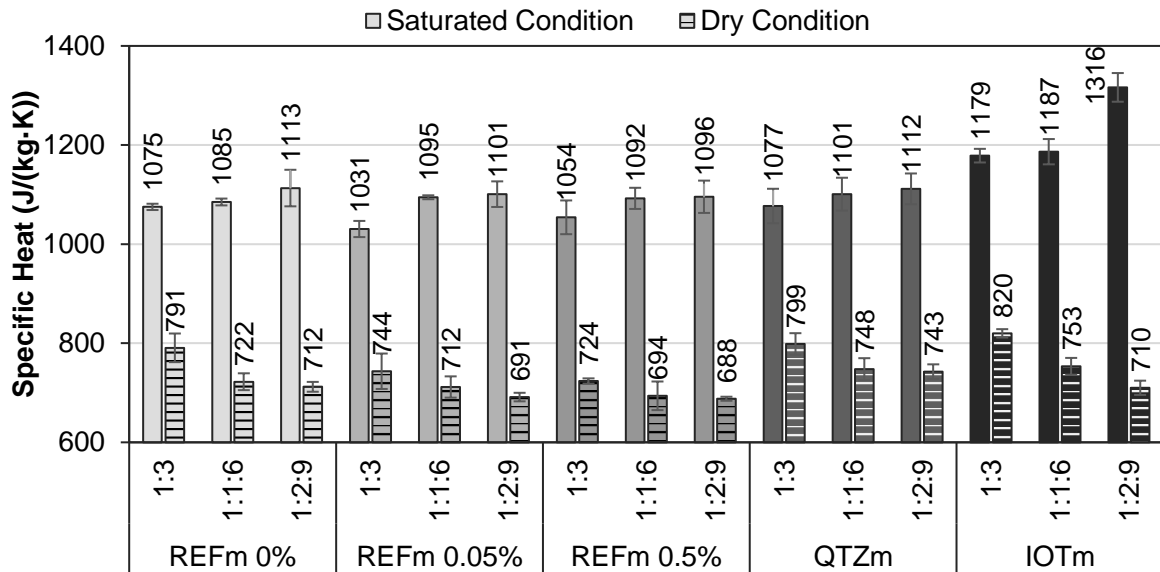


**Figure 4-11 – Saturated and oven-dried specific heats of mortars produced with natural aggregate (REFm) with 0%, 0.05% and 0.5% AEA content; friable quartzite (QTZm) and iron ore tailings (IOTm).**

Initially, it is observed that the dry specific heats of all samples fall within the expected from their chemical composition, between 600 and 900 J/(kg·K). In general, QTZm presented a slightly higher dry specific heat than REFm, possibly due to the higher quartz (740 J/(kg·K)) and kaolinite (974 J/(kg·K)) contents of QTZ in relation to river sand. IOTm demonstrates the highest result, 820 J/(kg·K), probably a function of the chemical composition of IOT, with relatively high contents of kaolinite and gibbsite (1180 J/(kg·K)). The results obtained for REFm were in agreement with the reported by Li et al. (2013).

The dry specific heat presents a decreasing trend with the increase in lime content (from mortar 1:3 to 1:2:9) and with the addition of AEA (REFm 0.05% and 0.5%). These results are initially unexpected since mortars with higher AEA and lime content presented higher void indexes (Figure 4-6), and the air has higher specific heat than the cement paste, respectively 1005 J/(kg·K) and 700-800 J/(kg·K) (Xu & Chung, 2000a). Again, the microstructure of the matrix is probably the main factor influencing the results.

As previously mentioned, hydrated lime enhances water retention (Mehta & Monteiro, 2014) (Sébaïbi, et al., 2003). Matrices with more water in the fresh state will present more capillary channels when excess water evaporates during curing, generating an interconnected pore system. In turn, an interconnected pore system facilitates the evaporation of unbound water (approximately 4200 J/(kg·K)) from the matrix during the drying of the samples. Therefore, the facilitated exit of water from the matrices with higher

lime content and AEA led to a reduction in their overall specific heat. This result is corroborated by Mendes et al. (2017), who verified a greater shrinkage of mortars as the air entrainment increases.

Confirming this observation, the opposite effect is observed in the saturated condition. When the pore system is filled by water, the higher the water absorption of the samples, promoted by an interconnected pore system, the higher their specific heat. This is a result of the much higher specific heat of water (over 4 times that of the cement hydration products and the air) filling the pores.

It is noticeable that the difference between the specific heat values in dry and saturated conditions are much more significant than among the dry specific heat from different aggregate types and mixture proportions. This affirmation is in agreement with the reported by Neville (2012) for concretes – that their specific heat is little affected by the mineralogical properties of the aggregate, but is substantially increased if the moisture content of the concrete increases. The difference between this property in dry and saturated conditions is highlighted in Figure 4-12.

The trend on this graph follows closely that of the void index and water absorption (Figure 4-6). The higher the porosity of the mortars, the larger the difference between the specific heat on dry and saturated conditions. On average, the specimens when saturated presented a specific heat 48% higher than when dry. It reaches 620 J/(kg·K) or 87% for mortar IOTm 1:2:9. This is a direct effect of lime content, w/b content and the microstructure generated by the aggregates.

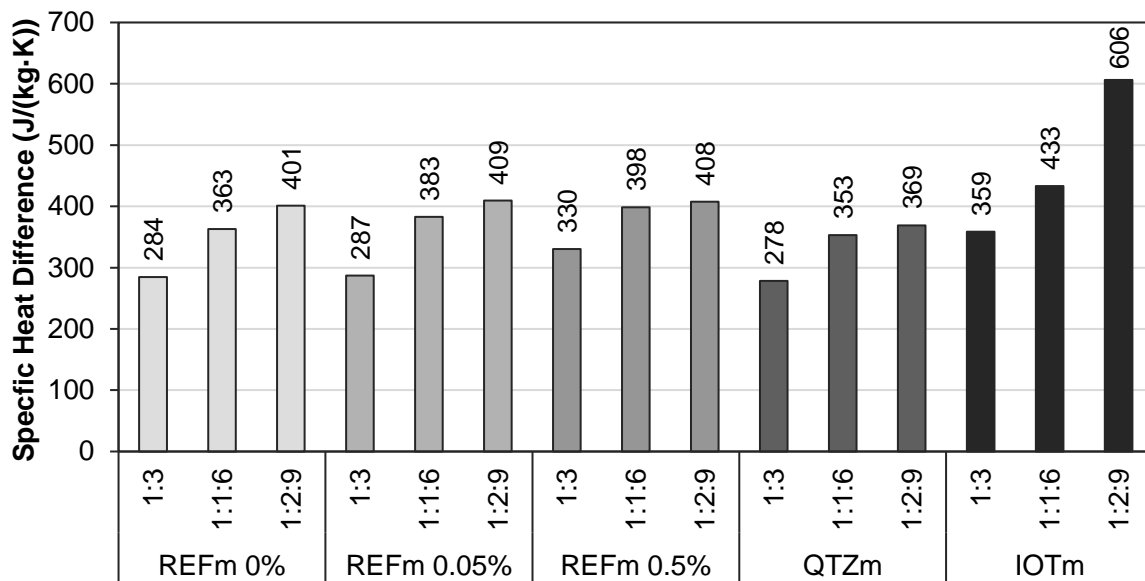


**Figure 4-12 - Difference between the average specific heat on saturated and dry conditions of mortars produced with natural aggregate (REFm) with 0%, 0.05% and 0.5% AEA content; friable quartzite (QTZm) and iron ore tailings (IOTm).**

#### 4.6 DISCUSSIONS ON THE ENERGY PERSPECTIVE

The reduction of the thermal conductivity is important to improve the thermal performance of the buildings, as it reduces the heat transfer rate between the internal and external environments. In addition to improving habitability, this factor promotes the reduction of the energy employed in conditioning over the operation years of the construction (Carabaño, et al., 2017) (Bustamante, et al., 2009) (Lamberts, et al., 1997).

In the aspect of thermal storage and energy-efficient design, Figure 4-13 shows the energy density (the product between dry specific heat and specific gravity) of the mortars. A high value of energy density means a high ability for retaining heat, what is desirable for energy conservation in buildings (Song, et al., 2018) (de Gracia & Cabeza, 2015). Therefore, construction materials with high energy density would leave the building less exposed to the variation of the external temperature. On the other hand, in tropical regions, a reduced energy density prevents overheating during the night (Lam, et al., 2008) (Lamberts, et al., 1997) and is, thus, rather beneficial.

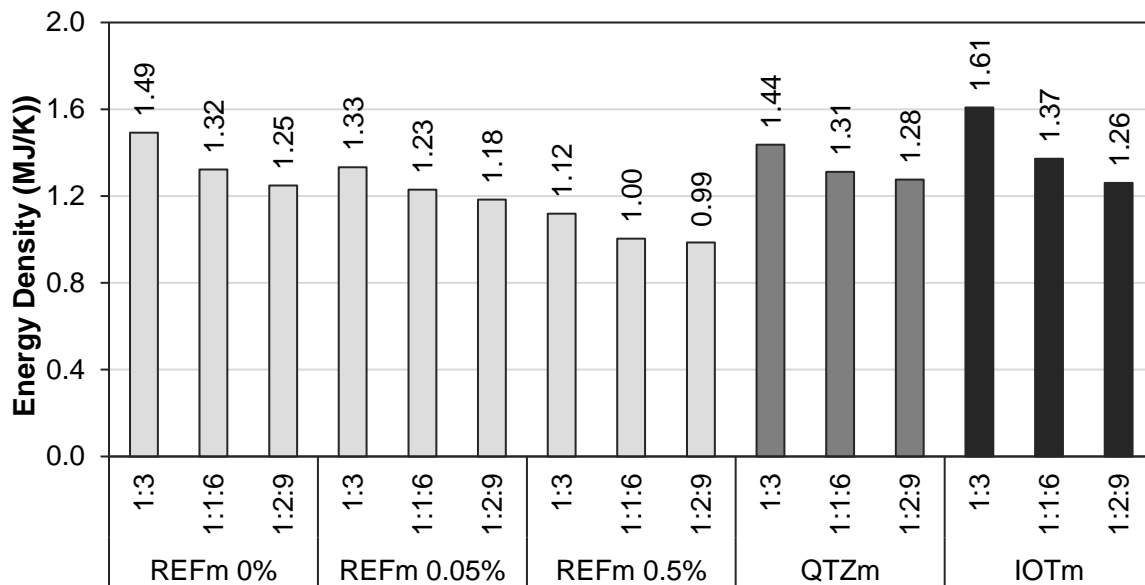


**Figure 4-13 – Energy density (on the dry condition) of mortars produced with natural aggregate (REFm) with 0%, 0.05% and 0.5% AEA content; friable quartzite (QTZm) and iron ore tailings (IOTm).**

Among the mortars studied, IOTm 1:1:6 and 1:2:9 showed the lowest effective thermal conductivity, followed by REFm 0.5% AEA 1:1:6 and 1:2:9. IOTm also presented the highest energy density of all mortars, thus demonstrating the highest thermal inertia amongst them. Mortars with AEA (REFm 0.05% and 0.5%) presented relatively low thermal conductivity and energy density, being indicated for tropical climates with small daily thermal amplitude. QTZm and REFm present similar physicochemical characteristics and similar thermal properties. It means that, although QTZ does not significantly improve the thermal performance, it does not worsen it. Therefore, the use of the studied residues and air-entraining agents potentially contribute to the thermal performance of the building envelope.

Paulsen & Sposto (2013) affirmed that the social housing sector in Brazil presents a higher embodied energy in comparison to other countries (7.2 GJ/m<sup>2</sup> versus the world average of 5.8 GJ/m<sup>2</sup> per 50 years). In this scenario, the incorporation of non-conventional cement-based composites can a) decrease the energy consumption of the buildings, b) reduce the carbon footprint of the use of natural aggregates, c) mitigate the environmental impacts of the deposit of the residues, and d) decrease the costs associated to these improvements.

Since the lifespan of envelope components are usually larger than service systems, the enhanced thermal performance obtained from the non-conventional mortars is long-lasting and demands low or no maintenance. These results do not depend on (and may even

be improved by) user behaviour. Also, the use of residues demands no changes in the mortars' production or application methods, like PCMs usually do.

In this sense, depending on the temperature fluctuation pattern, design requirements, and location, all non-conventional mortars have potential application in passively improving the thermal performance of buildings. This improved thermal performance potentially leads to a higher comfort of the occupants with lesser need for artificial conditioning (Felix & Elsamahy, 2017) .

Also, the enhanced thermal performance promoted by the non-conventional composites may increase health, productivity, and happiness, thus reducing the social deprivation suffered by families in thermally stressful environments (Patino & Siegel, 2018). The consequences are not only social but also economic and environmental, given the more rational use of resources through lower energy consumption and reuse of residues (Carabaño, et al., 2017) (Triana, et al., 2015). Non-conventional cement-based composites are, thus, durable and stable materials that can passively improve the thermal performance of the building during its whole lifecycle.

It should be noticed that, even for reference mortars (REFm 0%), a significant difference is observed between the experimental results (0.82-1.26 W/(m·K)) and the thermal conductivity value of conventional mortars provided by Brazilian standard NBR 15220: 1.15 W/(m·K) (ABNT, 2003). The same deviation occurs concerning the experimental specific heat of conventional mortars (712-791 J/(kg·K) in the dry state and 1075-1113 J/(kg·K) in the saturated condition) versus the generic value provided by NBR 15220: 1000 J/(kg·K) (ABNT, 2003). Additionally, the standards do not mention the methodology for obtaining these properties, the mixture proportion referred to, neither the moisture condition considered. These discrepancies highlight the importance of updated, experimental results when evaluating the thermal performance of buildings.

## **4.7 ULTRASONIC PULSE VELOCITY**

### *4.7.1 Average UPV*

Figure 4-14 presents the average results of UPV and specific gravity (density) for mortars with natural aggregate, with varying contents of AEA, and for mortars with residues.

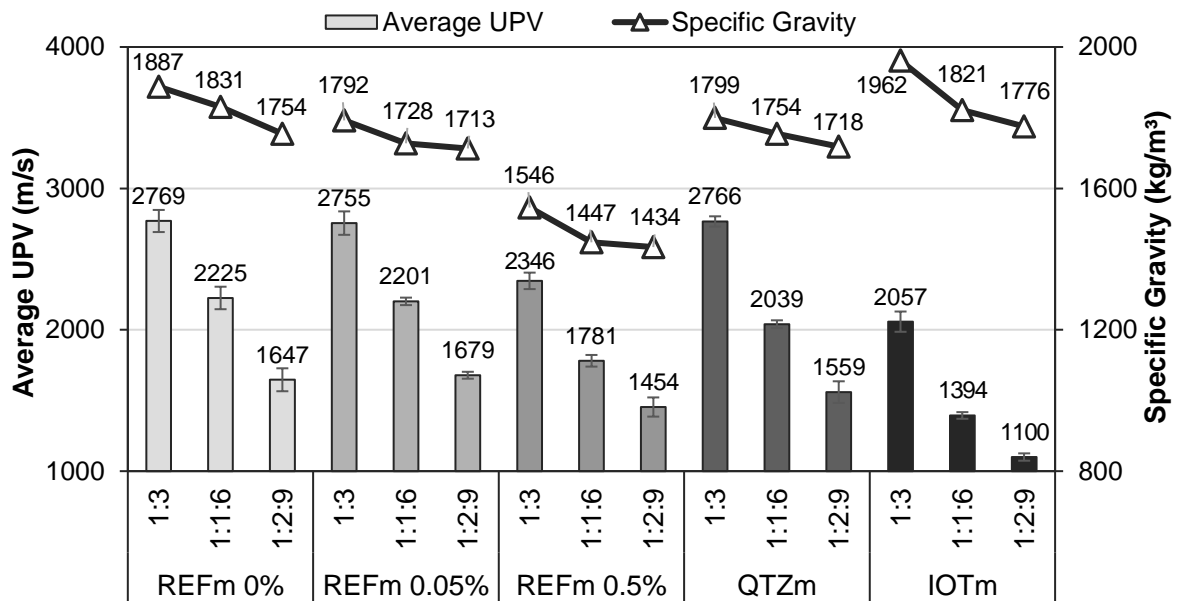


**Figure 4-14 – Average UPV and average specific gravity of mortars produced with natural aggregate (REFm) with 0%, 0.05% and 0.5% AEA content; friable quartzite (QTZm) and iron ore tailings (IOTm).**

The UPV trend originates from the increase in reflection and refraction that occur when sound waves interact with interfaces air/aggregates/cement hydration products. The more interfaces (i.e. pores) exist and the lower the rigidity of the sample, the longer will be the transit time of the ultrasonic pulses (ACI Committee, 2013) (Komlos, et al., 1996). These phenomena explain the decrease of UPV of mortars with high AEA and lime contents. A similar relationship between porosity and UPV was observed by Lafhaj, et al. (2006) and Lafhaj & Goueygou (2009) for mortars, and by Punurai, et al. (2007) for cement pastes. All these authors verified that the pulse velocity decreases with porosity and permeability.

The lime promotes water retention, which contributes to an increased and refined porosity (Mehta & Monteiro, 2014) (Fontes, et al., 2016) (Sébaïbi, et al., 2003), as noticed in the thermal conductivity results (Figure 4-7). As consequence, both the specific gravity and the UPV of all mortars are reduced when the lime content is increased from mixtures 1:3 to 1:2:9.

For the REFm mortars with varying AEA content, it is observed that the specific gravity decreases slightly from mortars without AEA (0%) to those with 0.05% AEA; on the other hand, there is a pronounced difference when the AEA content is increased to 0.5%. This reduction is due to the effects of the AEA, and stabilising pores from the fresh to the

hardened state and reducing the weight of the matrix (Mendes, et al., 2017) (Ouyang, et al., 2008) (Du & Folliard, 2005).

Mortars REFm 0.05%, however, behaved abnormally. These mortars presented UPV values similar or higher than REFm 0% AEA, even though they presented, on average, 5% lower specific gravity and 5% higher void index (Figure 4-6). This behaviour is a combination of the effects of air-entrainment promoted by the AEA with the reduction on the w/b ratio also promoted by this admixture (Figure 4-3).

On the one hand, the AEA increases the porosity of the matrix by stabilising air bubbles. On the other hand, the AEA improves workability, leading to a reduced w/b ratio, which, in turn, decreases porosity and increases mechanical properties (Mendes, et al., 2019) (Mendes, et al., 2017) (Łaźniewska-Piekarczyk, 2012). In high AEA concentrations (0.5%), the first effect (porosity increase) outweighs the second (lower w/b ratio). In low AEA concentrations (0.05%), these two phenomena culminated in a slightly more porous matrix (as shown by their void index), but their refined pore system promoted by a low w/b content did not significantly affect their elastic modulus (thus maintaining similar UPV values).

Mortars with QTZ followed the trend formerly established in the thermal conductivity tests: values usually similar and slightly lower than REFm 0%. However, the remarkably low UPV verified for IOTm in comparison to REFm 0% is initially unexpected, since IOTm presents similar or higher specific gravity than REFm; and IOT presents a much higher apparent specific gravity than natural river sand.

These results can be explained by the pore system formed within the matrices, as shown by the previous microstructural analysis. In general, the reference mortars (REFm 0%) present a more compact matrix, with fewer amounts of isolated bigger voids. For IOTm, the filler effect and lower water mobility promoted by the IOT led to the formation of a larger number of interconnected capillary pores in the mortars. The elastic properties of composite materials vary depending on the pore volume and size, as well as the connections between them (Kumar & Bhattacharjee, 2003) (Roberts & Garboczi, 2000). The particular pore system of IOTm thus resulted in the lowest UPV values among all tested mortars. The increase in lime content emphasised this effect.

#### 4.7.2 Thermal Conductivity versus Specific gravity

Initially, Figure 4-15 presents the plot thermal conductivity versus specific gravity of all mortars produced – with the different aggregates, as well as with different AEA contents.

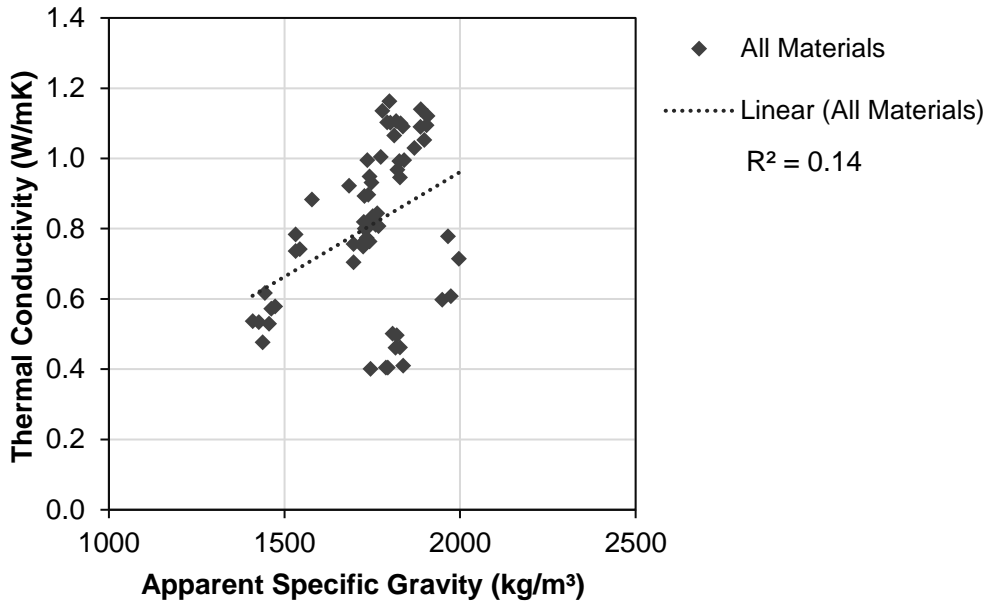


**Figure 4-15 – Relationship between thermal conductivity and specific gravity of all mortars produced**

It is observed that, combined, the values show a large degree of scattering and a low coefficient of determination ( $R^2 = 0.14$ ). This result highlights the influence of the type of matrix in this property. Since the aggregates present significantly different chemical compositions, specific gravities, particle sizes and shapes, the resulting mortars also present remarkably different structure and pore system.

Figure 4-16 shows the relationship between thermal conductivity and specific gravity when the mortars are broken down by aggregate type. These correlations are now in agreement with the reported in the literature ( $0.8 < R$  or  $R^2 < 0.95$ ) (Marie, 2017) (Liu, et al., 2015) (Demirboga & Gül, 2003).

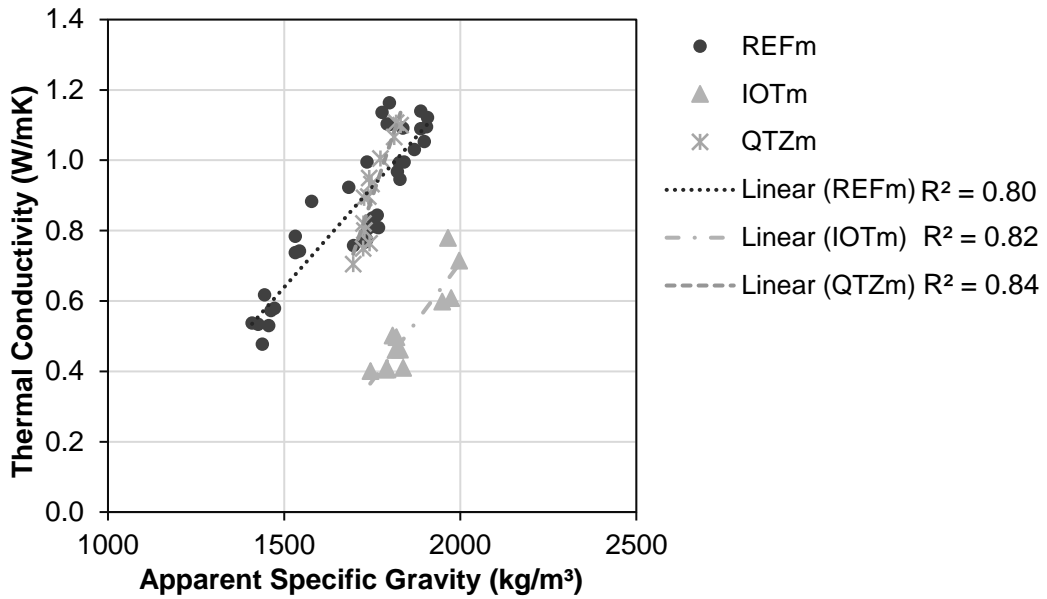


**Figure 4-16 – Relationship between thermal conductivity and specific gravity of mortars, separated by aggregate type.**

#### 4.7.3 Thermal Conductivity versus UPV

Regarding the correlation between thermal conductivity and ultrasonic pulse velocity, Figure 4-17 presents the results obtained for all mortars.

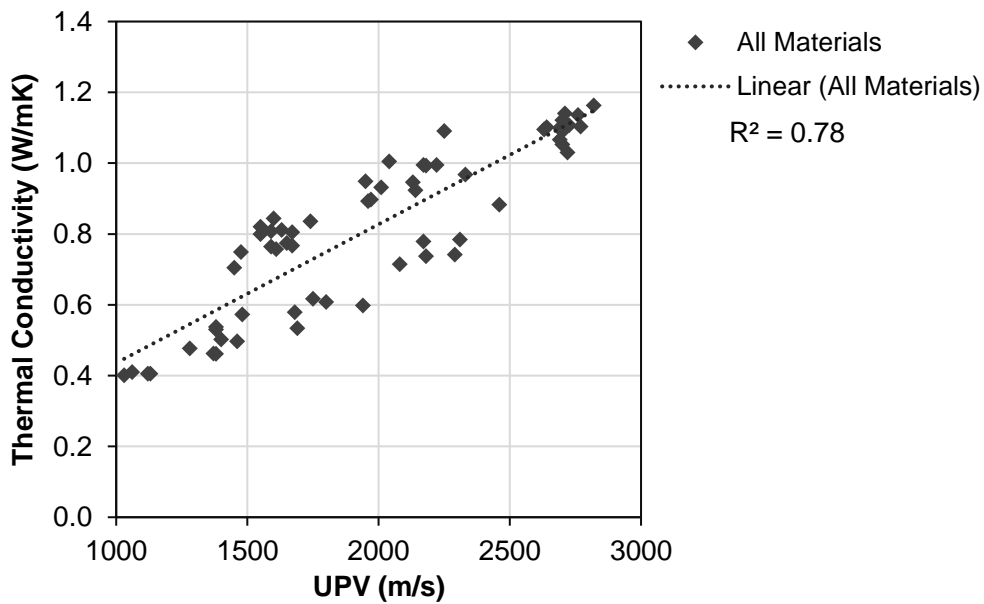


**Figure 4-17 – Relationship between thermal conductivity and Ultrasonic Pulse Velocity (UPV) of all mortars.**

Again, a slightly poor coefficient of determination was observed ( $R^2 = 0.78$ ) when all mixtures were evaluated together; although this result is not as low as the one observed between the thermal conductivity and specific gravity of all matrices ( $R^2 = 0.14$ ).

An improved result was obtained when mortar types were split by aggregate type, as shown by Figure 4-18.

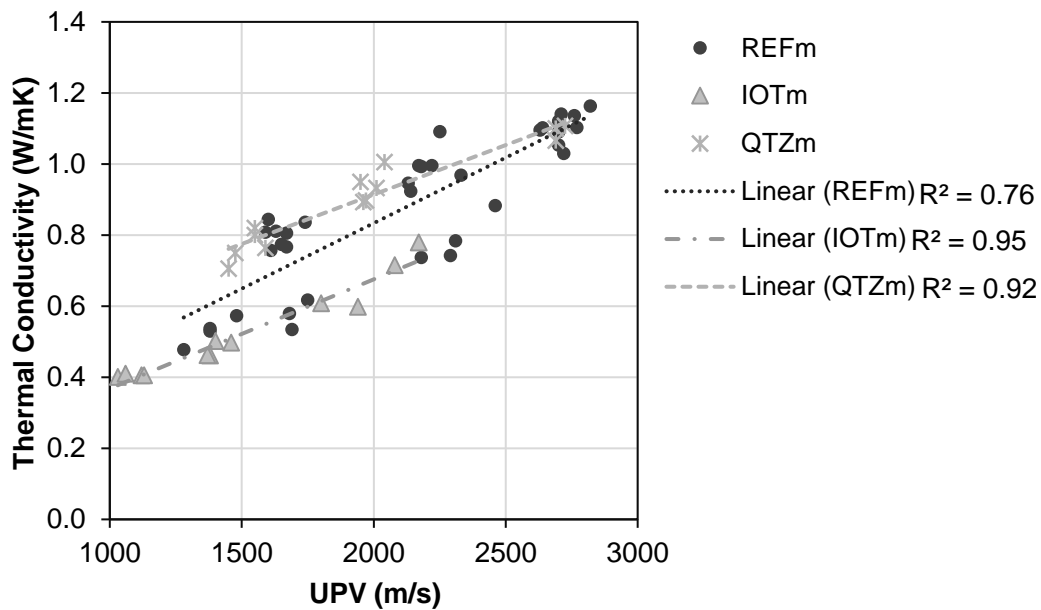


**Figure 4-18 - Relationship between thermal conductivity and Ultrasonic Pulse Velocity (UPV) of mortars, separated by aggregate type.**

The correlation between thermal conductivity and UPV was significantly improved for IOTm ( $R^2 = 0.95$ ) and QTZm ( $R^2 = 0.92$ ). However, REFm still presented an unsatisfactory determination coefficient ( $R^2 = 0.76$ ).

This scenario changed when REFm were then evaluated according to their AEA content, seen in Figure 4-19. By splitting the mortars with none and low AEA content (0% and 0.05%) from those with a relatively high AEA content (0.5%), their determination coefficient grew to 0.92 and 0.93, respectively. Determination coefficients higher than 0.9 are generally accepted as indicators that one property can be sufficiently well predicted by the other. This relationship has only been previously observed by Davraz, et al. (2016) in a brief paper focused on foaming concretes, with  $R^2 = 0.92$ . However, the authors did not include a discussion of the aspects responsible or affecting this interaction.

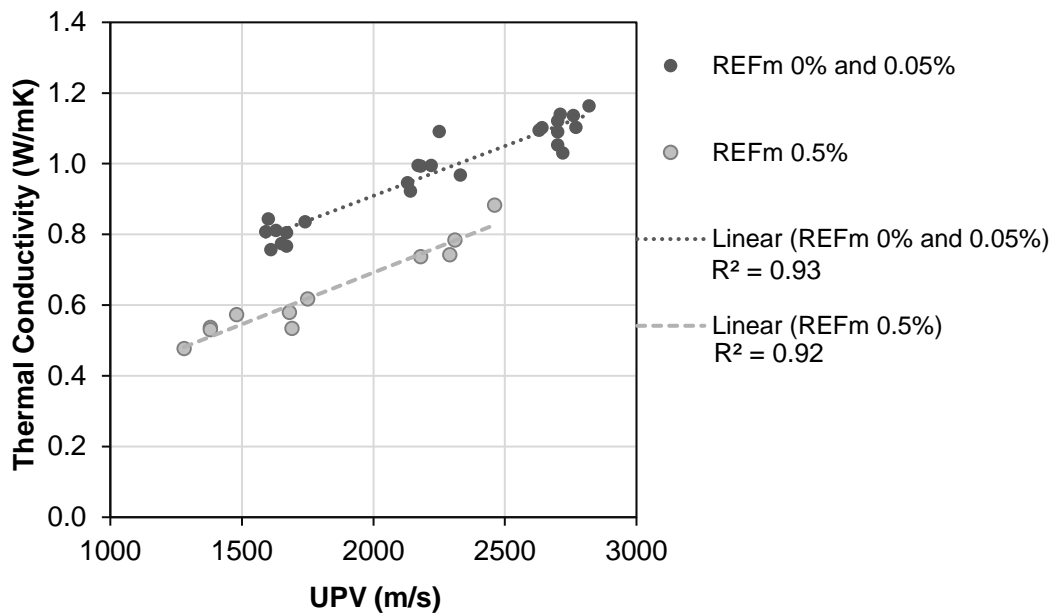


**Figure 4-19 - Relationship between thermal conductivity and UPV of mortars produced with natural aggregate, with 0% and 0.05% AEA and with 0.5% AEA.**

It is known that a high AEA content increases the number of voids with larger diameters together with the total porosity (Mendes, et al., 2017) (Łaźniewska-Piekarczyk, 2012) (Ramachandran, 1995). Larger pores and higher total porosity generate a less rigid and less uniform matrix, meaning that the sonic pulses must travel through longer and more varied paths (ACI Committee, 2013) (Komlos, et al., 1996). In this case, the alterations promoted by the 0.5% AEA content in the mortars' pore system were so significant that they no longer could be compared to the others.

Remarkably, when separated by mortar type, the plot 'thermal conductivity x UPV' (Figure 4-18 and Figure 4-19) presented better correlation values than 'thermal conductivity x Specific gravity' (Figure 4-16). This is possibly due to the fact that the apparent specific gravity is only influenced by the constituents' densities and total porosity, while UPV and thermal conductivity also depend on the resulting pore system (sizes, orientation and interconnection) (Smith, et al., 2013) (Francl & Kingery, 1954).

Regarding testing conditions, it should be noticed that, while thermal conductivity testing with the HFM equipment took 2-3h per specimen, the UPV only requires a few minutes. This is an important advantage of the UPV method. Additionally, although the current results are based on laboratory-scale correlations, the lightness and flexibility of the UPV equipment allow it to be used *in situ* as well. Techniques and calibration curves for direct and indirect measurements can now be developed for conventional wall systems. This

possibility would allow a quick non-destructive assessment of the thermal conductivity of building envelopes.

In summary, a linear relationship with a satisfactory coefficient of determination was found between thermal conductivity and UPV for mortars. This result is valid for composites with similar components and matrix structure. It is now possible for researchers with materials similar to those studied here to evaluate their thermal conductivity with the curves presented. Additionally, developers of cement-based composites can reduce the time and cost required for the testing of several samples by using the UPV method. Since UPV is a comparative method, it is possible to use thermal conductivity tests for some key samples and use UPV to interpolate the others.

# 5

---

## Chapter 5: Conclusion

## 5 CONCLUSION

---

Several industries worldwide currently hold millions of tonnes of reusable wastes in their deposits. Concomitantly, the construction sector compulsively withdraws from rivers and quarries another millions of tons of aggregates. The financial, environmental and social impacts of these activities can be severely reduced by recycling the residues as construction materials. Several researchers around the world have already investigated the chemical, physical and mechanical properties of many of these residues with successful results.

Now, to further disseminate their use, the current work evaluates the thermal properties of non-conventional cement-based composites. To this purpose, we investigated three mortar mixes (1:3, 1:1:6 and 1:2:9); three types of aggregates (river sand, iron ore tailings, and friable quartzite); and three dosages of air-entraining admixture (0%, 0.05% and 0.5%). The materials' proportions, chemical compositions, sizes and shapes influence the microstructure of the matrix, which in turn result in a greater/lesser heat transfer potential.

In this sense, the main findings can be summarised as follows:

- Within the mortars with air-entraining admixture (AEA), REFm 0.05% and 0.5%, more porous mortars led to lower thermal conductivity (up to 40%), due to the low thermal conductivity of air.
- Among the mortars with different aggregates (REFm, QTZm, and IOTm), pores below 20  $\mu\text{m}$  were more effective than larger pores in reducing the thermal conductivity. This observation was verified even if the specific gravity (density) of the mortar was high. This result is a consequence of the phonon scattering phenomenon, enhanced in the matrices containing a higher number of smaller pores and capillary channels, and hence, more interfaces.
- An increased lime content, together with filler effect (QTZ and IOT) and water retention (IOT) promoted by the aggregates led to a refined pore system. These characteristics were especially marked for IOTm, which thus presented the lowest thermal conductivity among all the tested aggregates (0.75 – 0.55 W/(m·K), up to 50% reduction from REFm).
- Among the studied mixtures, the higher the lime content, the lower the thermal conductivity and the dry specific heat, due to the elevated porosity and refinement of pores promoted by the lime.

- Among the materials tested, mortars with IOT presented the highest specific heats (1179 – 1316 J/(kg·K) in the saturated condition).
- The higher the porosity of the mortars, the higher their specific heat in the saturated condition, and the higher the difference between saturated and dry conditions.
- Therefore, the specific heat is, too, more influenced by the microstructure of the mortars than by their chemical composition or mixture proportion, due to the easiness of inlet/exit of moisture in a more interconnected pore system.
- Since the specific heat of cement-based composites is strongly influenced by the pore system of the matrix and its moisture content, adiabatic calorimetry should preferably be used to evaluate this property. Besides being an inexpensive equipment, the sample's size and non-destructive preparation process maintain the representativity of the microstructure.
- No clear trend was observed between the results of specific heat and thermal conductivity of the mortars, or between their specific heat and density.
- The components, mix proportion and pore system of the composites strongly influenced the UPV as well. The main evidence of this conclusion is the behaviour of IOTm, which presented the lowest values (2057 – 1100 m/s). This outcome is a result of the microstructure generated by the particularities of IOT aggregates.
- A better correlation was found between the UPV and thermal conductivity than between the thermal conductivity and specific gravity of the mortars. The physicochemical characteristics of the aggregates and the pore system of the composites strongly influence the UPV, as they do to the thermal conductivity. On the other hand, the specific gravity is only influenced by the chemical properties and overall porosity of the matrix.
- UPV is a feasible alternative to predict the thermal conductivity of mortars, with a relatively high determination coefficient ( $R^2 > 0.9$ ). The main advantage of this method is the speed of measurement and portability of the equipment.

In summary, the aggregates and admixtures adopted had a significant influence on the thermal properties of the mortars; not only because of their chemical and mineralogical

properties, but mainly due to the microstructure they generated in the composites. In this sense, UPV and adiabatic calorimetry are two cost-effective and efficient alternatives to investigate the thermal conductivity and specific heat of cement-based composites, respectively. They have the advantage of being non-destructive techniques that use macroscopic samples, thus evaluating the microstructure of the composite along with other parameters.

The use of AEA and residues culminated in mortars with similar or improved thermal properties in relation to the reference ones. In this sense, these non-conventional composites can potentially improve energy-efficiency of buildings by passively enhancing the thermal performance of the envelope. More studies related to the impact of the improved thermal properties in real applications, through energy simulation, reduced-scale models or large-scale prototypes should be carried out.

Some other recommendations for further investigations are to study the effect of the pore system on the thermal properties of concretes, and to investigate the effect of additional residues, such as steelmaking slag, recycled aggregates, IOT with varying hematite contents, sewer sludge, among others. Finally, more calibration curves should be built for improving the reliability of the ‘thermal conductivity  $\times$  UPV’ correlation for various materials.

In conclusion, this work seeks to improve the comprehension of the factors affecting the thermal properties of cement-based composites. As consequence, we hope to promote materials with lower environmental impact for buildings and industries, and ultimately contribute to the technological development of cement-based composites.



# 6

---

## Chapter 6: References

## REFERENCES

---

ABNT, 2003. *NBR 15220 - Thermal performance in buildings*. Rio de Janeiro, Brazilian Association of Technical Standards.

ABNT, 2004a. *NBR 10004 - Solid waste - Classification*, Rio de Janeiro: ABNT.

ABNT, 2004b. *NBR 10007 - Sampling of solid waste*, Rio de Janeiro: Brazilian Association of Technical Standards.

ABNT, 2005a. *NBR 13276 - Mortars applied on walls and ceilings - Determination of the consistence index*, Rio de Janeiro: Brazilian Association of Technical Standards.

ABNT, 2005b. *NBR 13280 - Mortars applied on walls and ceilings - Determination of the specific gravity in the hardened stage*, Rio de Janeiro: Brazilian Association of Technical Standards.

ABNT, 2006. *NBR NM 45 - Aggregates - Determination of the unit weight and air-void content*, Rio de Janeiro: Brazilian Association of Technical Standards - ABNT.

ABNT, 2009. *NBR 9778 - Hardened mortar and concrete - Determination of absorption, voids and specific gravity*, Rio de Janeiro: Brazilian Association of Technical Standards.

ABNT, 2013. *NBR 15575 - Residential buildings — Performance*, Rio de Janeiro: Brazilian Association of Technical Standards.

ABNT, 2018. *NBR 16697 - Portland cement - Requirements*, Rio de Janeiro: Brazilian Association of Technical Standards.

ACI Committee, 2013. *ACI 228.2R Nondestructive Test Methods for Evaluation of Concrete in Structures*, s.l.: American Concrete Institute.

Adom-Asamoah, M., Tuffour, Y. A., Afrifa, R. O. & Kankam, C. K., 2014. Strength characteristics of hand-quarried partially-weathered quartzite aggregates in concrete.. *American Journal of Civil Engineering*, 2(5), pp. 134-142.

Akutstu, M. & Sato, N., 1988. Thermophysical properties of building materials and components. In: *Tecnologia de Edificações*. São Paulo: PINI/IPT (in Portuguese), pp. 519-522.

Aligizaki, K. K., 2005. *Pore structure of cement-based materials: testing, interpretation and requirements*.. 1st ed. s.l.:CRC Press.

Allesch, A. & Brunner, P. H., 2014. Assessment methods for solid waste management: A literature review. *Waste Management & Research*, 32(6), pp. 461-473.

Al-Nu'man, B., Aziz, B., Abdulla, S. & Khaleel, S., 2016. Effect of Aggregate Content on the Concrete Compressive Strength - Ultrasonic Pulse Velocity Relationship. *American Journal of Civil Engineering and Architecture*, 4(1), pp. 1-5.

ANEPAC, 2015. *Brazilian Aggregate Market*, São Paulo: National Association of Entities of Producers of Construction Aggregates.

Asadi, I., Shafigh, P., Hassan, Z. F. B. A. & Mahyuddin, N. B., 2018. Thermal conductivity of concrete-A review. *Journal of Building Engineering*, Volume 20, pp. 81-93.

ASTM International, 2018. *ASTM E1269 - Standard Test Method for Determining Specific Heat Capacity by Differential Scanning Calorimetry*, West Conshohocken: American Society for Testing and Materials.

Ávila, J., 2012. *Tailing Dams in Brazil (in Portuguese)*. Rio de Janeiro: CGDB – Bazillian Comitee of Dams .

Bastos, L. A. C., Silva, G. C., Mendes, J. C. & Peixoto, R. A. F., 2016. Using iron ore tailings from tailing dams as road material. *J. Mater. Civ. Eng.*, Issue 10.1061/(ASCE)MT.1943-5533.0001613.04016102.

Benmansour, N. et al., 2014. Thermal and mechanical performance of natural mortar reinforced with date palm fibers for use as insulating materials in building. *Energy and Buildings*, Volume 81, pp. 98-104.

Bodach, S. & Hamhaber, J., 2010. Energy efficiency in social housing: Opportunities and barriers from a case study in Brazil. *Energy Policy*, Stembro.pp. 7898-7910.

Brazil, 2016. *Recommendation No. 014/2016-MPF-GAB / FT*, Brasília: Brazilian Federal Prosecution Service.

Brigaud, F. & Vasseur, G., 1989. Mineralogy, porosity and fluid control on thermal conductivity of sedimentary rocks.. *Geophysical Journal International*, 98(3), pp. 525-542.

Burger, N. et al., 2016. Review of thermal conductivity in composites: mechanisms, parameters and theory.. *Progress in Polymer Science*, Volume 61, pp. 1-28.

Bustamante, W. et al., 2009. Thermal Improvement of Perforated Ceramic Bricks. *Revista de la Construcción*, pp. 8 (1) 24-35.

Cahill, D. G. & Pohl, R. O., 1987. Thermal conductivity of amorphous solids above the plateau.. *Physical review B*, 35(8), p. 4067.

Callister Jr., W., 2001. *Fundamentals of Materials Science and Engineering*. s.l.:John Wiley & Sons, Inc..

Carabaño, R., Hernando, S., Ruiz, D. & Bedoya, C., 2017. Life Cycle Assessment (LCA) of building materials for the evaluation of building sustainability: the case of thermal insulation materials. *Revista de la Construcción*, pp. 16 (1) 22-32.

Carrasco, E. V. M. et al., 2017. Characterization of mortars with iron ore tailings using destructive and nondestructive tests. *Construction and Building Materials*, Volume 131, pp. 31-38.

Carvalho, J. M. F. et al., 2019. More eco-efficient concrete: An approach on optimization in the production and use of waste-based supplementary cementing materials.. *Construction and Building Materials*, Volume 206, pp. 397-409.

Çengel, Y. & Ghajar, A., 2012. *Heat and Mass Transfer: Fundamentals and Applications*. 4a ed. New York: McGraw-Hill.

Cha, J., Seo, J. & Kim, S., 2011. Building materials thermal conductivity measurement and correlation with heat flow meter, laser flash analysis and TCI. *Journal of Thermal Analysis and Calorimetry*, 109(1), pp. 295-300.

Cheng, Y. et al., 2016. Test research on the effects of mechanochemically activated iron tailings on the compressive strength of concrete. *Construction and Building Materials*, Volume 118, pp. 164-170.

Coakley, D., Raftery, P. & Keane, M., 2014. A review of methods to match building energy simulation models to measured data.. *Renewable and sustainable energy reviews*, Volume 37, pp. 123-141.

Corinaldesi, V., Mazzoli, A. & Moriconi, G., 2011. Mechanical behaviour and thermal conductivity of mortars containing waste rubber particles.. *Materials & Design*, 32(3), pp. 1646-1650.

D&R International, 2009. *Buildings energy data book, buildings technologies program, energy efficiency and renewable energy*, s.l.: U.S. Department of Energy.

Davraz, M., Kilincarslan, S., Koru, M. & Tuzlak, F., 2016. Investigation of relationships between ultrasonic pulse velocity and thermal conductivity coefficient in foam concretes.. *Acta Physica Polonica A*, 130(1), pp. 469-470.

de Gracia, A. & Cabeza, L. F., 2015. Phase change materials and thermal energy storage for buildings.. *Energy and Buildings*, Volume 103, pp. 414-419.

Defáveri, K. et al., 2019. Iron ore tailing-based geopolymer containing glass wool residue: A study of mechanical and microstructural properties.. *Construction and Building Materials*, Volume 220, pp. 375-385.

Demirboga, R., 2003. Influence of mineral admixtures on thermal conductivity and compressive strength of mortar. *Energy and Buildings*, p. 35 189–192.

Demirboga, R. & Gül, R., 2003. The effects of expanded perlite aggregate, silica fume and fly ash on the thermal conductivity of lightweight concrete. *Cement and Concrete Research*, Volume 33, p. 723–727.

Demirboga, R., Turkmen, I. & Karakoç, M., 2004. Relationship between ultrasonic velocity and compressive strength for high-volume mineral-admixed concrete. *Relationship between ultrasonic velocity and compressive strength for high-volume mineral-admixed concrete*, Volume 34, p. 2329–2336.

Dias, L. et al., 2017. *REJEITOS DE MINERAÇÃO DE QUARTZITO PARA PRODUÇÃO DE ARGAMASSA COLANTE*. Natal, 22º CBECiMat - Congresso Brasileiro de Engenharia e Ciência dos Materiais.

Dowson, M., Poole, A., Harrison, D. & Susman, G., 2012. Domestic UK retrofit challenge: Barriers, incentives and current performance leading into the Green Deal.. *Energy Policy*, Volume 50, pp. 294-305.

Duan, P., Yan, C., Zhou, W. & Ren, D., 2016. Fresh properties, compressive strength and microstructure of fly ash geopolymer paste blended with iron ore tailing under thermal cycle. *Construction and Building Materials*, Volume 118, pp. 76-88.

Du, L. & Folliard, K. J., 2005. Mechanisms of air entrainment in concrete. *Cement and Concrete Research*, Volume 35, pp. 1463-1471.

Dzaye, E. D., De Schutter, G. & Aggelis, D. G., 2018. Study on mechanical acoustic emission sources in fresh concrete.. *Archives of Civil and Mechanical Engineering*, 18(3), pp. 742-754.

Edraki, M. et al., 2014. Designing mine tailings for better environmental, social and economic outcomes: a review of alternative approaches. *Journal of Cleaner Production*, 1 December, Volume 84, pp. 411-420.

Faleiro, F. F. & Lopes, L. M., 2010. ASPECTS OF IMPACTS OF MINING AND EXPLORATION QUARTZITE IN PIRENÓPOLIS-GO. *Ateliê Geográfico*, 4(11), pp. 148-162.

Faraone, N., Tonello, G. & Furlani, E. M. S., 2009. Steelmaking slag as aggregate for mortars: effects of particle dimension on compression strength. *Chemosphere*, 77(8), pp. 1152-1156.

FEAM, 2009. *Plano de Ação para Sustentabilidade do Setor de Rochas Ornamentais – Quartzito São Thomé das Letras*, Belo Horizonte: State Foundation for the Environment.

Felice, R., Freeman, J. & Ley, T., 2014. Durable Concrete with Modern Air Entraining Admixtures.. *Concrete International*, Volume August, pp. 37-45.

Felix, M. & Elsamahy, E., 2017. The Efficiency of Using Different Outer Wall Construction Materials to Achieve Thermal Comfort in Various Climatic Zones. *Energy Procedia*, Volume 115, pp. 321-331.

Fontes, W. et al., 2018. Iron ore tailings in the production of cement tiles: a value analysis on building sustainability. *Ambiente Construído*, 18(4), pp. 395-412.

Fontes, W., Mendes, J., Silva, S. & Peixoto, R., 2016. Mortars for laying and coating produced with iron ore tailings from tailing dams. *Construction and Building Materials*, Volume 112, p. 988–995.

Francl, J. & Kingery, W. D., 1954. Thermal conductivity: IX, experimental investigation of effect of porosity on thermal conductivity. *Journal of the American Ceramic Society*, Volume 37, pp. 99-107.

Franks, D. M., Boger, D. V., Côte, C. M. & Mulligan, D. R., 2011. Sustainable development principles for the disposal of mining and mineral processing wastes. *Resources Policy*, Volume 36, pp. 114-122.

Fundação João Pinheiro, 2016. *Housing deficit in Brazil 2013-2014*, Belo Horizonte: Centro de Estatística e Informação (In Portuguese).

Fu, X. & Chung, D., 1997. Effects of silica fume, latex, methylcellulose, and carbon fibers on the thermal conductivity and specific heat of cement paste. *Cement and concrete research*, 27(12), pp. 1799-1804.

Galvão, J. L. B. et al., 2018. Reuse of iron ore tailings from tailings dams as pigment for sustainable paints. *Journal of Cleaner Production*, Volume 200, pp. 412-422.

Givoni, B., 1992. Comfort, climate analysis and building design guidelines. *Energy and buildings*, 18(1), pp. 11-23.

Gomes, R. B., De Tomi, G. & Assis, P. S., 2016. Iron ore tailings dry stacking in Pau Branco mine, Brazil.. *Journal of Materials Research and Technology*, 5(4), pp. 339-344.

Gonçalves, D. R. et al., 2016. Evaluation of the economic feasibility of a processing plant for steelmaking slag.. *Waste Management & Research*, 34(2), pp. 107-112.

Gopal, E., 1966. *Specific Heats at Low Temperatures*. New York: Springer Science & Business Media.

GOV.UK, 2017. *Energy consumption in the UK*, London: Department for Business, Energy & Industrial Strategy.

Guimarães, G. & Philippi, P., 1993. *Métodos transientes para a medição de propriedades termofísicas de materiais*. Florianópolis, ANTAC ENCONTRO NACIONAL DE CONFORTO NO AMBIENTE CONSTRUÍDO, pp. 131-137.

Guyot, G., Sherman, M. H. & Walker, I. S., 2018. Smart ventilation energy and indoor air quality performance in residential buildings: A review. *Energy & Buildings*, Volume 165, p. 416–430.

Hall, M., 2010. *Materials for energy efficiency and thermal comfort in buildings*. s.l.:Elsevier.

Han, Z. & Fina, A., 2011. Thermal conductivity of carbon nanotubes and their polymer nanocomposites: a review.. *Progress in polymer science*, 36(7), pp. 914-944.

Horai, K. & Simmons, G., 1969. THERMAL CONDUCTIVITY OF ROCK-FORMING MINERALS. *EARTH AND PLANETARY SCIENCE LETTERS*, Volume 6, pp. 359-368.

IEA, 2013. *Transition to Sustainable Buildings - Strategies and Opportunities to 2050*, Paris: International Energy Agency .

Incropera, F., 2007. *Fundamentals of heat and mass transfer*. 6<sup>a</sup> ed. s.l.:John Wiley.

Jenkins, H. & Yakovleva, N., 2006. Corporate social responsibility in the mining industry: Exploring trends in social and environmental disclosure.. *Journal of cleaner production*, 14(3-4), pp. 271-284.

Jones, R., 1962. *Non destructive testing of concrete*, s.l.: University Press.

Kaviany, M., 2012. *Principles of heat transfer in porous media*. 1st ed. s.l.:Springer Science & Business Media.

Khan, M., 2002. Factors affecting the thermal properties of concrete and applicability of its prediction models. *Building and Environment*, Volume 37, p. 607–614.

Khedari, J., Suttisonk, B., Pratinthong, N. & Hirunlabh, J., 2001. New lightweight composite construction materials with low thermal conductivity. *Cement and Concrete Composites*, 23(1), pp. 65-70.

Kim, K., Jeon, S., Kim, J. & Yang, S., 2003. An experimental study on thermal conductivity of concrete. *Cement and Concrete Research*, Volume 33, p. 363–371.

Komlos, K. et al., 1996. Ultrasonic Pulse Velocity Test of Concrete Properties as Specified in Various Standards. *Cement and Concrete Composites* , Volume 18, pp. 357-364.

Kośny, J. & Kossecka, E., 2002. Multi-dimensional heat transfer through complex building envelope assemblies in hourly energy simulation programs. *Energy and Buildings*, 34(5), pp. 445-454.

Kossoff, D. et al., 2014. Mine tailings dams: characteristics, failure, environmental impacts, and remediation.. *Applied Geochemistry*, Volume 51, pp. 229-245.

Kumar, R. & Bhattacharjee, B., 2003. Porosity, pore size distribution and in situ strength of concrete. *Cement and Concrete Research*, Volume 33, pp. 155-164.

Lafhaj, Z. & Goueygou, M., 2009. Experimental study on sound and damaged mortar: Variation of ultrasonic parameters with porosity.. *Construction and building materials*, 23(2), pp. 953-958.

Lafhaj, Z., Goueygou, M., Djerbi, A. & Kaczmarek, M., 2006. Correlation between porosity, permeability and ultrasonic parameters of mortar with variable water/ cement ratio and water content. *Cement and Concrete Research*, 36(4), pp. 625-633.

Lamberts, R., Dutra, L. & Pereira, F., 1997. *Energy Efficiency in Architecture*, Rio de Janeiro: Eletrobrás Procel.

Lam, J., Wan, K., Tsang, C. & Yang, L., 2008. Building energy efficiency in different climates. *Energy Conversion and Management*, 49(8), pp. 2354-2366.

Larkin, B. K. & Churchill, S. W., 1959. Heat transfer by radiation through porous insulations.. *AIChE Journal*, 5(4), pp. 467-474.

Łaźniewska-Piekarczyk, B., 2012. The influence of selected new generation admixtures on the workability, air-voids parameters and frost-resistance of self compacting concrete. *Construction and Building Materials*, Volume 31, pp. 310-319.

Lea, F., 1971. *The Chemistry of Cement and Concrete*. Nova York: Chemical Publishing Company.

Ledhem, A., Dheilily, R. M., Benmalek, M. L. & Quéneudec, M., 2000. Properties of wood-based composites formulated with aggregate industry waste. *Construction and Building Materials*, 14(6-7), pp. 341-350.

Li, M., Wu, Z. & Tan, J., 2013. Heat storage properties of the cement mortar incorporated with composite phase change material.. *Applied energy*, Volume 103, pp. 393-399.

Li, S., Jones, B., Thorpe, R. & Davis, M., 2016. An investigation into the thermal conductivity of hydrating sprayed concrete.. *Construction and Building Materials*, Volume 124, pp. 363-372.

Liu, K. et al., 2015. An experimental study on thermal conductivity of iron ore sand cement mortar.. *Construction and Building Materials*, Volume 101, pp. 932-941.

Ma, B. G., Cai, L. X., Li, X. G. & Jian, S. W., 2016. Utilization of iron tailings as substitute in autoclaved aerated concrete: physico-mechanical and microstructure of hydration products.. *Journal of Cleaner Production*, Volume 127, pp. 162-171.

Manzano-Agugliaro, F., Montoya, F. G., Sabio-Ortega, A. & García-Cruz, A., 2015. Review of bioclimatic architecture strategies for achieving thermal comfort. *Renewable and Sustainable Energy Reviews*, Volume 49, p. 736–755.

Marie, I., 2017. Thermal conductivity of hybrid recycled aggregate–Rubberized concrete. *Construction and Building Materials*, Volume 133, pp. 516-524.

Marinho, A. et al., 2017. Ladle Furnace Slag as Binder for Cement-based composites. *Journal of Materials in Civil Engineering*, 29(11), p. 04017207.

McHugh, J., Fideu, P., Herrmann, A. & Stark, W., 2010. Determination and review of specific heat capacity measurements during isothermal cure of an epoxy using TM-DSC and standard DSC techniques. *Polymer Testing*, 29(6), pp. 759-765.

McPhail, G., 2006. *Implications of different tailings disposal options on future rehabilitation.*, Brisbane: Mine tailings 2006.

Mehta, P. & Monteiro, P. J. M., 2014. *Concrete: Microstructure, Properties, and Materials*. 2<sup>a</sup> ed. São Paulo: IBRACON.

Mendes, J., 2013. *Post Occupancy Evaluation of a Retrofit for the Future project: 55 Wolvercote Road, Thamesmead*. Londres: Brunel University (Trabalho de Final de Período Sanduíche).

Mendes, J. et al., 2017. Mechanical, rheological and morphological analysis of cement-based composites with a new LAS-based air entraining agent. *Construction & Building Materials*, Volume 145, p. 648–661.

Mendes, J. et al., 2019. Macroporous Mortars for Laying and Coating. *Revista de la Construcción*, 18(1), pp. 29-41.

Ministry of Mines and Energy, 2018. *Brazilian Mineral Yearbook 2018*, Brasília: Federal government.

NETZSCH, 2014. *Heat Flow Meter – HFM 436 Lambda*. Selb: NETZSCH.

NETZSCH, 2015. *Determinação da Difusividade Térmica e da Condutividade Térmica*. [Online]

Available at: <https://www.netzsch-thermal-analysis.com/pt/landing-pages/determinacao-da->

[Accessed 20 12 2015].

Neville, A. M., 2012. *Properties of concrete*. 5th ed. London: Longman.

Oliveira, R., Souza, R. & Silva, R., 2017. Issues to be improved on the Thermal Performance Standards for Sustainable Buildings consolidations: an overview of Brazil. *Energy Procedia*, Volume 111, pp. 71-80.

Olivier, D., 2001. *Building in ignorance - Demolishing complacency: improving the energy performance of 21st century homes*, Leominster: Energy Efficiency Advice Services for Oxfordshire.

O'Neill, M. J., 1966. Measurement of Specific Heat Functions by Differential Scanning Calorimetry.. *Analytical chemistry*, 38(10), pp. 1331-1336.

Ouyang, X., Guo, Y. & Qiu, X., 2008. The feasibility of synthetic surfactant as an air entraining agent for the cement matrix. *Construction and Building Materials*, Volume 22, p. 1774–1779.

Pacheco, R., Ordóñez, J. & G., M., 2012. Energy efficient design of building: A review. *Renewable and Sustainable Energy Reviews*, Volume 16, p. 3559–3573.

Pacheco-Torgal, F. et al., 2017. *Cost-Effective Energy Efficient Building Retrofitting*. 1<sup>a</sup> ed. s.l.:Woodhead Publishing.

Pahuja, O., 2005. *Solid State Physics*. s.l.:Firewall Media.

Passuello, A. C. B., Oliveira, A. F. D., Costa, E. B. D. & Kirchheim, A. P., 2014. Application of the Life Cycle Assessment in the analysis of the environmental impacts of innovative building materials: a case study of the carbon footprint of alternative clinkers. *Ambiente Construído (in Portuguese)*, October/December, 14(n°4), pp. 7-20.

Patinoa, E. D. L. & Siegel, J. A., 2018. Indoor environmental quality in social housing: A literature review. *Building and Environment*, Volume 131, p. 231–241.

Paulsen, J. S. & Sposto, R. M., 2013. A life cycle energy analysis of social housing in Brazil: Case study for the program “MY HOUSE MY LIFE”. *Energy and Buildings*, Volume 57, p. 95–102.

Pereira, O. C. & Bernardin, A. M., 2012. Ceramic colorant from untreated iron ore residue. *Journal of Hazardous Materials*, Volume 233-234, pp. 103-111.

Philip, P. & Fagbenle, L., 2014. DESIGN OF LEE’S DISC ELECTRICAL METHOD FOR DETERMINING THERMAL CONDUCTIVITY OF A POOR CONDUCTOR IN THE FORM OF A FLAT DISC. *International Journal of Innovation and Scientific Research*, 9(2), pp. 335-343.

Popovics, S., Rose, J. & Popovics, S., 1990. The behavior of ultrasonic pulses in concrete. *Cement and Concrete Research*, Volume 20, pp. 259-270.

Powers, T., 1968. *The Properties of Fresh Concrete*. New York: John Wiley & Sons.

Punurai, W. et al., 2007. Characterization of multi-scale porosity in cement paste by advanced ultrasonic techniques. *Cement and Concrete Research*, 37(1), pp. 38-46.

Química Amparo LTDA, 2011. *FISPQ - Detergente Ypê Neutro*. [Online] Available at: [http://www.ype.ind.br/wp-content/uploads/2014/08/FISPQ\\_LAVA-LOUCAS\\_YPE\\_CLEAR.zip](http://www.ype.ind.br/wp-content/uploads/2014/08/FISPQ_LAVA-LOUCAS_YPE_CLEAR.zip)

[Accessed 14 setembro 2015].

Rabbani, A., Jamshidi, S. & Salehi, S., 2014. An automated simple algorithm for realistic pore network extraction from micro-tomography images.. *Journal of Petroleum Science and Engineering*, Volume 123, pp. 164-171.

Raheem, A. A. & Adesanya, D. A., 2011. A study of thermal conductivity of corn cob ash blended cement mortar.. *The Pacific Journal of Science and Technology*, 12(2), pp. 106-111.

Ralid, R., 2003. *Post Occupancy Evaluation as a tool for Better Quality Low-income Housing*, Brasília: Secretaria de Estado de Habitação, Regularização e Desenvolvimento Urbano.

Ramachandran, V., 1995. *Concrete Admixtures Handbook*. 2a ed. New Jersey: Noyes Publications.

Ramirio, R. F., Pamplona, D. R. P., Francklin Junior, I. & Collares, E. G., 2008. Estudo comparativo de rejeitos de quartzito com outros agregados comercialmente utilizados como materiais de construção no Sudoeste de Minas Gerais. *Ciência et Praxis*, 1(1), pp. 25-32.

Roberts, A. & Garboczi, E., 2000. Elastic Properties of Model Porous Ceramics. *Journal of the American Ceramic Society*, 83(12), p. 3041–3048.

Rosen, B. W. & Hashin, Z., 1970. Effective thermal expansion coefficients and specific heats of composite materials. *International Journal of Engineering Science*, 8(2), pp. 157-173.

Sadineni, S., Madala, S. & Boehm, R., 2011. Passive building energy savings: A review of building envelope components. *Renewable and Sustainable Energy Reviews*, Volume 15, p. 3617–3631.

Saint-Pierre, F., Philibert, A., Giroux, B. & Rivard, P., 2016. Concrete Quality Designation based on Ultrasonic Pulse Velocity. *Construction and Building Materials*, Volume 125, p. 1022–1027.

Sant'Ana Filho, J. N. et al., 2017. Technical and Environmental Feasibility of Interlocking Concrete Pavers with Iron Ore Tailings from Tailings Dams. *Journal of Materials in Civil Engineering*, 29(9), p. 04017104.

Santos, D., 2015. *Substituição total do agregado natural por quartzito friável para produção de argamassas mistas de assentamento e revestimento*, Ouro Preto: Federal University of Ouro Preto (Master's Thesis).

Schackow, A. et al., 2014. Mechanical and thermal properties of lightweight concretes with vermiculite and EPS using air-entraining agent.. *Construction and building materials*, Volume 57, pp. 190-197.

Schulle, W. & Schlegel, E., 1991. Fundamentals and properties of refractory thermal insulating materials (High-temperature insulating materials). *Ceramic Monographs – Handbook of Ceramics*, 40(7), p. 1–12.

Sébaïbi, Y., Dheilly, R. M. & Queneudec, M., 2003. Study of the water-retention capacity of a lime–sand mortar: influence of the physicochemical characteristics of the lime. *Cement and Concrete Research*, 33(5), pp. 689-696.

Shettima, A. U., Hussin, M. W., Ahmad, Y. & Mirza, J., 2016. Evaluation of iron ore tailing as replacement for fine aggregate in concrete. *Construction and Building Materials*, Volume 120, pp. 72-79.

Silva, M. et al., 2016. Feasibility Study of Steel Slag Aggregates in Precast Concrete Pavers. *ACI MATERIALS JOURNAL*, 113(4), pp. 439-446.

Siwinska, A. & Garbalinska, H., 2011. Thermal conductivity coefficient of cement-based mortars as air relative humidity function. *Heat Mass Transfer*, 47(1), p. 1077–1087.

Slack, G. A., 1964. Thermal conductivity of pure and impure silicon, silicon carbide, and diamond.. *Journal of Applied physics*, 35(12), pp. 3460-3466.

Smith, D. S. et al., 2013. Thermal conductivity of porous materials. *Journal of Materials Research*, 28(17), pp. 2260-2272.

Song, M., Niu, F., Mao, N. & Hu, Y. D. S., 2018. Review on building energy performance improvement using phase change materials.. *Energy and Buildings*, Volume 158, pp. 776-793.

Stancato, A., 2000. *Determinação da condutividade térmica e da resistência mecânica em argamassa leve*, Campinas: UNICAMP (Master's Thesis).

Thermtest, 2015. *HFM Theory of Operation*. [Online] Available at: <https://www.thermtest.com/index.php?page=hfm-theory-of-operation> [Accessed 20 12 2015].

Triana, M., Lamberts, R. & Sassi, P., 2015. Characterisation of representative building typologies for social housing projects in Brazil and its energy performance. *Energy Policy*, Agosto, Volume 87, pp. 524-541.

Trtnik, G., Kavcic, F. & Turk, G., 2009. Prediction of concrete strength using ultrasonic pulse velocity and artificial neural networks. *Ultrasonics*, Volume 49, p. 53–60.

Tuladhar, R. & Yin, S., 2019. Sustainability of using recycled plastic fiber in concrete.. In: *Use of Recycled Plastics in Eco-efficient Concrete*. s.l.:Woodhead Publishing, pp. 441-460.

Viegas, G. M., Jodra, J. I., San Juan, G. A. & Díscoli, C. A., 2018. Heat storage wall made of concrete and encapsulated water applied to mass construction social housing in temperate climates. *Energy and Buildings*, Volume 159, p. 346–356.

Waples, D. W. & Waples, J. S., 2004. A review and evaluation of specific heat capacities of rocks, minerals, and subsurface fluids. Part 1: Minerals and nonporous rocks.. *Natural resources research*, 13(2), pp. 97-122.

Weishi, L., Guoyuan, L., Ya, X. & Qifei, H., 2018. The properties and formation mechanisms of eco-friendly brick building materials fabricated from low-silicon iron ore tailings. *Journal of cleaner production*, Volume 204, pp. 685-692.

Xu, Y. & Chung, D. D. L., 1999. Increasing the specific heat of cement paste by admixture surface treatments.. *Cement and Concrete Research*, 29(7), pp. 1117-1121.

Xu, Y. & Chung, D. D. L., 2000a. Cement of high specific heat and high thermal conductivity, obtained by using silane and silica fume as admixtures.. *Cement and concrete research*, 30(7), pp. 1175-1178.

Xu, Y. & Chung, D. D. L., 2000b. Effect of sand addition on the specific heat and thermal conductivity of cement. *Cement and concrete research*, 30(1), pp. 59-61.

Yaman, Y., Inei, G., Yesiller, N. & Aktan, H., 2001. Ultrasonic Pulse Velocity in Concrete Using Direct and Indirect Transmission. *ACI Materials Journal*, 98(6), pp. 450-458.

Yang, Q., Zhu, P., Wu, X. & Huang, S., 2000. Properties of concrete with a new type of saponin air-entraining agent. *Cement and Concrete Research*, Volume 30, pp. 1313-1317.

Yao, R., Li, B. & Steemers, K., 2005. Energy policy and standard for built environment in China. *Renewable Energy*, 30(13), pp. 1973-1988.

Yellishetty, M., Karpe, V., Reddy, E. & Subhash, K., 2008. Reuse of iron ore mineral wastes in civil engineering constructions: A case study.. *Resources, Conservation and Recycling*, 52(-), p. 1283–1289.

Yunsheng, X. & Chung, D., 2000. Effect of sand addition on the specific heat and thermal conductivity of cement. *Cement and Concrete Research*, p. 30 59–61.

Zhao, S., Fan, J. & Sun, W., 2016. Utilization of iron ore tailings as fine aggregate in ultra-high performance concrete. *Construction and Building Materials*, Volume 50, pp. 540-548.

Ziman, J. M., 1960. *Electrons and phonons: the theory of transport phenomena in solids*. 1<sup>a</sup> ed. Oxford: Oxford university press.

# Publications

---

# PUBLICATIONS BY THE AUTHOR

---

Listed below are the peer-reviewed journal articles published with excerpts from this thesis.

1. On the relationship between morphology and thermal conductivity of cement-based composites.
  - Authors: Júlia Castro Mendes, Rodrigo Rony Barreto, Ana Carolina Barbieri de Paula, Fernanda Pereira da Fonseca Elói, Guilherme Jorge Brigolini, Ricardo André Fiorotti Peixoto;
  - DOI: <https://doi.org/10.1016/j.cemconcomp.2019.103365>
  - Journal: Cement and Concrete Composites (0958-9465);
  - Impact Factor: 6.486 (JCR 2018), 2.715 (SJR 2018).
  
2. Macroporous Mortars for Laying and Coating
  - Authors: Júlia Castro Mendes, Paloma Bárbara Pinto, Henrique Emanuel Américo da Silva, Rodrigo Rony Barreto, Taís Kuster Moro, Ricardo André Fiorotti Peixoto;
  - DOI: <https://doi.org/10.7764/RDLC.18.1.29>
  - Journal: Revista de la Construcción (0718-915X, 0717-7925)
  - Impact Factor: 0.468 (JCR 2018), 0.266 (SJR 2018).
  
3. Factors affecting the specific heat of conventional and residue-based mortars
  - Authors: Júlia Castro Mendes, Rodrigo Rony Barreto, Arthur Silva Santana Castro, Guilherme Jorge Brigolini Silva, Ricardo André Fiorotti Peixoto;
  - DOI: <https://doi.org/10.1016/j.conbuildmat.2019.117597>
  - Journal: Construction and Building Materials (0950-0618)
  - Impact Factor: 4.046 (JCR 2018), 1.522 (SJR 2018)
  
4. (Under review) Correlation between ultrasonic pulse velocity and thermal conductivity of cement-based composites
  - Authors: Júlia Castro Mendes, Rodrigo Rony Barreto, Laís Cristina Barbosa Costa, Guilherme Jorge Brigolini Silva, Ricardo André Fiorotti Peixoto;
  - Journal: Journal of Nondestructive Evaluation (1573-4862)
  - Impact Factor: 2.139 (JCR 2018)

5. (Under review) Coating mortars based on mining and industrial residues
  - Authors: Júlia Castro Mendes, Rodrigo Rony Barreto, Vanessa de Freitas Vilaça, Amanda Vitor Lopes, Henor Artur de Souza, Ricardo André Fiorotti Peixoto;
  - Journal: Journal of Material Cycles and Waste Management (1611-8227)
  - Impact Factor: 2.004 (JCR 2018)